UNIVERSITY OF NAPLES FEDERICO II

PHD IN AEROSPACE AND NAVAL ENGINEERING
XXXII CYCLE

Surf-riding/Broaching Assessment within Second Generation Intact Stability Criteria

DOCTORAL THESIS IN NAVAL ARCHITECTURE (ING-IND/01)

PhD candidate
Barbara RINAURO

Supervisor
Prof. Ermina BEGOVIC

Naples, Italy
2020

Acknowledgements

First and foremost, I would like to express my gratitude to my supervisor Prof. Ermina Begovic for guiding me and helping me throughout all my research, and for encouraging me and supporting me in all my achievements.

I would like to thank Prof. Carlo Bertorello who has inspired my studies and research with his expertise and passion, Prof. Guido Boccadamo for providing me the basic skills to start my research, Gennaro Rosano for his friendship and support, and the towing tank technicians, for their politeness and willingness.

I am extremely grateful to Prof. Hrvoje Jasak and Inno Gatin, Ph.D, who gave me the opportunity to work with them and were very warm and willing during my staying at the University of Zagreb.

A special thanks to Prof. Gabriele Bulian who brought light in my doubts especially in the last period of my research.

Many thanks to Maria Acanfora, Ph.D, Silvia Pennino, Ph.D, and Riccardo Pigazzini, Ph.D, who helped me during my research.

And last but not least, I would like to thank my Family who supports me in all my choices and helped me overcome all the difficulties.

I would like to dedicate this thesis to my Grandmother Anna, who was always very proud of my studies and achievements. She always participated to all my important life successes and this time I know she will continue from the highest heaven.

Abstract

This thesis focuses on the study of surf-riding phenomenon, that is one of the failure modes dealt by the Second Generation Intact Stability Criteria (SGISC). The SGISC are based on the physics of "realistic failure modes" that analyse the nonlinear dynamic behaviour of ships in waves. Their development started in 2002 and they have been finalized in the 7th session of the International Maritime Organization (IMO) sub-committee on Ship Design and Construction (SDC) in 2020, in view of approval in 2021. Surf-riding occurs when a ship, sailing in quartering or following waves, is accelerated to wave celerity. In this condition ships are normally directionally unstable and an uncontrollable turn to beam position, known as broaching, and eventually capsizing can occur despite the maximum steering effort being applied. Because surf-riding usually precedes broaching, which has a more complex dynamics, the likelihood of surf-riding occurrence is studied to detect the vulnerability to broaching.

After an overview on the surf-riding/broaching state of the art, the surf-riding phenomenon has been studied with the aims to analyse the effect of the different mathematical models, to investigate the effect of the hull forms, to search for possible "semi-empirical" improvements in one Degree Of Freedom (DOF) methodology and to provide Operational Measures for surf-riding criterion.

The occurrence of the phenomenon has been studied by three numerical approaches: 1-DOF surge mathematical model, solved by nonlinear dynamics and bifurcation analysis; 6-DOF Potential Theory (PT) simulations, based on the combination of seakeeping and manoeuvring models; 3-DOF CFD simulations performed with Naval Hydro Pack of OpenFOAM software, that has been specifically developed to study ships dynamics in waves.

The test case selected for the application is the semi-displacement Systematic Series D of Kracht and Jacobsen (1992), whose models have characteristics of ships that are considered typically vulnerable to surf-riding, due to the narrow and relatively short hull form and fast service speed.

Having found the series D vulnerable to surf-riding Level 2 IMO criterion, the study based on ship dynamics considerations has started by performing 1-DOF approach. In a first attempt, this approach considered calm water approximations for resistance and thrust formulations, and the wave force was simplified by considering regular waves modelled only by the Froude-Krylov component under calm water profile, neglecting the diffraction component.

Surf-riding limits in terms of wave heights, for different ship speeds and wave periods, have been found with 1-DOF approach, with and without the diffraction effect, and have been compared to the occurrence of surf-riding phenomenon experienced by CFD and 6-DOF potential theory simulations. At service speed the D1 hull was found vulnerable to surf-riding phenomenon at wave lengths comparable to ship length and for relatively low wave heights.

From the comparison of the results obtained by the different approaches, the introduction of the diffraction component and the contribution of the wave particle velocities on ship speed have been identified as possible improvement for the 1-DOF approach. It has been observed that the introduction of the diffraction component resulted in a greater and more significant improvement than the wave particle contribution.

Since the series D has been found vulnerable to surf-riding Level 2 and surf-riding occurrence has been observed for low wave heights, Operational Measures, following IMO guidelines, have been discussed and provided for D1 ship, in view of an hypothetical route in the Mediterranean Sea. The Operational Limitations restricted the operations in the Mediterranean Sea for significant wave heights up to 3.8 m, and the Operational Guidance provided limited speeds and headings for specific sea states.

A final discussion in view of a Direct Stability Assessment application has been outlined, underlining the limitations of the three numerical approaches, the time durations and their possible applicability.

Contents

Chapter 1

Introduction

1.1 Regulatory Framework

Adequate intact stability is one of the fundamental requirements for the design and operations of any type of ship or floating vessel. Since the 1930ies, different stability criteria have been developed including national stability standards and classification society rules, mainly based on Rahola's work (Rahola, 1939). First attempts in the development of international intact stability standards followed a statistical approach and they led to the so-called "Rahola type" intact stability criteria or statistical stability criteria (IMO Res. A.167 (ES IV) and IMO Res. A.168 (ES IV), 1968). The Rahola Criteria judged the stability of seagoing vessels evaluating the values of the transversal metacentric height, GM, and righting lever, GZ, curves in calm water conditions and at zero speed. They were statistical since the relationship between the GZ curve and the ship stability safety were obtained by a statistical analysis of stability parameters of a wide dataset of ships including both ships that capsized and ships that were judged safe by the stability point of view.

After the capsizing of ships compliant with Rahola Criteria, it became clear that further improvements in intact stability standards were needed. Therefore, to take into account the environmental conditions, the Weather Criterion was adopted by the International Maritime Organization (IMO) Assembly Resolution A.562, in 1984. It was developed to guarantee the safety against capsizing for a ship losing all propulsive and steering power in severe beam wind and waves. The Weather Criterion was in part based on a simplified one degree-of-freedom physical model of the wind and wave actions, even though some parameters were calibrated on a sample of ships, therefore their applicability was strongly dependent on the dataset of ships used at the time.

The first generation of stability criteria was originally encoded at IMO in 1993 as a set of recommendations, and after a revision process, they were codified in the 2008 IS Code and became effective as a part of both the SOLAS and International Load Line Conventions in 2010. They are based on calm water and zero-speed conditions and consist in the statistical criteria (Rahola criteria) and Weather criterion. The waves influence on ship motions was considered only in seakeeping studies with the aim to improve ship comfort and operability, but not for ships security.

Over the last several decades, significant changes in ships' design and operations, that differentiated the ships from the reference sample, have impacted on the intact stability performance. In addition, the occurrence of stability-related accidents, due to the nonlinear dynamics of sailing ships, clearly demonstrated that the "actual" intact

stability criteria were not adequate and motivated the development of a new generation of criteria.

The development of the Second Generation Intact Stability Criteria (SGISC) started in 2002 with the re-establishment of the intact-stability working group by IMO's Subcommittee on Stability and Load Lines and on Fishing Vessels Safety (SLF). Nevertheless, due to the priority of revising the Intact Stability Code for approval, the actual work on the SGISC did not commence until the 48th session of the SLF in September 2005. Since then, many efforts have been done to understand and develop criteria suitable to describe possible modes of stability failure. During the 7th session of the IMO sub-committee on Ship Design and Construction (SDC) in 2020 the SGISC have been finalized. The SGISC draft interim guidelines have been submitted to the Maritime Safety Committee (MSC) 102 (May 2020) for approval with the aim of providing them for trial use to the industry. A correspondence group will work on the explanatory notes to the interim guidelines until SDC 8 (January 2021), with a view to approval at MSC 104 (June 2021).

The five stability failure modes dealt by IMO Intact Stability working group are: Parametric roll, Pure loss of stability, Surf-riding/broaching, Dead ship condition and Excessive acceleration.
The aim of these criteria is to prevent dangerous loss of stability that may lead to capsizing or endanger passengers, crew and cargo when ships are sailing in dangerous weather conditions. All these criteria are based on "realistic failure modes" that analyse the nonlinear dynamic behaviour of ships in waves and consider large amplitude motions. The seakeeping theory, that studies the influence of waves on ships' motions, even though could not be directly applied since it is based on approximated linearisation, considering motions of small amplitude and normally neglects surge motion, nevertheless it provides wave descriptions used to develop mathematical models to study ship motions in waves.

Due to the complexity of physical modelling and the substantial additional design analysis expense, the SGISC are structured with a multi-tiered approach, as described in Figure 1.1. Vulnerability checks are performed at three levels to ensure simplicity and prevent unnecessary computational efforts. Level 1 (L1) vulnerability check is simple and conservative to distinguish ships that are clearly not vulnerable. Level 2 (L2) is less conservative than Level 1 and is based on a more sophisticate physical model to reduce conservatism but a certain number of assumptions are made to contain the computational effort. The Direct Stability Assessment (DSA) has to be performed using the most advanced state of art methodology to predict, as close as possible, actual ship behaviour in waves. At the beginning the levels were thought to be applied in sequence starting from the first, but in the finalization of the SGISC the three levels have been adopted without any hierarchy. In a given loading condition, if the ship is found vulnerable to one level, the next one has to be applied, otherwise the ship design has to be modified. If L2 or the DSA are not satisfied for one or more loading conditions and no changes in ship design are practicable, Operational Measures (OM) can be provided to avoid dangerous situations and reduce the likelihood of stability failures. Operational Measures (OM) are divided in Operational Limitations (OL) related to areas or routes and season and related to maximum significant wave heights, and in Operational Guidance (OG), that defines sailing conditions that are not recommended or to be avoided in relevant sea states. While Level 1 and Level 2 vulnerability assessments are defined by clear procedures and explanatory notes, the applications of the Direct Stability Assessment and the Operational Measures, are still under discussion.
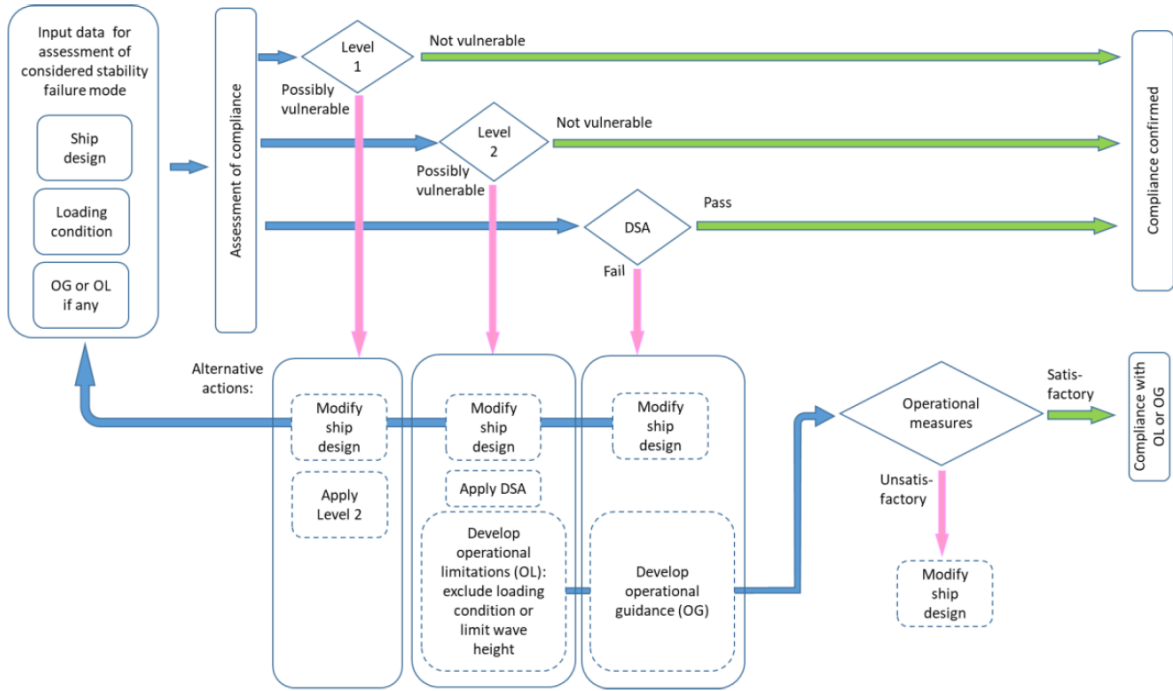
Figure 1.1: Simplified scheme of the application structure of SGISC (SDC7/5, 2019).

All the failure modes considered in the SGISC, except surf-riding/broaching, are described by the roll motion and, for given displacement and initial trim values, the vulnerability detected varies as function of the position of the centre of gravity. For this reason, the limits of compliance are provided as a function of the limiting values of the KG. The surf-riding/broaching criterion in this framework is an isolated failure mode that does not depend on the variation of KG values but is related to ships' manoeuvrability and to ship velocity. Moreover, the surf-riding phenomenon is described by the surge motion, which is normally neglected when studying ship seakeeping.

In this thesis the surf-riding/broaching criterion has been chosen and studied, since, due to its different dynamics, it is one of the less studied phenomena and criteria.

Surf-riding and broaching normally occur in following to quartering seas when the ship and wave lengths are comparable and the ship speed is slightly lower than the wave celerity. Large following waves acting on the hull can accelerate the ship and force her to move with the same speed: this phenomenon is called surf-riding. During surf-riding condition, ships are normally directionally unstable and an uncontrollable turn to beam position, known as broaching, can occur despite the maximum steering effort being applied. Broaching may induce significant violent yaw moments and the resulting centrifugal forces may lead to capsizing. Small-size high-speed ships, high-speed RoPax ferries, naval ships and fishing vessels are most vulnerable to this stability failure.

If the ship speed is slightly higher than the wave celerity and the wave crest is around bow position, the ship may be blocked by the wave and forced to decelerate to wave celerity. This phenomenon is called wave blocking and it is less dangerous than surf-riding because it does not lead to capsizing, although, once wave blocking phenomenon stops, the ship may experience bow diving.

While surf-riding phenomenon can be described by one-degree-of-freedom surge motion equation, broaching is regarded as a manoeuvrability problem and must be described

by at least 4 degrees of freedom.

Surf-riding usually precedes broaching, which has a more complex dynamics, therefore, its likelihood of occurrence is used to formulate the vulnerability assessment for surf-riding/broaching criterion.

In order to allow surf-riding to occur, several conditions need to be satisfied: the wave length must be in a range of 1.0-3.0 times the ship length, the wave must be sufficiently steep and the ship speed should be comparable to the wave celerity, around 75%.

When a ship proceeds in following waves, the forces acting in the axial direction are: hull resistance, propeller thrust and surging wave force, pushing the ship forward or backwards when the ship is on the face or on the back of the wave.

Depending on the magnitude of these forces, three conditions may occur:

- **Surging motion**: when the magnitude of the wave surging force is less than the difference between the propeller thrust and hull resistance, and the only possible motion is surge;

- **Surf-riding motion under certain initial condition**: when the amplitude of the wave surging force exceeds the difference between propeller thrust and resistance, and under certain initial conditions surf-riding phenomenon becomes possible and both surging and surf-riding motions may occur. The condition when surf-riding becomes possible represents the first threshold of surf-riding;

- **Surf-riding motion under any initial condition**: when the amplitude of the surging force exceeds the difference between propeller thrust and resistance and surf-riding occurs in any condition. This situation in which surging ceases to exist and surf-riding becomes inevitable represents the second threshold of surf-riding.

Figure 1.2 represents the forces acting on a ship as function of the wave crest position on the hull, x, in surf-riding condition over the second threshold. In this condition, the three forces: resistance, thrust and wave force, reach equilibrium for infinite relative wave-hull positions, defining two types of equilibrium points:

- stable when wave trough is around amidships;

- unstable when the crest is around amidships

The ship represented in the figure is the parent hull of the Systematic Series D, Kracht and Jacobsen (1992), scaled to 90 m length, advancing at speed of 9.95 m/s, equal to Froude number Fn = 0.335, in following regular waves with wavelength to ship length ratio equal to $\lambda/L = 1$ and steepness equal to $H/\lambda = 0.1 \rightarrow H = 9$ m.
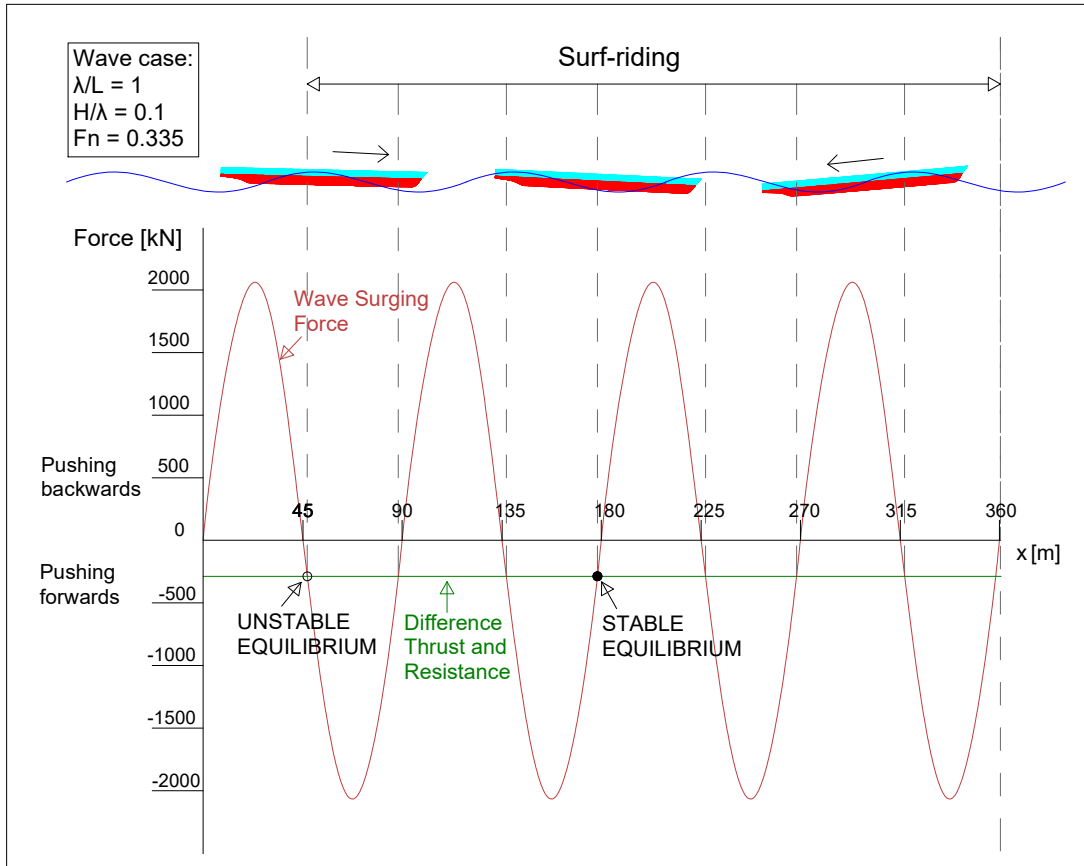
Figure 1.2: Forces acting on the ship in surf-riding condition

1.2 State of the Art

The surf-riding/broaching phenomenon is a rare event occurred in actual existing ships. Not many experiences and accidents related to this failure are described and reported but some testimonies of its occurrence go back to the 1600 and 1700ies.

Du-Cane and Goodrich (1962) reported some experiences of broaching in actual ships starting for example with the loss of the Sussex East India and the broaching of a Four-Masted Barque in High Latitudes. Authors underline that sailing ships in following seas best used the strong winds "... to keep the ship running as fast as possible and yet avoid the dreaded broach". Moreover Authors described that: a fleet of small fishing vessel were lost in on gale in 1954, "... trying to run out and make port to leeward as fast as possible, had in many cases, broached..."; and in 1971 an old power-driven battleship H.M.S. St. Vincent experienced "... a violent and uncontrolled yaw or "broach" into the trough of the sea...".

Conolly (1972) illustrated the disaster of the Lyttelton–Wellington ferry Wahine sinking in 1968, which was one of the most serious accidents referred to as broaching stability failure.

In the last decades researchers have made significant theoretical and experimental efforts to study the physics and highly nonlinear and chaotic nature of the surf-riding/broaching phenomena. Different approaches have been studied in literature starting from analytical approaches, passing through potential flow numerical methods based on 4 or 6 Degrees Of Freedom (DOF), all the way to Computational Fluid Dynamics (CFD) applications.

Since the pioneering work of Grim (1963) it has been pointed out that the highly nonlinear surging motion of a ship in following sea is found to be the most important pre-condition for broaching. The Author concluded that broaching probably will be more severe for a slow running than for a fast running ship, provided that the slow running ship can still be accelerated by the sea to the dominant wave speed. Grim suggested that the criterion for an acceleration of the ship to the dominant wave speed can be used as an important criterion for broaching. These considerations have been "solved" for the surging motion in regular following waves. The law of superposition cannot be used to treat the nonlinear surging motion in an irregular sea and it is not possible to extend the results obtained in regular waves to predict the behaviour in an irregular sea. The occurrence of surf riding in irregular sea has been studied first by Grim (1963) who proposed the analytical method which was re-considered recently by Themelis et al. (2016).

The first systematic experimental research of surf-riding and broaching was carried out in the 1960's by Du-Cane and Goodrich (1962), for ships in severe following or quartering seas. Authors discussed directional stability in calm water and performed an experimental campaign on a self-propelled model in following waves. As the Authors concluded, the most interesting result from these experiments was the large range of wavelengths (100 to 800 ft at full scale) over which the model was carried along the wave crest speed. Furthermore, Authors compared these results with their previous campaign on four high speed craft in regular following waves, concluding that the persistence of tendency to broaching beyond the condition "ship speed approximately equal to wave celerity" is due to a hydrodynamic lift at slight angle of attack.

Kan et al. (1994) confirmed that, in an extensive experimental campaign of two container ships tested in quartering regular waves at constant propeller rate, not only surf-

riding occurred at wave lengths $\lambda/L \simeq 1$, but also many capsizing were observed in longer waves such as $\lambda/L \simeq 1.75$. Authors commented that it should be recognized that the most dangerous wave lengths were in the range of 1.00 to 1.75.

J. O. De Kat and W. L. Thomas III (1998) performed tests on a frigate hull form in following regular and irregular waves. Model tests showed that for speeds corresponding to $Fn \leq 0.3$ surf-riding did not occur. For $Fn = 0.35$ Authors reported that "a drastic change in surge character occurs, as at this speed setting the frigate model does experience wave capture and surf-riding events". Authors furthermore reported that the frigate experienced two modes of broaching under certain condition at $Fn = 0.35$:

- High speed broach preceded by surf riding with rapidly and monotonically increasing heading deviation in following and stern quartering sea;

- Large amplitude, low frequency yaw (heading) oscillations in stern quartering waves

Dynamic instability in quartering seas has been analysed by Spyrou between 1996 and 1997. In Spyrou (1996b) the dynamics of the broaching phenomenon in steady state and transient analysis have been carried out from the customary periodic motions with the astern regular waves overtaking the vessel. The attempt was to clarify the role of surf-riding by concentrating on the system's state-space topological definition and by analysing the bifurcating behaviour. The problem formulation took into account the motions of the actively steered or controls-fixed vessel in surge-sway-yaw-roll with consideration of Froude-Krylov and diffraction wave excitation. Spyrou (1996a) studied the ship capsizing specifically in connection with the broaching phenomenon. Figure 1.3 displays how the four qualitatively different types of ship behaviour existing in stern quartering waves, namely, surf-riding, ordinary periodic motion, broaching and capsize, are related to each other, for two different initial motion patterns of the ship.
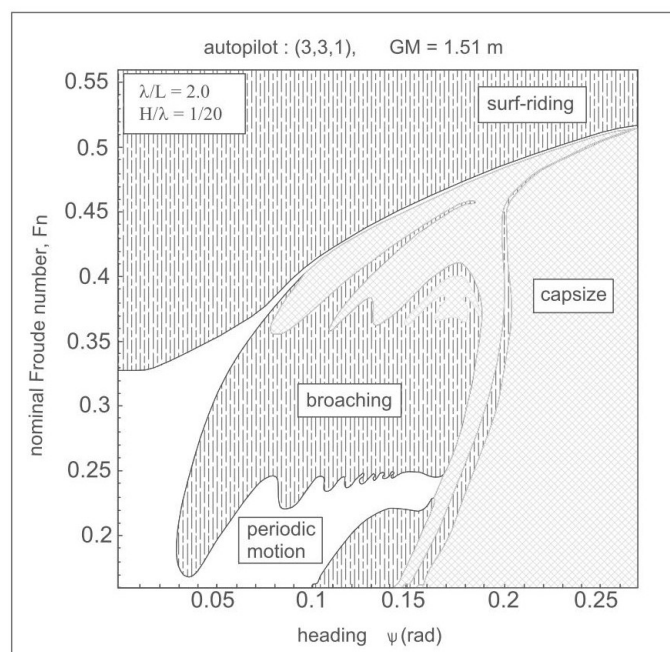

Figure 1.3: "Multiple-effect" global analysis helps to locate the domains of surf-riding, periodic-motion, broaching and capsize Spyrou (1996a).

Umeda (1999) applied a nonlinear dynamic approach to the surge–sway–yaw–roll mathematical model of a ship running with an autopilot in following and quartering seas. Fixed points and unstable manifolds defining surf-riding domains were systematically investigated by phase plan analysis and the existence of heteroclinic bifurcation was identified. Numerical experiments confirmed that this heteroclinic bifurcation represented reasonably well the critical condition for capsizing due to broaching.

An analytical approach for the study of asymmetric surging and surf-riding in extreme following seas has been developed by Spyrou (2006). The two main aims were to better understand the nature of ship surging in the strongly nonlinear region and to develop some relatively simple formulas as a guidance for ship design and operation.
The surf-riding occurrence has been predicted by Melnikov's method which is a powerful tool for predicting the occurrence of the tangency of homoclinic orbits of a dynamical system. In a phase plane representation of the ship position on the wave and surge velocity, such tangency would mean the destruction of the periodic surge motion and the capture into surf-riding irrespective of the initial condition. This situation corresponds to the second threshold of surf-riding.
Explicit analytical closed-form solutions that describe asymmetric surging up to the limit of surf-riding have been developed. For the first time the effect of water particle velocity has been introduced on ship resistance and thrust in steep following waves. This effect was found not negligible but unlikely to influence the qualitative character of surge dynamics. The Author concluded that the analytical approach seems to have limitations as the mathematical model incorporates extra detail in the representation of loads that act on the ship.

In Maki et al. (2014) different methods for solving surge motion equation have been compared. Authors reported results of surf-riding and wave-blocking thresholds obtained from: experimental tests, numerical bifurcation analysis and two analytical formulae: the Melnikov's method and the continuous piecewise linear (CPL) approximation. For the particular case, both analytical methods have provided accurate results.

Similar approach, i. e. improvement of the Melnikov's method, has been applied by Wu et al. (2010). Authors proposed an extended version of the Melnikov method to large damping systems, with the idea to provide "semi-empirical" formula between purely analytical approaches (such as Melnikov method) and full computationally intensive simulations.

Recent studies are devoted to detect the phenomenon of surf-riding in irregular seas (Spyrou et al. (2014), Belenky et al. (2016), Themelis et al. (2016)). The extension of consolidated methodology in regular waves requires the definition of the celerity of irregular waves (in order to find equilibria) and the formulation of a mathematical model of surf riding in spatial-temporal framework, i.e. all variables must be functions of position and time. Another approach is to evaluate broaching probability or probability of capsizing due to broaching in irregular waves, as Grim (1963) proposed.

Themelis et al. (2016) developed a simulation-based method on the direct counting of "high runs" and applied the semi-analytical method of Grim (1963). "High runs" are identified when a ship operates in steep irregular waves and can attain, in intermittent time intervals, abnormally high speed, due to waves' effect. Authors compared results from these two approaches and concluded that "In comparison to the direct counting method, the analytical one seems to overestimate the probability of high runs with longer duration".

Important contributions towards the validation of IMO methodologies have been the

works by Yu et al. (2014) and Feng et al. (2015) and Feng et al. (2017), where different hydrodynamic numerical approaches were applied to predict the surf riding occurrence.

Yu et al. (2014) applied a 6-DOF weakly nonlinear unified model considering nonlinear restoring and Froude-Krylov forces over instantaneous wetted surfaces for the numerical simulation of ship stability failure events in quartering seas for ITTC A2 fishing vessel of 34.5 m length (Japan sample ship data). Authors showed that the weakly nonlinear model is capable of simulating ship stability failure events including broaching after surf-riding and capsizing due to loss of stability in quartering seas. It was also found that the ship tended to capsize at high Froude number in following and quartering seas, since she may be overtaken by wave from astern with high speed close to wave celerity.

Yu et al. (2017) investigated the possibility of mitigating surf-riding occurrence by adjusting the centre of buoyancy of the ITTC A2 fishing vessel in the design stage using the 6-DOF weakly non-linear model developed from Yu et al. (2014). Surf-riding motions in regular following seas for cases with different LCBs and Froude numbers have been simulated using the numerical model. Results showed that the surf-riding cannot be prevented by the adjusting of LCB, although thresholds of the surf riding are affected.

Feng et al. (2015) performed a sensitivity analysis on calm water resistance, propulsion coefficients and wave force variations on the final assessment result for a purse seiner ship of 42.5 m length. Conclusions reported that the uncertainty of 5% in resistance prediction affected 16% difference in the attained index C value of Level 2 vulnerability criterion. Even more important was the uncertainty due to the order of the polynomials for curve fitting; Authors reported as much as 29.5% difference of C value for fitting by 3rd and 5th order polynomials. Influence of $\pm 10\%$ variation of propulsion coefficients K_T, w_p and t_p resulted in 1 to 3 % difference in the attained index C value. The major influence is due to the wave induced surge force, for which the Authors reported up to 50% different result for the expression with and without diffraction correction to the Froude Krylov force. This latter has been further studied in Feng et al. (2017) for the small fishing vessel. Wave surge force has been measured through captive model tests at zero speed and at Fn = 0.30 for two sets of wave steepness. Measured results were compared against the ones calculated by HydroSTAR ® Software and those calculated according to the IMO documents. Authors concluded that the diffraction effect should be included into the calculation of wave force while speed and wave steepness have only secondary influence on the wave force and therefore can be acceptable to neglect the speed effect and to adopt linear theory assumptions for the Level 2.

Bonci et al. (2018) studied the vulnerability of broaching of high speed craft with time domain simulations based on potential flow boundary element method theory. For different speed conditions, the direct assessment has been used to evaluate the number of broaches occurring during a time realization of the sea spectrum. This method has been compared with a regular wave stochastic approach, where the probability of broaching to is associated to the probability of encountering a local regular wave that causes a dynamic instability given a certain sea state. The number of instability failures have shown opposite trends: with the stochastic approach they decrease when ship speed increases; in irregular waves the trend is opposite. However, Authors highlighted the importance of numerical tools to provide statistical description of the phenomenon in irregular seas.

The technological progress and computing power give the possibility to perform surf-riding and broaching occurrence by CFD softwares. Among few numerical CFD studies, one of the first application of an unsteady Reynolds-Averaged Navier Stokes method

(RANS) has been demonstrated for an auto piloted ONRT (Office of Naval Research Thumblehome) by Carrica et al. (2008) using CFDShip-Iowa software. The equations of motions have been solved only on the water side and the waves have been implemented through initial and boundary conditions. The propellers have been modelled by an actuator disk/body force approach. Authors concluded that the use of complex codes to study dynamic stability problems could help the design of hull and appendages for safer ships although at a larger cost than other simpler methods.

The effect of different wave induced force assessments (linear Froude Krylov, captive model test by experimental fluid dynamics (EFD) and CFD) on the surging/surf-riding boundaries has been analysed in Sadat-Hosseini et al. (2011). Although the linear Froude Krylov formulation overestimated the wave induced forces, Authors concluded that this estimation resulted in non-significant loss in overall assessment of the boundaries. The CFD simulations in waves (for surging, surf-riding, and broaching conditions) were performed on the ONRT model scale hull and used an actuator disk model with a fixed number of revolutions set to gain the desired Fn in calm water condition. Authors underlined that in the simulations the calculation of thrust and torque did not depend on the local flow field near the propeller but on the velocity of the ship; and that the body force was axisymmetric. Simulations for different target headings led to surge, surf-riding or broaching conditions, and in each case, motions, forces and moments have been analysed, predicting the instability boundaries that were found in good agreement with the ones obtained by EFD.

Studies of the influence that the ship form has on the wave field in following sea conditions when surf-riding phenomenon is likely to occur, have been conducted by Hashimoto et al. (2016) and Yang and Wang (2017). Hashimoto et al. (2016) have analysed the wave induced force variations on different hull forms, derived from the ONRT hull, throughout 2-DOF CFD simulations. The aim was to improve the prediction accuracy of the wave-induced surge force in IMO surf-riding criterion taking into account the effect of hull form parameters. Furthermore, the consideration of the dynamic vertical position in waves slightly improved the prediction accuracy. Authors concluded that, although the RANS solver showed fairy good agreement with the experiment, it is not realistic to use CFD for practical design and safety assessment, except for the direct stability assessment, due to time and costs of computations; so further investigation, based on the their outcomes, to propose a more reliable correction formula, has been encouraged.

Yang and Wang (2017) studied the stability properties of a ship in surging and surf-riding conditions, highlighting great difference in the stability curve values obtained by two methods: one that does not consider the effect of ship motions on the wave field and the other obtained performing CFD simulations that take into account the actual wave profile influenced by ship's motions.

To have a brief overview, surf-riding is a precondition for broaching and therefore its occurrence is used to predict and avoid broaching. The surf-riding phenomenon is related to an heteroclinic bifurcation and analytically solved with a closed form solution of Melnikov's Method, which is the approach used in Level 2 of the SGISC. The diffraction component in evaluating wave excitation forces has a non negligiable influence. CFD simulations are found to predict well the ships' motions and forces, and there fore a valuable approach to study and predict surf-riding phenomenon.

1.3 Objectives and Outline of the Thesis

This thesis focuses on the assessment of surf-riding failure mode from a physical and regulatory point of view. From the detailed analysis of the state of the art, the following study has been concentrated on the main aspects and parameters found to be significantly influential on the surf-riding phenomenon.

The Objectives of the thesis have been to:

- Analyse the accuracy of the different mathematical models applied to identify surf-riding phenomenon;

- Investigate the effect of the hull form on the occurrence of surf-riding;

- Search for possible "semi-empirical" improvements to be implemented in a 1-DOF methodology;

- Verify the impact of the Operational Measures;

- Provide Operational Measures for surf-riding criterion;

To analyse the various aspects of the phenomenon, the test case selected for the application has been chosen in order to be different from the classical benchmark ships and with characteristics of ships that are considered typically vulnerable to surf-riding, as narrow and relatively short hull forms and fast service speed.
The surf-riding study has therefore been performed on the semi-displacement, transom stern, round bilge, twin-screw, Systematic Series D of Kracht and Jacobsen (1992), scaled to 90 m length, which has service speed corresponding to Fn=0.433. The series consists of 7 hull forms obtained by linear distortion or scaling of the parent model D1. A ranking list has been obtained among the different hulls, to evaluate which were the best and worst form from the surf-riding point of view, as reported in Begovic et al. (2018).

The phenomenon has been analysed comparing various numerical approaches used in literature:

- 1-DOF mathematical model, on which Level 2 IMO procedure is based, solved by a nonlinear dynamics procedure and bifurcation analysis;

- 6-DOF potential flow theory approach based on Matusiak (2013) mathematical model, that combines seakeeping and manoeuvrability and solves motion equations in time domain;

- CFD simulations performed with OpenFOAM software Vukčević et al. (2017), which has a specific package, Naval Hydro, implemented to study the dynamic motions of ships sailing in waves.

The thesis is structured according to the following parts.
A description of IMO Level 1 and 2 vulnerability assessment procedures is given in Section 2. The numerical models are introduced in Section 3 for 1-DOF approach, in Section 4 for the potential theory model, and in Section 5 for the CFD modelling.

The test case application is described in Section 6. After a description of the test case hull form in Section 6.1, Section 6.2 reports a first verification of the vulnerability of the hull forms, performed by the application of Level 1 and 2 assessments.

Surf-riding limits obtained by 1-DOF model are described in Section 6.3. Simulations in time domain are reported in Section 6.4 for the 6-DOF potential theory mathematical model, and in Section 6.5 for the CFD approach. Possible improvements for the 1-DOF model are discussed and implemented in Section 7.

Surf-riding limits, obtained by 1-DOF approach, have been compared with the surge and surf-riding motions observed by numerical potential flow theory and CFD simulations, as reported in Section 8.

Operational Measures are presented in Section 9 and conclusions and future works are discussed in Section 10.

Chapter 2

IMO Second Generation Intact Stability Criteria

2.1 Surf-riding/Broaching Criterion

The study on the vulnerability criteria of Level 1 and 2 for the surf-riding/broaching failure mode has been made according to the following IMO draft amendments:

- SDC2/WP4 (2015) (Annex 3 (02/2015)) - Draft amendments to Part B of the Is code with regard to Vulnerability criteria of Level 1 and 2 for the surf-riding/broaching failure mode;

- SDC3/INF10 (2015)(Annex 18 (11/2015)) and SDC3/WP5 (2016), (Annex 5 (01/ 2016)) - Draft explanatory notes on the vulnerability of ships to the surf-riding/broaching stability failure mode;

- SDC4/5/4 (2016) and SDC4/5/6 (2016) (11/2016) - Comments on Level 2 criteria for surf-riding/broaching stability failure mode.

- SDC7/WP6 (2020) - Finalization of the Second Generation Intact Stability Criteria;

2.1.1 Level 1

A ship is considered not to be vulnerable to the surf-riding/broaching stability failure mode if either of the following conditions is fulfilled:

$$L \geq 200m \tag{2.1}$$

$$Fn \leq 0.3 \tag{2.2}$$

where:
$Fn = u/\sqrt{Lg}$ is the Froude number;
u is the service speed in calm water [m/s];
L is the length of the ship between perpendiculars [m];
g is the gravitational acceleration of 9.80665 $[m/s^2]$.

The criterion and the standard for the Froude number in Level 1 criterion were adopted as a part of the MSC.1/Circ.707 (1995) and then superseded as MSC.1/Circ.1228 (2007).

This guidance concludes that surf-riding may occur when the ship speed, in knots, is higher than:

$$u \geq \frac{1.8\sqrt{L}}{\cos(180° - \alpha)} \tag{2.3}$$

where: α is wave heading (0 ° is head waves).

Assuming following seas ($\alpha = 180°$) and transforming the equation above into the form of length-based Froude number yields:

$$Fn \geq (1.8 \times 0.51444)/\sqrt{g} = 0.296 \sim 0.3 \tag{2.4}$$

This is considered the lower limit of threshold for surf-riding under any initial condition for conventional ships in the worst waves.

2.1.2 Level 2

Level 2 vulnerability assessment defines a long-term probability index, based on the identification of the surf-riding second threshold combined with the probability of encountering a local regular wave that causes this instability, given a certain sea state, and weighted on the probability of occurrence of each sea state.

Surf-riding is described by analysing the surge motion equation (Equation 2.5) described by the forces acting on a ship sailing in following wave in direction of forward speed, as represented in Figure 2.1: resistance, R, propeller thrust, T_e, and wave surging force, F_X, that pushes the ship forward or backward depending on whether the ship is on the face or back of a wave.
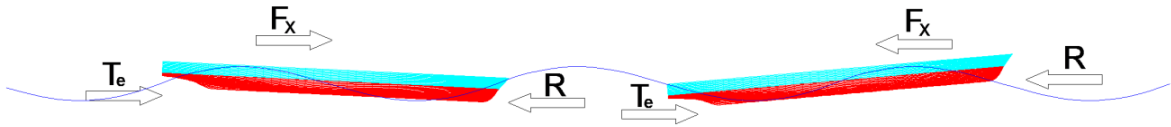
$$(M + M_X)\dot{u} + R - T_e = F_X \tag{2.5}$$

Figure 2.1: Forces acting on a ship sailing in following waves

Surf-riding occurs when the difference between resistance and thrust balance the wave surging force, as described in Section 1.1.

The solution of the surge motion equation and the identification of surf-riding second threshold is obtained by Melnikov's method, as described in Spyrou (2006), that identifies the critical number of revolution for which surf-riding occurs at the second threshold, for a specific loading condition and sea state.

Level 2 IMO procedure to detect surf-riding vulnerability, can be split into four parts.

The first part considers the calculation of the critical number of revolutions of the propeller, n_{cr}, obtained by the Melnikov's analysis. The n_{cr} is the solution of a second order algebraic equation whose parameters are:

- ship geometrical data: Mass, M, and section data;

- calm water resistance $R_,$;

- propeller thrust T_e;

- thrust deduction t_p, wake fraction w_p, propeller diameter D_p;

- wave steepness, $s_j = H_{ij}/\lambda_i$, varying from 0.03 to 0.15 with increment $\Delta s = 0.0012$, for a total of cases $N_\lambda = 81$;

- wavelength to ship length ratio, $r_i = \lambda_i/L$, varying from 1.0 to 3.0 with increment $\Delta r = 0.025$, for a total of cases $N_a = 101$.

All the parameters depending on the velocity have been calculated considering the ship speed equal to the wave celerity: $u = c_i$. The second order equation is:

$$2\pi \frac{T_e(c_i, n_{cr}) - R(c_i)}{f_{ij}} + 8a_0 n_{cr} + 8a_1 - 4\pi a_2 + \frac{64}{3}a_3 - 12\pi a_4 + \frac{1024}{15}a_5 = 0 \qquad (2.6)$$

where:
the thrust and the resistance are formulated as:

$$T_e(c_i, n_{cr}) = \tau_0 n_{cr}^2 + \tau_1 c_i n_{cr} + \tau_2 c_i^2 \qquad (2.7)$$
$$R = r_0 + r_1 c_i + r_2 c_i^2 + r_3 c_i^3 + r_4 c_i^4 + r_5 c_i^5 \qquad (2.8)$$

the wave celerity, wave number and wave height are respectively:

$$c_i = \sqrt{\frac{g}{k_i}} \qquad (2.9)$$

$$k_i = \frac{2\pi}{\lambda_i} \qquad (2.10)$$

$$H_{ij} = s_j r_i L \qquad (2.11)$$

the coefficients are:

$$a_0 = -\frac{\tau_1}{\sqrt{f_{ij}k_i(M + M_X)}} \qquad (2.12)$$

$$a_1 = \frac{r_1 + 2r_2 c_i + 3r_3 c_i^2 + 4r_4 c_i^3 + 5r_5 c_i^4 - 2\tau_2 c_i}{\sqrt{f_{ij}k_i(M + M_X)}} \qquad (2.13)$$

$$a_2 = \frac{r_2 + 3r_3 c_i + 6r_4 c_i^2 + 10r_5 c_i^3 - \tau_2}{k_i(M + M_X)} \qquad (2.14)$$

$$a_3 = \frac{r_3 + 4r_4 c_i + 10r_5 c_i^2}{\sqrt{k_i^3(M + M_X)^3}}\sqrt{f_{ij}} \qquad (2.15)$$

$$a_4 = \frac{r_4 + 5r_5 c_i}{k_i^2(M + M_X)^2}f_{ij} \qquad (2.16)$$

$$a_5 = \frac{r_5}{\sqrt{k_i^5(M + M_X)^5}} \qquad (2.17)$$

23

M_X is the added mass and f_{ij} is the amplitude of the wave surge force calculated considering only the Froude Krylov component:

$$f_{ij} = \rho g k_i \frac{H_{ij}}{2} \sqrt{Fc_i^2 + Fs_i^2} \tag{2.18}$$

where:
ρ is the water density, $[kg/m^3]$;

$$Fc_i = \sum_{m=1}^{N} \Delta x_m S(x_m) \sin(k_i x_m) \exp\left(-0.5 k_i d(x_m)\right) \tag{2.19}$$

$$Fs_i = \sum_{m=1}^{N} \Delta x_m S(x_m) \cos(k_i x_m) \exp\left(-0.5 k_i d(x_m)\right) \tag{2.20}$$

where:
Δx_m is length of the ship strip associated with station m, [m];
x_m is the longitudinal distance from the center of ship mass to a m-th station , positive for a bow section, [m];
$d(x_m)$ is the local draft at m-th station in calm water, [m];
$S(x_m)$ is the area of submerged portion of the ship at m-th station in calm water, $[m^2]$;
N is the number of stations.

The thrust coefficients τ_0, τ_1, τ_2 are calculated as:

$$\tau_0 = k_0(1 - t_p)\rho D_p^4 \tag{2.21}$$
$$\tau_1 = k_1(1 - t_p)(1 - w_p)\rho D_p^3 \tag{2.22}$$
$$\tau_2 = k_2(1 - t_p)(1 - w_p)^2 \rho D_p^2 \tag{2.23}$$

where:
the thrust deduction t_p can be:

$$t_p = 1; \qquad \text{for single screw ship} \tag{2.24}$$

$$t_p = 0.325\, C_B - 0.1185 \frac{D_P}{\sqrt{Bd}} \quad \text{for double screw ship} \tag{2.25}$$

where: C_B is the block coefficient, B the ship breath and d the ship draft, and the wake fraction w_p can be approximated to 0.1.

The approximation coefficients for the propeller thrust coefficient $K_T(J)$ in calm water, k_0, k_1, k_2 are obtained from the second order polynomial fit of propeller thrust curve:

$$K_T(J) \sim \sum_{i=0}^{2} k_i J^i = k_0 + k_1 J + k_2 J^2 \tag{2.26}$$

where J is the advanced ratio defined as:

$$J = \frac{u(1 - w_p)}{n_{cr} D_p}$$

In case of a ship having multiple propellers, the overall thrust can be calculated by summing the effect of the individual propellers, that is the thrust calculated in Equations 2.7 and 2.28 and the thrust coefficients of Equations 2.21 - 2.23 are obtained by considering the effect of the total number of propellers.

The second part regards the calculation of the critical Froude number, Fn_{cr}, corresponding to the second threshold of surf-riding which occurs under any initial condition. The critical Froude number is obtained by the critical ship speed, u_{cr}, determined by solving the equation of equilibrium between the thrust, T_e, and resistance R. The thrust is function of ship speed in calm water and the critical number of revolutions, n_{cr}, and the resistance is function of the ship speed in calm water. This time the involved parameters have been calculated considering the ship speed in calm water.

$$Fn_{cr} = u_{cr}/\sqrt{Lg} \qquad (2.27)$$

u_{cr} is the solution of the following equation:

$$T_e(u_{cr}, n_{cr}) - R(u_{cr}) = 0 \qquad (2.28)$$

where the resistance and the thrust are written as:

$$R(u_{cr}) = r_0 + r_1 u_{cr} + r_2 u_{cr}^2 + r_3 u_{cr}^3 + r_4 u_{cr}^4 + r_5 u_{cr}^5 \qquad (2.29)$$

$$T_e(u_{cr}, n_{cr}) = (1 - t_p)\rho n_{cr}^2 D_p^4 \{k_0 + k_1 J + k_2 J^2\} \qquad (2.30)$$

Depending on the Fn_{cr} value, a specific number $C2_{ij}$ is taken to be one or zero depending on whether the Froude number, Fn, corresponding to the service speed, is greater or smaller than the critical one Fn_{cr}.

$$C2_{ij} = \begin{cases} 1 \text{ if } Fn > Fn_{cr} \\ 0 \text{ if } Fn \leq Fn_{cr} \end{cases} \qquad (2.31)$$

The third part defines a short-term index. A statistical weight of a wave, W_{ij}, is evaluated and represents the joint probability density function of local steepness and local wavelength under the stationary wave state with a Pierson-Moskwitz type wave spectrum.

The formulation of W_{ij}, as in Equation 2.32, is function of the wave steepness, s_j and wavelength to ship length ratio, r_i, the significant wave height, H_s, and zero-crossing wave period, T_z, given in Table 2.1. This formulation originates from the Loguet-Higgins' theory (Longuet-Higgins, 1983), based on the wave envelope theory.

$$W_{ij} = \frac{4\sqrt{g}}{\pi\nu} \frac{L^{5/2}T_{01}}{(H_s)^3} s_j^2 r_i^{3/2} \left(\frac{\sqrt{1+\nu^2}}{1+\sqrt{1+\nu^2}}\right) \Delta r \Delta s \cdot exp\left[-2\left(\frac{L \cdot r_i \cdot s_j}{H_s}\right)^2 \left\{1 + \frac{1}{\nu^2}\left(1 - \sqrt{\frac{gT_{01}^2}{2\pi r_i L}}\right)^2\right\}\right]$$
$$(2.32)$$

where: $\nu = 0.425$ and $T_{01} = 1.086 T_Z$.

The values of n_{cr}, u_{cr}, $C2_{ij}$ and W_{ij} have to be determined for each case of wave steepness and wavelength to ship length ratio, which define a corresponding values of wave celerity. The sum of the products of $C2_{ij} \cdot W_{ij}$, for each combination of s_j and r_i,

for a specific significant wave height, H_s, and the zero-crossing wave period, T_z, defines a value of $C2$ which represents the Short Term Prediction:

$$C2(H_s, T_z) = \sum_{i=1}^{N_\lambda} \sum_{j=1}^{N_a} W_{ij} C2_{ij} \tag{2.33}$$

The fourth part gives a value of the probability Index C of Long Term Prediction formulated by averaging the Short Term Prediction by means of the weighting factor, $W2$, of short-term sea state, which is function of the significant wave height, H_s, and of the zero-crossing wave period, T_z. A ship is then considered not to be vulnerable to surf-riding/broaching failure mode if the value of Index C is less than a threshold equal to $R_{SR} = 0.005$.

$$C = \sum_{H_s} \sum_{T_z} (W2(H_s, T_z) \cdot C2(H_s, T_z)) \leq R_{SR} \tag{2.34}$$

The value of $W2(H_s, T_z)$ is the probability of wave occurrence of each sea state and is obtained by dividing number of occurrence of in each sea state condition by the total number of observations equal to 100000, reported in the North Atlantic scatter diagram in Table 2.1.

This mathematical procedure has been implemented into a numerical code created in Matlab® software, as illustrated in flowchart in Figure 2.2.

Table 2.1: Wave case occurrences, after IMO SDC2/WP4 (2015), Annex 3.

Wave case occurrences																	
Number of occurrences: 100 000 / Tz (s) = average zero up-crossing wave period																	
Hs (m)	3.5	4.5	5.5	6.5	7.5	8.5	9.5	10.5	11.5	12.5	13.5	14.5	15.5	16.5	17.5	18.5	**SUM**
0.5	1.3	134	865.6	1186	634.2	186.3	36.9	5.6	0.7	0.1	0	0	0	0	0	0	**3050**
1.5	0	29.3	986	4976	7738	5569.7	2375.7	703.5	160.7	30.5	5.1	0.8	0.1	0	0	0	**22575**
2.5	0	2.2	197.5	2158.8	6230	7449.5	4860.4	2066	644.5	160.2	33.7	6.3	1.1	0.2	0	0	**23810**
3.5	0	0.2	34.9	695.5	3226.5	4675	5099.1	2838	1114.1	337.7	84.3	18.2	3.5	0.6	0.1	0	**19128**
4.5	0	0	6	196.1	1354.3	3288.5	3857.5	2685.5	1275.2	455.1	130.9	31.9	6.9	1.3	0.2	0	**13269**
5.5	0	0	1	51	498.4	1602.9	2372.7	2008.3	1126	463.6	150.9	41	9.7	2.1	0.4	0.1	**8328**
6.5	0	0	0.2	12.6	167	690.3	1257.9	1268.6	825.9	386.8	140.8	42.2	10.9	2.5	0.5	0.1	**4806**
7.5	0	0	0	3	52.1	270.1	594.4	703.2	524.9	276.7	111.7	36.7	10.2	2.5	0.6	0.1	**2586**
8.5	0	0	0	0.7	15.4	97.9	255.9	350.6	296.9	174.6	77.6	27.7	8.4	2.2	0.5	0.1	**1309**
9.5	0	0	0	0.2	4.3	33.2	101.9	159.9	152.2	99.2	48.3	18.7	6.1	1.7	0.4	0.1	**626**
10.5	0	0	0	0	1.2	10.7	37.9	67.5	71.7	51.5	27.3	11.4	4	1.2	0.3	0	**285**
11.5	0	0	0	0	0.3	3.3	13.3	26.6	31.4	24.7	14.2	6.4	2.4	0.7	0.2	0	**124**
12.5	0	0	0	0	0.1	1	4.4	9.9	12.8	11	6.8	3.3	1.3	0.4	0.1	0	**51**
13.5	0	0	0	0	0	0.3	1.4	3.5	5	4.6	3.1	1.6	0.7	0.2	0.1	0	**21**
14.5	0	0	0	0	0	0.1	0.4	1.2	1.8	1.8	1.3	0.7	0.3	0.1	0	0	**8**
15.5	0	0	0	0	0	0	0.1	0.4	0.6	0.7	0.5	0.3	0.1	0.1	0	0	**3**
16.5	0	0	0	0	0	0	0	0.1	0.2	0.2	0.2	0.1	0.1	0	0	0	**1**
SUM	**1**	**165**	**2091**	**9280**	**19922**	**24879**	**20870**	**12898**	**6245**	**2479**	**837**	**247**	**66**	**16**	**3**	**1**	**100000**

Start

ship data file

Resistance & thrust file

Calculation of resistance (r_1-r_5) and thrust coefficients (k_1-k_2)

for r_i=1:0.025:3
for s_j=0.03:0.0012:0.15
calculate: λ_i, H_{ij}, c_i

sections data file

W2, T$_z$, H$_s$ file

1st Part

3rd Part

for i=1:length r_i
for j=1:length s_j
calculate:
- H_{ij}, k_i, c_i (wave parameters)
- t_p (thrust deduction)
- w_p (wake fraction)
- f_{ij} (surging force)
- t_i (thrust approx. coefficients t_1-t_2)
- a_i (coefficients a_0-a_5)
solve equation (Eq. 2.6):
$T(c_i, n_{cr}) - R(c_i) + coeff=0$

for h=1:length H$_s$
for t=1:length T$_z$
for i=1:length r_i
for j=1:length s_j
calculate W_{ij}

$n_{cr,ij}$

2nd Part

for i=1:length r_i
for j=1:length s_j
for v=1:length Fn
solve equation (Eq. 2.28):
$T_e(u_{cr}, n_{cr})-R(u_{cr})=0$

$u_{cr,ij}$ -> Fn$_{cr,ij}$

Fn$_{cr,ij}$ < Fn

Yes   No

C2$_{ij}$=1   C2$_{ij}$=0

4th Part

for h=1:length H$_s$
for t=1:length T$_z$
for i=1:length r_i
for j=1:length s_j
calculate:
$C= \Sigma\Sigma W2 \ x \ (\Sigma\Sigma W_{ij}*C_{ij})$

C

C < 0.005

Yes   NOT Vulnerable

No   Vulnerable

Figure 2.2: Flow chart of Matlab code for the 2nd level vulnerability check for Surf-riding criterion.

2.2 Matlab Code Validation According to IMO Benchmark Fishing Vessel

The Matlab code developed for surf-riding Level 2 assessment has been validated on the IMO benchmark fishing vessel ITTC A2 reported in SDC3/INF10 (2015). With the hull data available, mainly ship dimensions, resistance and propulsion coefficients, two types of checks have been made: on the critical Froude number for 5 different combinations of wave steepness, H_{ij}/λ_i, and wavelength to ship length ratio, λ_i/L, and on the final value of probability Index C for the considered 5 Froude number cases. The results obtained by the Matlab code differ about 3% for the critical Froude number and about 0-10% for the Index C values from the values reported in IMO documents, as shown in Figure 2.3. In the figure, the Index C has been calculated in two cases: using linear wave celerity (Linear c) and non linear wave celerity (Nonlinear c) formulations.

These differences are justified by numerical accuracy coming from the number of decimal places used for polynomials coefficients and are in line with the findings of Feng et al. (2015) as order of magnitude.
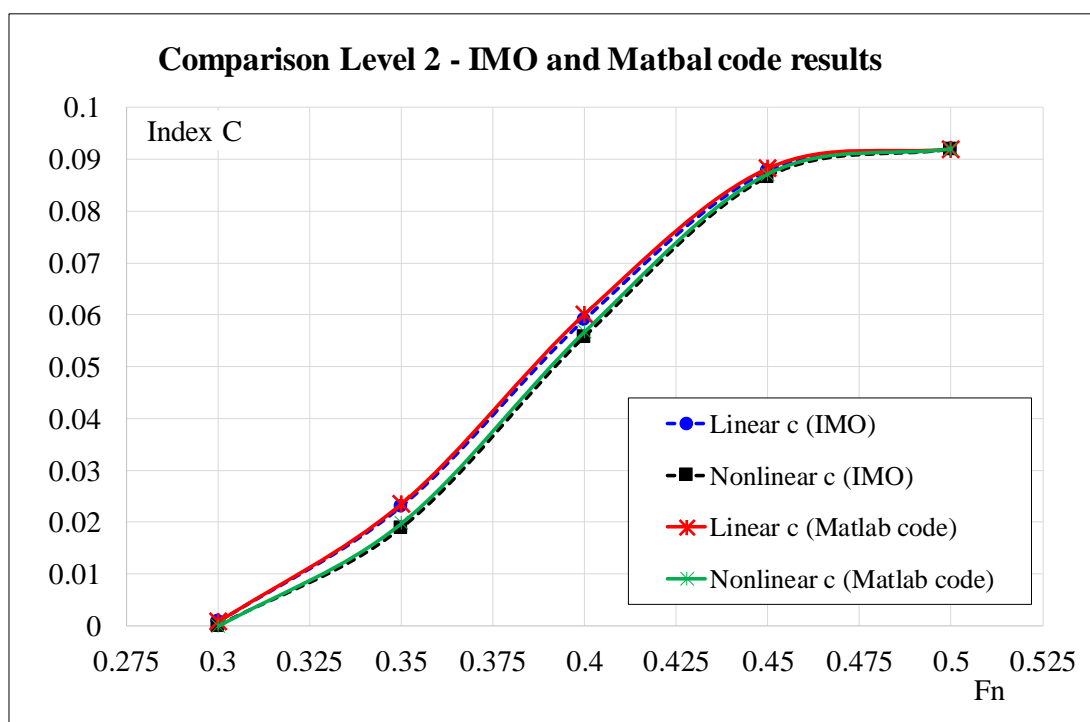
Figure 2.3: Level 2 Comparison between the Index C values obtained by the Matlab code and the ones reported in IMO SDC3/INF10 (2015).

Chapter 3

Surf-riding 1-DOF Model: Bifurcation Analysis

3.1 Mathematical Model

A first step towards a direct approach of surf-riding occurrence has been done by studying a 1-DOF mathematical model of the surge motion equation, that describes a ship sailing in following regular waves.

Two reference systems have been taken into consideration, as shown in Figure 3.1.

- the $(O;X, Y, Z)$ reference frame fixed to Earth, where the X-Y plane coincides with the still water level, Z coordinate points upwards and at time zero the origin O is located at the aft perpendicular of the ship;

- the $(G;x, y, z)$ reference frame fixed to the ship, where the x-y plane is parallel to the still water level, the x coordinate points to bow, the z coordinate point upwards and G is the ship's center of gravity. At zero time the wave trough is aligned with the ship center of gravity, G.

X represents the distance from the origin of the reference frame fixed to Earth to the wave trough;
X_G is the distance of the center of gravity from the origin of the reference frame fixed to Earth;
x is the distance between the ship center of gravity and the wave trough;
$\dot{x}$ is the surging velocity, i.e. relative velocity between ship speed, u, and wave celerity, c, and $\ddot{x}$ is the surging acceleration.

The formulas for the transformation of the coordinates and velocity from one system to the other are:

$$X = X_G + x = ut + x \tag{3.1}$$

$$\dot{x} = u - c \rightarrow \begin{cases} u = & \dot{x} + c \\ \dot{u} = & \ddot{x} \end{cases} \tag{3.2}$$
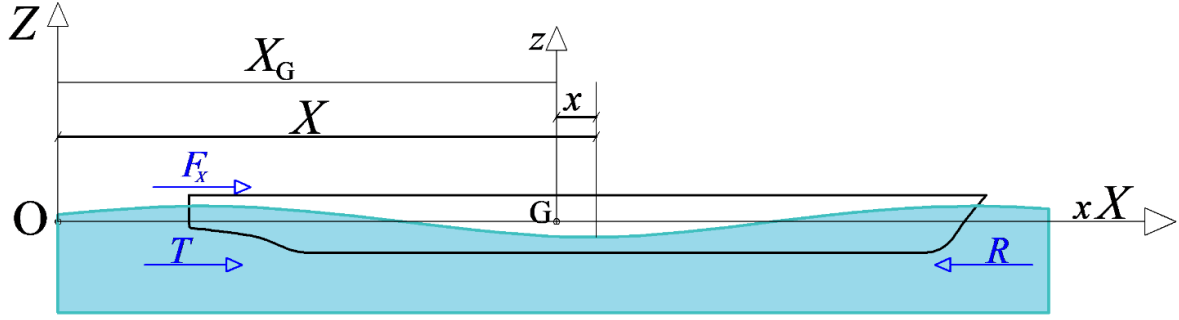
Figure 3.1: Reference systems for surge motion equation.

The surge motion equation derives from Newton's second law and represents the equilibrium of forces acting on the ship in the direction of forward speed, X. In the fixed to Earth reference system it is formulated as:

$$(M + M_X)\dot{u} + R(u) - T_e(u, n) = F_X(X) \tag{3.3}$$

where:
M is the ship displacement, $[kg]$;
M_X is the added mass of the ship for surge motion, $[kg]$, assumed equal to $0.1M$;
u is the ship speed, $[m/s]$, and $\dot{u}$ is the corresponding acceleration, $[m/s^2]$;
R is the calm water resistance, $[N]$;
T_e is the thrust delivered by the propeller in calm water condition, $[N]$;
F_X is the wave induced force, $[N]$.

The calm water resistance is normally achieved by EFD tests or CFD simulations. The resistance curve can be approximated with a 5th order polynomial function of ship speed, formulated as Equation (2.29).

The thrust delivered by the propeller in calm water condition can be expressed as:

$$T_e = N_P(\tau_0 n^2 + \tau_1 un + \tau_2 u^2) \tag{3.4}$$

where:
N_P is the number of propellers;
n is the propeller's number of revolutions, $[rps]$;
τ_0, τ_1, τ_2 are the thrust coefficients as expressed in Equations (2.21) - (2.23)

The wave excitation can be expressed in the reference frame fixed to Earth:

$$F_X = f_X \sin(\omega t - kX) \tag{3.5}$$

where:
f_X is the wave amplitude that can be expressed either:

- considering only the linear Froude-Krylov component calculated by Strip theory method, as in Equation (2.18) (SDC3/WP5, 2016);

- considering both Froude Krylov and diffraction components calculated by a 3-D panel method software.

$k = \frac{2\pi}{\lambda}$ is the wave number, $[rad/m]$;
ω is the wave frequency, $[rad/s]$;

In the fixed to ship reference system the wave force can be expressed as:

$$F_X = f_X \sin\left(\omega t - k(X_G + x)\right) = f_X \sin\left((\omega - ku)t - kx\right) = f_X \sin\left((\omega_e t - kx\right) \quad (3.6)$$

where:
$\omega_e = \omega - ku\cos\beta = \omega - ku$ is the wave encounter frequency for heading angle $\beta = 0$.

3.1.1   Non Linear Dynamics of Surge Motion Equation

Substituting the formulations for resistance, thrust and wave force in Equation (3.3) and expressing all forces as function of the surge variables, following Equations (3.2), the surge motion equation becomes:

$$
\begin{aligned}
(M + M_X)\ddot{x} + r_0 + r_1(\dot{x} + c) + r_2(\dot{x} + c)^2 + r_3(\dot{x} + c)^3 + r_4(\dot{x} + c)^4 + r_5(\dot{x} + c)^5 + \\
- N_P\left[\tau_0 n^2 + \tau_1(\dot{x} + c)n + \tau_2(\dot{x} + c)^2\right] = f_X\sin(\omega_e t - kx)
\end{aligned}
\quad (3.7)
$$

then solving the powers of the terms in brackets and ordering the surge variables the equation becomes:

$$
\begin{aligned}
(M + M_X)\ddot{x} + (r_0 + r_1 c + r_2 c^2 + r_3 c^3 + r_4 c^4 + r_5 c^5) - N_P(\tau_0 n^2 + \tau_1 cn + \tau_2 c^2) + \\
\dot{x}\left[r_1 + 2(r_2 - N_P\tau_2)c + 3r_3 c^2 + 4r_4 c^3 + 5r_5 c^4 - N_P\tau_1 n\right] + \dot{x}^2\left[r_2 + 3r_3 c + 6r_4 c^2 + 10r_5 c^3 - N_P\tau_2\right] + \\
\dot{x}^3\left[r_3 + 4r_4 c + 10r_5 c^2\right] + \dot{x}^4\left[r_4 + 5r_5 c\right] + \dot{x}^5 r_5 = f_X\sin(\omega_e t - kx)
\end{aligned}
$$

$$(3.8)$$

The terms in brackets are constant for a specific ship and wave case and represented by the following expressions:

$$R_c = r_0 + r_1 c + r_2 c^2 + r_3 c^3 + r_4 c^4 + r_5 c^5 \quad (3.9)$$

$$T_c = N_P(\tau_0 n^2 + \tau_1 cn + \tau_2 c^2) \quad (3.10)$$

$$A_1 = r_1 + 2(r_2 - N_P\tau_2)c + 3r_3 c^2 + 4r_4 c^3 + 5r_5 c^4 - N_P\tau_1 n \quad (3.11)$$

$$A_2 = r_2 + 3r_3 c + 6r_4 c^2 + 10r_5 c^3 - N_P\tau_2 \quad (3.12)$$

$$A_3 = r_3 + 4r_4 c + 10r_5 c^2 \quad (3.13)$$

$$A_4 = r_4 + 5r_5 c \quad (3.14)$$

$$A_5 = r_5 \quad (3.15)$$

These Equations are comparable to those used in IMO SDC3/WP5 (2016) for Melnikov's method to determine the critical number of revolutions. The only difference between the two formulations is found in the number of propellers, N_P, that is explicitly defined and included in the reported formulas.

The surge motion equation can be written as:

$$\ddot{x} = \frac{1}{M + M_X}\left[T_c - R_c - (A_1\dot{x} + A_2\dot{x}^2 + A_3\dot{x}^3 + A_4\dot{x}^4 + A_5\dot{x}^5) + f_X\sin(\omega_e t - kx)\right]$$

$$(3.16)$$

This equation is a non-linear second order differential equation and the exact solution cannot be found analytically, therefore the system's behaviour is studied following the procedures of non-linear dynamics, with a numerical approach. Numerical methods are intended to solve differential equations and systems of differential equations of the first order. At the same time, all motion equations have second order derivatives, so the first step is to transform the second order equation into a system of the first order equations.

This is done by introducing a new function:

$$\begin{cases} y_1 = x \\ y_2 = \dot{x} \end{cases} \Rightarrow \begin{cases} \dot{y}_1 = \dot{x} = y_2 \\ \dot{y}_2 = \ddot{x} \end{cases} \tag{3.17}$$

and, applying the variable transformation to Equation (3.17), Equation (3.16) is transformed into a system of first order differential equations:

$$\overrightarrow{F}(\overrightarrow{y}) = \begin{cases} \dot{y}_1 = y_2 \\ \dot{y}_2 = \frac{1}{(M+M_X)} \left[T_C - R_C - \left(A_1 y_2 + A_2 y_2^2 + A_3 y_2^4 + A_4 y_2^4 + A_5 y_2^5 \right) + f_X \sin(-ky_1) \right] \end{cases} \tag{3.18}$$

In following sea and around surf-riding conditions the value of the encounter frequency is close to zero, therefore from now on the dependence on time may be ignored.

The second step is to study the system looking for the equilibrium positions (or fixed points) and analysing their stability.

Given a generic non linear system of differential equations:

$$\begin{cases} \dot{y}_1 = f(y_1, y_2) \\ \dot{y}_2 = f(y_1, y_2) \end{cases} \tag{3.19}$$

the fixed points, y_1^* and y_2^*, are found by imposing the system of equations equal to zero. The type of stability of the fixed points is studied throughout the analysis of the Jacobian matrix calculated in the fixed points:

$$J^* = \begin{vmatrix} J_{11} & J_{12} \\ J_{21} & J_{22} \end{vmatrix} = \begin{vmatrix} \frac{\partial \dot{y}_1}{\partial y_1} & \frac{\partial \dot{y}_1}{\partial y_1} \\ \frac{\partial \dot{y}_2}{\partial y_2} & \frac{\partial \dot{y}_2}{\partial y_2} \end{vmatrix} y_1 = y_1^*, \ y_2 = y_2^* \tag{3.20}$$

From the determination of the trace, τ, and the determinant, Δ:

$$\tau = J_{11} + J_{22} \tag{3.21}$$
$$\Delta = J_{11} J_{22} - J_{21} J_{12} \tag{3.22}$$

the characteristic equation of the system is given by:

$$\lambda^2 - \tau\lambda + \Delta = 0 \tag{3.23}$$

and the eigenvalues are evaluated as:

$$\lambda_{1,2} = \frac{\tau \pm \sqrt{\tau^2 - 4\Delta}}{2} \tag{3.24}$$

The value of the discriminant, δ, of the characteristic equation is given by:

$$\delta = \tau^2 - 4\Delta \tag{3.25}$$

If fixed points exist, the type of stability or instability is determined according to the values of eigenvalues, trace, determinant and delta, as shown in Figure (3.2).
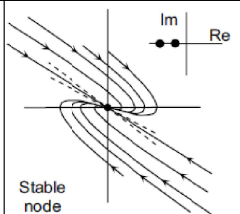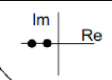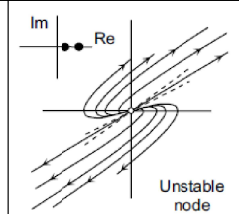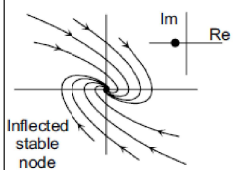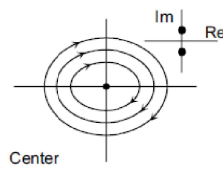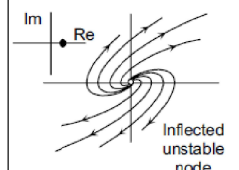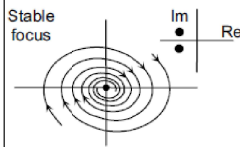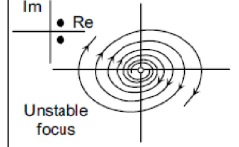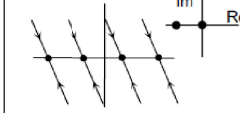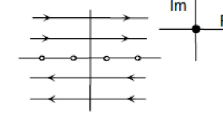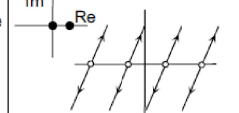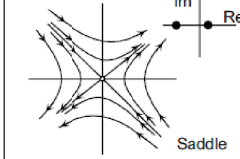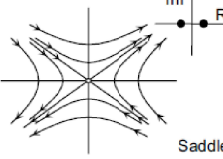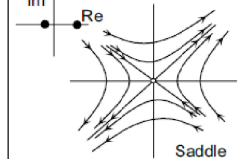

Figure 3.2: Types of stability of fixed points, after Belenky and Sevastianov (2007).

For the surge motion equation the fixed points are found setting Equation (3.18) to zero:

$$\overrightarrow{F}(\overrightarrow{y}) = 0 \Rightarrow \overrightarrow{F}(\overrightarrow{y}^*) = \begin{cases} y_2^* = 0 \\ \frac{1}{(M+M_X)}[T_C - R_C + f_X \sin(-ky_1^*)] = 0 \end{cases} \tag{3.26}$$

This brings to 2 results:

- the surge velocity equals to zero $\rightarrow y_2^* = \dot{x} = 0$;

- the system of differential equations becomes a non-linear algebraic equation that has a solution only if the sum of resistance and thrust, determined according to the wave celerity, are in equilibrium with the wave force.

$$T_C(c, n) - R_C(c) = -f_X \sin(-ky_1^*) \tag{3.27}$$

The fixed points can be determined from equation (3.27), and since the wave force depends on the sine function, which is an odd function, there will be two equilibrium

positions following the sine property $\sin(x) = \sin(\pi - x)$. Since $k = 2\pi/\lambda$, the fixed points are equal to:

$$y1^* = \begin{cases} y_2^* = 0 \\ y_{11}^* = \frac{1}{k}\left[-\sin^{-1}\left(\frac{R_C - T_C}{f_X}\right)\right] \end{cases} \tag{3.28}$$

$$y2^* = \begin{cases} y_2^* = 0 \\ y_{12}^* = \frac{1}{k}\left[\sin^{-1}\left(\frac{R_C - T_C}{f_X}\right)\right] - \frac{\lambda}{2} \end{cases} \tag{3.29}$$

For a chosen speed and wave condition, if no equilibrium points exist the only possible ship motion will be surging and no surf-riding phenomenon will occur. If equilibrium points exist the next step is to study their stability, analysing the Jacobian matrix calculated in the fixed point. The Jacobian matrix for the system (3.18) is:

$$J = \begin{vmatrix} 0 & 1 \\ \frac{-kf_X\cos(-ky_1)}{M+M_X} & \frac{-(A_1 + 2A_2y_2 + 3A_3y_2^2 + A_4y_2^3 + 5A_5y_2^4)}{M+M_X} \end{vmatrix} \tag{3.30}$$

and the Jacobian calculated in the fixed points are:

$$J_1^*(y1^*) = \begin{vmatrix} 0 & 1 \\ \frac{-kf_X\cos\left[\sin^{-1}\left(\frac{R_C - T_C}{f_X}\right)\right]}{M+M_X} & \frac{-(A_1)}{M+M_X} \end{vmatrix} \tag{3.31}$$

$$J_2^*(y2^*) = \begin{vmatrix} 0 & 1 \\ \frac{-kf_X\cos\left\{-k\left[\frac{1}{k}\sin^{-1}\left(\frac{R_C - T_C}{f_X}\right) - \frac{\lambda}{2}\right]\right\}}{M+M_X} & \frac{-(A_1)}{M+M_X} \end{vmatrix} \tag{3.32}$$

The trace and the determinant of the two Jacobian are:

$$\tau = \frac{-A_1}{M + M_X} \tag{3.33}$$

$$\Delta_1(y1^*) = \frac{kf_X\cos\left[\sin^{-1}\left(\frac{R_C - T_C}{f_X}\right)\right]}{M + M_X} \tag{3.34}$$

$$\Delta(y2^*) = \frac{kf_X\cos\left\{-k\left[\frac{1}{k}\sin^{-1}\left(\frac{R_C - T_C}{f_X}\right) - \frac{\lambda}{2}\right]\right\}}{M + M_X} \tag{3.35}$$

and the two couples of eigenvalues are:

$$\lambda_{11} = \frac{1}{2}\left[\frac{-A_1}{M+M_X} + \sqrt{\left(\frac{-A_1}{M+M_X}\right)^2 - 4\left\{\frac{1}{M+M_X}kf_X\cos\left[\sin^{-1}\left(\frac{R_C - T_C}{f_X}\right)\right]\right\}}\right] \tag{3.36}$$

$$\lambda_{12} = \frac{1}{2}\left[\frac{-A_1}{M+M_X} - \sqrt{\left(\frac{-A_1}{M+M_X}\right)^2 - 4\left\{\frac{1}{M+M_X}kf_X\cos\left[\sin^{-1}\left(\frac{R_C - T_C}{f_X}\right)\right]\right\}}\right] \tag{3.37}$$

$$\lambda_{21} = \frac{1}{2} \left[\frac{-A_1}{M + M_X} + \sqrt{\left(\frac{-A_1}{M + M_X} \right)^2 - 4 \left\{ \frac{1}{M + M_X} k f_X \cos \left(-k \left[\frac{1}{k} \sin^{-1} \left(\frac{R_C - T_C}{f_X} \right) - \frac{\lambda}{2} \right] \right) \right\}} \right] \qquad (3.38)$$

$$\lambda_{22} = \frac{1}{2} \left[\frac{-A_1}{M + M_X} - \sqrt{\left(\frac{-A_1}{M + M_X} \right)^2 - 4 \left\{ \frac{1}{M + M_X} k f_X \cos \left(-k \left[\frac{1}{k} \sin^{-1} \left(\frac{R_C - T_C}{f_X} \right) - \frac{\lambda}{2} \right] \right) \right\}} \right] \qquad (3.39)$$

When the combination of ship speed and wave characteristics bring to the equilibrium of resistance, thrust and wave forces and to the existence of fixed points, surf-riding 1st threshold is reached. According to the values of trace, determinant and discriminant of the Jacobian Matrix two possible types of equilibrium are identified from Figure 3.2: stable focus, corresponding to the stable fixed point, and saddle, corresponding to the unstable fixed point.

3.1.2   Phase Plane and Bifurcation Analysis

Once determined which fixed point is stable and which is unstable, a phase plane analysis is conducted to evaluate if surf-riding is occurring between the 1st and the 2nd thresholds or over the 2nd threshold.

To evaluate surge displacement and velocity solutions in time, for the representation of the phase planes, Equation (3.16) has been solved using ODE 45, a Matlab routine which implements a Runge-Kutta method. Four points closed to the unstable fixed points (saddle) and laying on the corresponding separatrices are chosen as initial condition to determine the positive and negative unstable manifolds by integrating forward in time and to determine the positive and negative stable manifolds by integrating backwards in time.

The phase plane is obtained by plotting the surge velocity, dimensionless by celerity, x'/c, as function of surge displacement, dimensionless by wave length, x/λ, and can be of two types:

- Surf-riding occurrence between the 1st and the 2nd thresholds, as in Figure 3.3, where the stable manifolds (blue lines) define the only surf-riding domain, while the rest of the plane defines surge motion. The unstable manifolds (red lines) define the ship's convergence in time to the stable equilibrium point or to surging dynamic equilibrium.

- Surf-riding occurrence over the 2nd threshold, as in Figure 3.4, where only surf-riding phenomenon is possible and the stable manifolds divide the different domains of attractions (fixed points). The unstable manifolds (red lines) define the ship's convergence in time to the stable equilibrium points, on a successive or preceding wave.
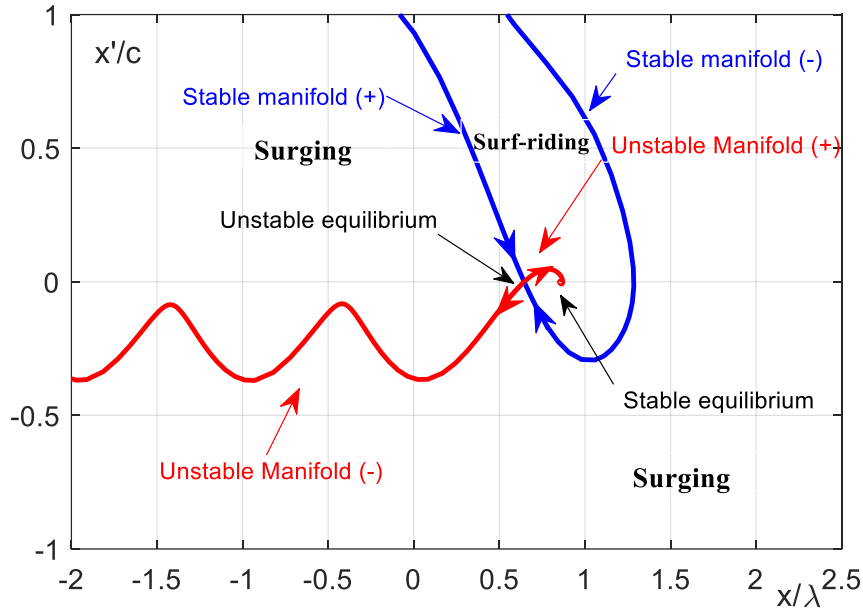
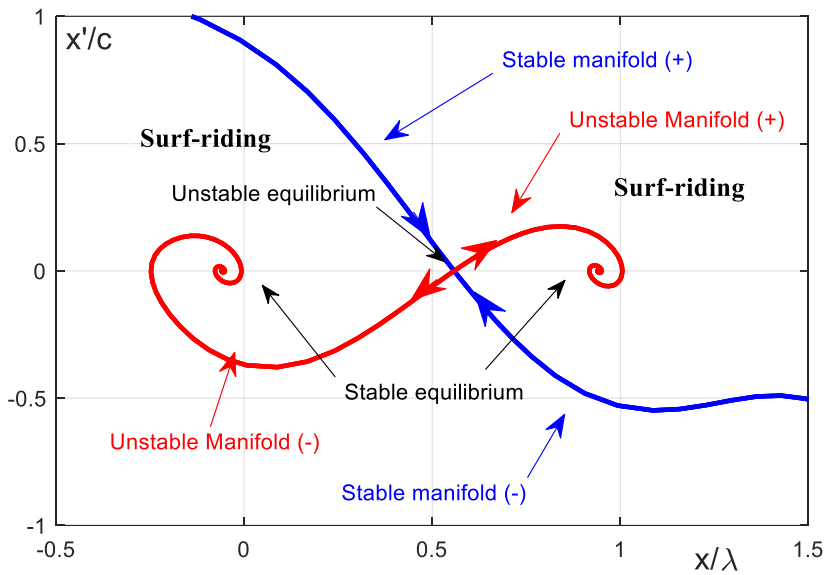Figure 3.3: Phase Plane for surging and surf-riding motions: between 1st and 2nd thresholds.

Figure 3.4: Phase Plane for the only surf-riding motion: over 2nd threshold.

The determination of the occurrence of surf-riding phenomenon and possible bifurcations is performed by choosing a control parameter and changing it to observe the behaviour of the system.

In the surge equation the possible control parameters are:

- the number of revolutions, n, corresponding to the nominal Froude number, therefore advancing speed, that would be achieved, if such a number of revolutions would be set in calm water;

- the wave length or ratio of wave to ship length, λ/L;

- the wave height or steepness, H/λ;

The change of the phase planes from the condition between the 1st and the 2nd thresholds, to the one over the 2nd threshold, shown in Figures 3.3 and 3.4, has been obtained for the same ship for fixed speed and wave length and increasing wave height. It can be noted that for a fixed wave height and length the same transition can be obtained by increasing the ship speed.

Using the phase plane analysis the heteroclinic connections of an invariant manifold to a saddle can be observed. This heteroclinic bifurcation occurs when the negative stable manifold, blue(-) curve, corresponding to one wave intersects the negative unstable manifold, red(-) curve, of the successive wave, as shown in Figure 3.5, where the phase plane changes have been obtained for fixed ship speed and wavelength and increasing wave heights. The heteroclinic bifurcation found for the surge motion equation corresponds to the 2nd threshold of surf-riding.
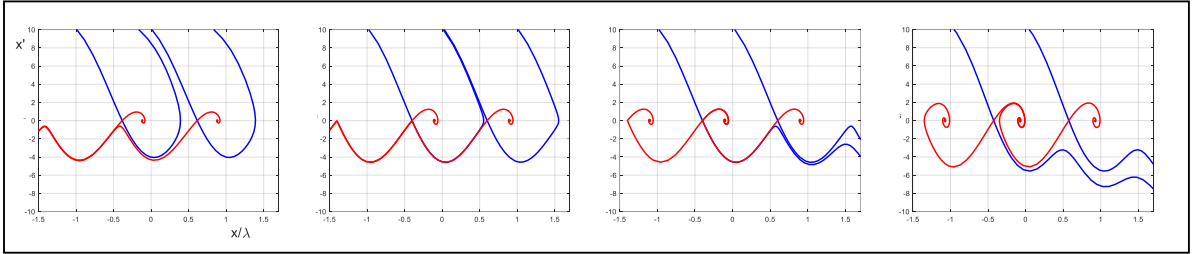

Figure 3.5: Heteroclinic bifurcation shown in a phase plane evolution for a fixed ship speed and wavelength and increasing wave heights

3.1.3 Separatrix Determination

A separatrix is a trajectory which approaches or leaves a fixed point tangent to a fixed radial direction. The directions of the separatrices of the unstable fixed point are needed to define the initial condition for the integration of the surge motion equation to define the stable and unstable manifolds. These directions, entering and leaving the saddle point are obtained by linearising the motion equation near the unstable equilibrium. The linearisation is done by introducing a disturbance, ε, to the dynamic equation governing the motion that becomes:

$$(M + M_X)\ddot{\varepsilon} + R(c + \dot{\varepsilon}) - T(c + \dot{\epsilon}, n) - F_X(\varepsilon) = 0 \qquad (3.40)$$

In the hypothesis of infinitesimal disturbance, resistance, thrust and wave force are linearised near the unstable equilibrium, that is $\dot{x} = 0$ and $x = x^* = y_{12}^*$:

$$R(c + \dot{\varepsilon}) \sim R(c) + \left.\frac{dR(\dot{x} + c)}{d\dot{x}}\right|_{\dot{x}=0} \dot{\varepsilon} = R(c) + [r_1 + 2r_2c + 3r_3c^4 + 4r_4c^3 + 5r_5c^4]\dot{\varepsilon} \quad (3.41)$$

$$T(c + \dot{\varepsilon}, n) \sim T(c) + \left.\frac{dT(\dot{x} + c, n)}{d\dot{x}}\right|_{\dot{x}=0} \dot{\varepsilon} = T(c) + N_P \left[\tau_1 n + 2\tau_2 c\right] \dot{\varepsilon} \qquad (3.42)$$

$$F_X(\varepsilon) \sim F(x) + \left.\frac{dF(x)}{dx}\right|_{x=x^*} \varepsilon = F(x) + k f_X \cos(-kx^*) \qquad (3.43)$$

Knowing that in surf-riding equilibrium $R(c) - T(c) - F(x) = 0$, and defining a damping and restoring term coefficient as:

$$B' = \frac{1}{M + M_X} \left[r_1 + 2r_2 c + 3r_3 c^4 + 4r_4 c^3 + 5r_5 c^4 - N_P \left(\tau_1 n + 2\tau_2 c \right) \right] \qquad (3.44)$$

$$C' = -\frac{1}{M + M_X} \left[k f_X \cos(-k x^*) \right] \qquad (3.45)$$

Equation (3.41) becomes:

$$(M + M_X)\ddot{\varepsilon} + B'\dot{\varepsilon} + C'\varepsilon = 0 \qquad (3.46)$$

To solve the problem the second order equation is transformed into a system of first order:

$$\overrightarrow{y} = \begin{pmatrix} \dot{y}_1 \\ \dot{y}_2 \end{pmatrix} = \begin{pmatrix} \dot{\varepsilon} \\ \ddot{\varepsilon} \end{pmatrix} = \begin{pmatrix} y_2 \\ -B'y_2 - C'y_1 \end{pmatrix} \qquad (3.47)$$

$$\overrightarrow{y} = \begin{bmatrix} \dot{y}_1 \\ \dot{y}_2 \end{bmatrix} \quad \begin{bmatrix} 0 & 1 \\ -C' & -B' \end{bmatrix} = \overrightarrow{y} \underline{\underline{\Phi}} \qquad (3.48)$$

If the solution is of the kind: $\overrightarrow{y} = \overrightarrow{v} e^{\lambda t}$ the system is equal to: $\overrightarrow{y} = \lambda \overrightarrow{y}$, therefore the problem reduces to the solution of the vector $\overrightarrow{v}$:

$$\underline{\underline{\Phi}}\overrightarrow{v} = \lambda \overrightarrow{v} \Rightarrow \left(\underline{\underline{\Phi}} - \underline{\underline{I}}\lambda \right) \overrightarrow{v} = 0 \qquad (3.49)$$

where λ and $\overrightarrow{v}$ are the eigenvalue and eigenvector of the matrix $\underline{\underline{\Phi}}$.

Equation (3.49) has solutions different from zero if the determinant satisfies the following:

$$\det|\underline{\underline{\Phi}} - \underline{\underline{I}}\lambda| = \det \begin{vmatrix} -\lambda & 1 \\ -C' & -B' - \lambda \end{vmatrix} = 0 \Rightarrow \lambda^2 + B'\lambda + C' = 0 \qquad (3.50)$$

Solving the characteristic equation, the eigenvalues are found to be equal to:

$$\lambda_{1,2} = \frac{-B' \pm \sqrt{B'^2 - 4C'}}{2} \qquad (3.51)$$

From Equation (3.49), written in matrix form, the eigenvectors can be determined as:

$$\begin{bmatrix} -\lambda & 1 \\ -C' & -B' - \lambda \end{bmatrix} \begin{bmatrix} v_x \\ v_y \end{bmatrix} = 0 \Rightarrow \begin{array}{c} -\lambda v_x + v_y = 0 \\ -C'v_x + (-B' - \lambda)v_y = 0 \end{array} \qquad (3.52)$$

Therefore the relation between the two eigenvectors corresponding to the two eigenvalues is:

$$v_{x1} = \lambda_1 v_{y1}$$
$$v_{x2} = \lambda_2 v_{y2}$$

The eigenvectors define the directions of the separatrices, therefore these two equations represent the straight line trajectories of the saddle point.

The eigenvectors relative to the negative eigenvalue $\lambda < 0$ correspond to the stable manifold because the solution $\overrightarrow{y}$ goes to zero with integration forward in time, for $t \to +\infty$. The eigenvectors relative to the positive eigenvalue $\lambda > 0$ correspond to the unstable manifold because the solution $\overrightarrow{y}$ goes to zero with integration backwards in time, for $t \to -\infty$.

Figure 3.6 represents the phase plane in surf-riding equilibrium over the 2nd threshold, where the green line represents the separatrix corresponding to the unstable manifold (red curve) and the cyan line represents the one corresponding to the stable manifold (blue curve).
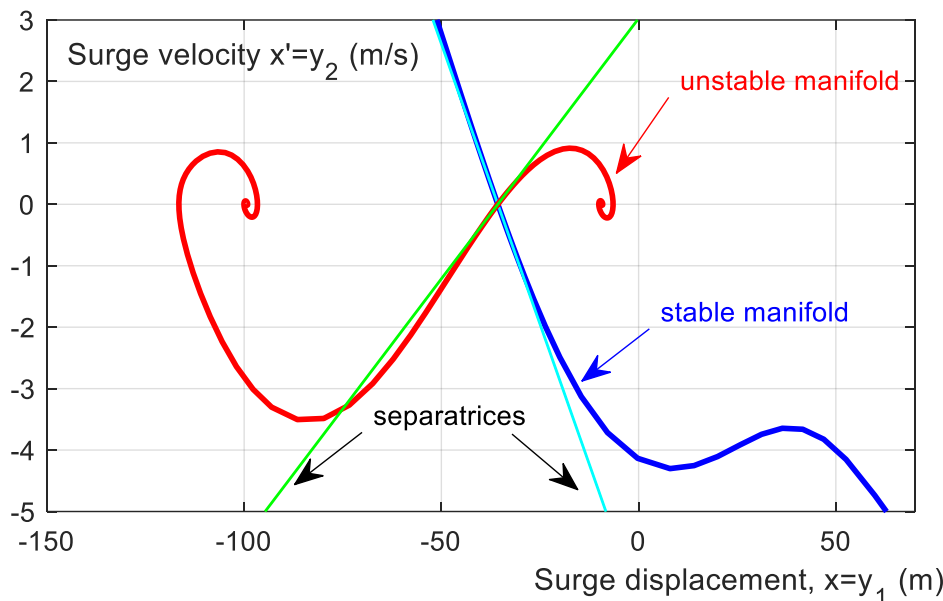

Figure 3.6: Phase plane with separtrices for surf-riding equilibrium over the 2nd threshold.

3.2 Matlab Code Validation According to ONRT Benchmark Vessel

The 1-DOF mathematical model has been implemented in a Matlab® software code and has been validated on the benchmark ship ONRT (The US Office of Naval Research Tumblehome vessel) in model scale. The hull geometry, resistance and thrust data have been obtained from Sadat-Hosseini et al. (2011) and Salmaso (2018) and is reported in Table 3.1. Surf-riding limits for the 2nd threshold evaluated by the present 1-DOF approach, considering only Froude Krylov component in the wave surge force, are compared with the once performed by the 1-DOF model of Salmaso (2018) in Figure 3.7 for different number of revolutions, different wave to ship lengths and for fixed wave steepness equal to 1/20. In the figure the surge and surf-riding motion observed by EFD tests reported in Maki et al. (2010) are represented together with the surf-riding thresholds.

Table 3.1: ONRT Hull Full Scale Main particulars.

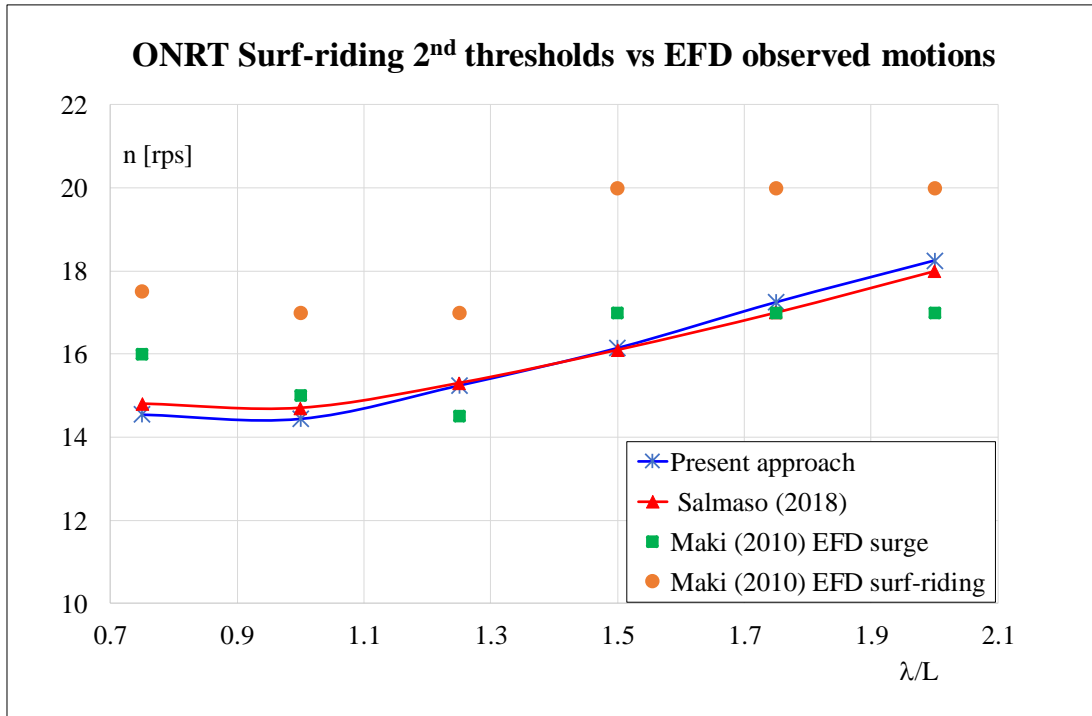| ONRT Main particulars		Ship	Model	
Length between perpendiculars	$\mathbf{L_{PP}}$	154	3.147	m
Draft	$\mathbf{T}$	5.494	0.1123	m
Breadth	$\mathbf{B}$	18.79	0.384	m
Block coefficient	$\mathbf{C_B}$	0.535	0.535	
Displacement	$\mathbf{M}$	8618000	73.2	kg
Added mass	$\mathbf{M_X}$	129270	1.098	kg

Figure 3.7: Surf-riding limits compared for present 1-DOF approach (blue line) and Salmaso (2018) (red line) and motion observed by Maki et al. (2010) (orange points for EFD surf-riding and blue points for EFD surge).

It can be observed that surf-riding threshold curves of the two numerical approaches, blue for the present model and red for Salmaso (2018), predict lower limits compared to the experimental motions reported in Maki et al. (2010).

The differences between the two numerical approaches, Salmaso and the present approach, may be due to the different methods of evaluating resistance and thrust values and to the approximation in reading the values reported in Salmaso (2018). Moreover, the conservatism of the numerical approaches related to the EFD results may be due to the overestimated wave induced force calculated only considering the Froude Krylov approximation without the diffraction corrections.

Chapter 4

6-DOF Potential Flow Theory Approach

4.1 Mathematical Model

A 6-DOF Potential Flow Theory (PT) mathematical model has been adopted to evaluate motions and forces variations for a ship sailing in following waves to predict environmental and loading conditions that lead to surge or surf-riding occurrence.

The potential flow numerical model, is based on the mathematical model, described in Matusiak (2013), that analyses the ship behaviour in waves. It combines seakeeping and manoeuvring motions and the ship is considered a intact rigid body. The model has been developed by the University of Aalto and initially implemented in a Fortran code, the LaiDyn software, (Acanfora and Matusiak, 2016), and validated in Shigunov et al. (2018). The model has then been implemented in a Matlab/Simulink ® code validated in Acanfora et al. (2019).

The equations of motions, presented in Matusiak (2013), are solved in time domain and simulation results provide ship motions in waves.

The main coordinate systems used to describe ship motion are presented in Figure 4.1, i.e the inertial system fixed to Earth, with the X-Y plane coincident with the still water level, and the body-fixed reference frame having its origin at ship center of gravity.
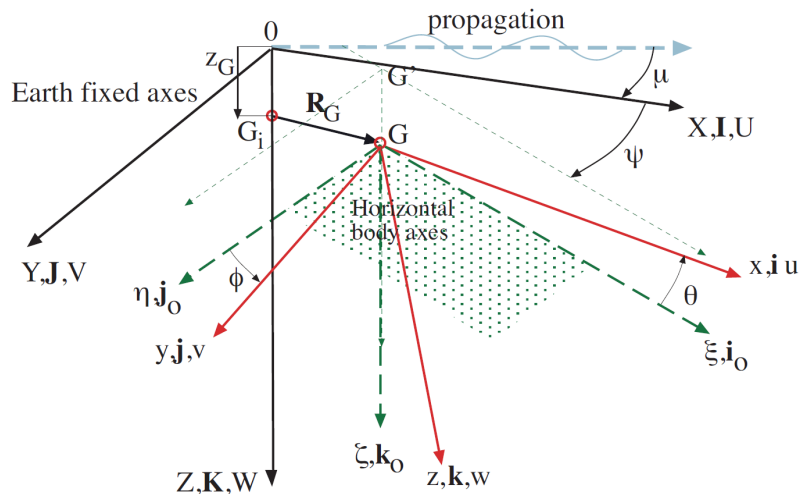

Figure 4.1: Co-ordinate systems used in ship dynamics (Matusiak, 2013).

41

The hull surface is discretized by means of triangular panels. For each panel, the surface S and the components of the normal vector at the control point (nx, ny, nz) are known. In Equation (4.1) the wave elevation is calculated in the control points of the hull surface X_c and Y_c (referring to the center of each panel), given in the Earth fixed co-ordinate system by means of a transformation matrix. The coordinates X_c and Y_c take into account the ship's position in waves.

$$\zeta(t) = A \cos\left[k\left(X_c \cos\mu - Y_c \sin\mu\right) - \omega t\right] \tag{4.1}$$

where: ω represents the wave frequency since the longitudinal coordinate X_c depends on the ship forward speed, u, and the angle, μ is the wave heading.

The non-linear 6-DOF equations of motions are represented by Equations (4.2). The numerical model can be defined as hybrid or blended, i.e. non-linearities are accounted for restoring and Froude-Krylov actions, while radiation and diffraction actions are obtained by linear strip-theory potential method (Matusiak, 2013).

$$\begin{cases} (m + a_{11})\dot{u} + m(qw - rv) + a_{15}\dot{q} = -mg\sin\theta + X_{wave} + X_{man} - b_{15}q + X_{prop} + X_{resistance} \\ (m + a_{22})\dot{v} + m(ru - pw) + a_{24}\dot{p} + a_{26}\dot{r} = mg\cos\theta\sin\phi + Y_{wave} + Y_{man} - b_{22}v - b_{24}p \\ (m + a_{33})\dot{w} + m(pv - qu) + a_{35}\dot{q} = mg\cos\theta\cos phi + Z_{wave} - b_{33}w - b_{35}q \\ (I_x + a_{44})\dot{p} + (I_z - I_y)qr + a_{42}\dot{v} + a_{46}\dot{r} = K_{wave} + K_{man} - b_{44}p - b_{42}v - b_{46}r \\ (I_y + a_{55})\dot{q} + (I_x - I_z)rp + a_{15}\dot{u} + a_{53}\dot{w} = M_{wave} - B_{55}q - b_{53}w - b_{51}u \\ (I_z + a_{66})\dot{r} + (I_y - I_x)pq + a_{62}\dot{v} + a_{64}\dot{p} = N_{wave} + N_{man} - b_{66}r - b_{64}p \end{cases} \tag{4.2}$$

The terms u, v, w represent the components of the velocity U of the ship's centre of gravity according to the inertial system expressed in the body-fixed system.

The angular velocity, $\mathbf{\Omega}$, of the ship in the body fixed co-ordinate system is expressed as:

$$\mathbf{\Omega} = \mathbf{pi} + \mathbf{qj} + \mathbf{rk} \tag{4.3}$$

where p, q and r are respectively x-, y- and z-directional components of the angular velocity.

The m and I_i terms define the mass and the mass moment of inertia of the body, respectively. The terms a_{ij} and b_{ij} are respectively the added mass and damping coefficients at the encounter wave frequency. The terms with the subscript "*wave*" include Froude-Krylov, diffraction and restoring forces and moments, while the terms with the subscript "*man*" refer to the manoeuvring forces and moments represented by hull forces related to yaw and sway velocities. The terms X_{prop} and $X_{resistance}$ model the ship propeller actions and hull resistance, respectively, at a given speed.

4.1.1 Forces Definition

The inertia, Froude-Krylov and restoring forces and moments are evaluated accounting for all the pertinent non-linearities. The pressure profile is assumed by applying the so-called "stretched distribution" above the waterline: $p = \rho g \left[\zeta e^{-k(Z_c + \zeta)} + Z_c\right]$
where ζ is the wave profile, k is the wave number and Z_c is the instantaneous depth of the control point of each panel, accounting for the actual ship motions.

This approach is a kind of extension of the linear wave theory to incorporate the nonlinear effects associated with the variation of the ship's wetted surface. Froude-Krylov forces and moments are evaluated by integrating the pressure over the wetted portion of hull surface depending on the effective ship's position in waves, thus on the local wave elevation at each point. The same non-linear approach is applied in computing the hydrostatic actions.

The damping, added mass and diffraction forces and moments are calculated beforehand by means of the Hydrostar ®, a 3-D panel method software, and then implemented in the numerical model.

The numerical model accounts for ship velocity given by the propeller behaviour, together with ship resistance in waves. The propeller actions are expressed in the body fixed reference frame and they move with the hull. The number of revolutions n is set to achieve the desired ship speed in still water. In such conditions, the thrust that the propellers have to supply for keeping the ship at the operational speed V is given by:

$$X_{resistance} = -R_T/(1 - t_p) = -0.5\rho u^2 S C_T/(1 - t_p) \tag{4.4}$$

where: R_T is the total resistance, t_p is the thrust deduction factor, S is the wetted surface and u is the forward velocity of the ship in the body-fixed co-ordinate system. The total resistance coefficient C_T is given in tabular form as a function of Froude number. The total thrust provided by the propellers is evaluated from the open water characteristic of the propeller, $K_T = K_T(J)$, as follows:

$$X_{prop} = N_P \rho n^2 D_P^4 K_T \tag{4.5}$$

where J is the advance number, N_P is the number of the propellers, n is the propeller revolutions per second and D_P is the propeller diameter. The required propeller revolutions n, for still water and constant forward speed, is set in order to obtain the equilibrium:

$$X_{prop} = X_{resistance} \tag{4.6}$$

The propeller characteristic curve $K_T(J)$, is implemented from known data. The propellers' number of revolutions is kept constant during the simulations in waves. Therefore, ship speed will be modified from the still water value, due to added resistance in waves. This is evaluated as a result of dynamic pressures forces, acting on the wetted panel on the ship, projected on the x-direction.

The model for ship manoeuvring is implemented and calculated together with seakeeping and resistance thrust models. In this way a unified seakeeping and manoeuvring approach is carried out; the manoeuvring forces and moments and the seakeeping forces and moments are calculated at the same time in the same system. Radiation and diffraction forces in seakeeping are related to ship motions in waves based on potential theory, while manoeuvring actions are estimated by a semi-empirical model.

The so-called slow motion hydrodynamic derivatives for manoeuvring motions are evaluated for the still water condition. Thus their application for the ship operating in waves may be questioned. A good compromise is to preserve only the terms of sway Y, and yaw, N, motions related to velocities, such as $Y_v = \partial Y/\partial v$, $Y_r = \partial Y/\partial r$, $N_v = \partial N/\partial v$, and $N_r = \partial N/\partial r$, without including added mass contribution in the manoeuvring model, as these are already included in the radiation forces model. The argument is that these terms include the effects that are related to slow motion, and they are mainly governed by the non-potential flow effects.

Moreover, the potential damping terms related to yaw and sway motions in following waves with encounter frequency close to zero are neglected. Therefore in order to include the existing damping effect even at encounter frequency close to zero, the seakeeping theory is combined with the manoeuvring model.

The implementation of manoeuvring forces in the equations of motion in waves, already presented in Acanfora and Matusiak (2016) and Matusiak (2013), allows estimating all the ship motions during manoeuvring in waves with a fair agreement of the results. A linear manoeuvring model is adopted. Although the non-linear model for ship manoeuvring is a more realistic approach, the non-linear coefficients cannot be easily evaluated.

The linear model for ship manoeuvring limits the manoeuvring forces only to the linear hydrodynamic derivatives, which can be easily estimated from the semi-empirical formulae, obtained with the aid of regression analysis, as a function of ship main dimensions (Brix, 1993):

$$Y_v = -\pi(T/L)^2[1 + 0.4C_B(B/T)]$$
$$Y_r = -\pi(T/L)^2[-0.5 + 2.2(B/L) - 0.08(B/T)]$$
$$N_v = -\pi(T/L)^2[0.5 + 2.4(T/L)]$$
$$N_r = -\pi(T/L)^2[0.25 + 0.039(B/T) - 0.56(B/L)])$$

Chapter 5

CFD Approach - Naval Hydro Pack

5.1 CFD Modelling

CFD simulations for a self-propelled ship sailing in regular following waves have been performed using Naval Hydro Pack software based on the open source object-oriented C++ foam-extend library version 4.1 OpenFOAM software for general computational continuum mechanics (Weller et al., 1998) (Jasak et al., 2007). Naval Hydro Pack is being developed with focus on ship dynamics, from resistance and wave calculations, to loading and hydrodynamic problem simulations.

The mathematical and numerical models used to describe a two–phase, incompressible and turbulent flow, concerning transient naval hydrodynamics, are the following:

- The flow model equations are described with RANS (Reynolds Averaged Navier-Stokes) equations (Versteeg and Malalasekera, 2007) and the turbulence closure is achieved via two equation eddy viscosity models described by k-ω Shear Stress Transport (SST) model (Menter et al., 2003), (Pereira et al., 2015).

- For the free–surface flow, the interface capturing is obtained with implicitly re-distanced Level Set (LS) method derived from the Phase Field (PF) equation (Sun and Beckermann, 2007) and the implicit treatment of free surface jump conditions is treated via the Ghost Fluid Method (GFM) (Bo and Grove, 2014), (Huang et al., 2007).

- For wave modelling, a solution decomposition is achieved via Spectral Wave Explicit Navier Stokes Equations (SWENSE) method (Ferrant et al., 2002) (Ducrozet et al., 2014) (Vukčević, 2016), and a domain decomposition method via relaxations zone, to prevent wave reflection (Jasak et al., 2015).

- The Finite Volume Method (FVM) (Jasak, 1996) is used for numerical discretization of the governing equations

The physical models used to describe a self-propelled ship sailing in waves are:

- Hydro-mechanical coupling combines fluid dynamics and mechanical rigid body motion (Gatin et al., 2019).

- The wave field is described by linear theory (Dean and Dalrymple, 2002).

- Propeller action is included by introducing an actuator disk associated with a pressure jump at disk interface (Bakica et al., 2019).

5.2 Numerical Modelling

5.2.1 Flow Model Equations

The mathematical model for incompressible, Newtonian, turbulent, two-phase flow of immiscible fluids with sharp interface in gravitational field, is described by Reynolds-Averaged Navier Stokes equations. Following Vukčević (2016) and applying the Ghost Fluid Method (GFM) (described in Section 5.2.3), the Continuity Equation (5.1) and Momentum Equation (5.2), for water, air and free surface, are:

$$\nabla \bullet \mathbf{u} = 0 \tag{5.1}$$

$$\frac{\partial \mathbf{u}}{\partial t} + \nabla \bullet (\mathbf{u}\mathbf{u}) - \nabla \bullet (\nu_e \nabla \mathbf{u}) = -\frac{1}{\rho}\nabla p + \mathbf{g} \tag{5.2}$$

where $\mathbf{u}$ is the velocity field, ν_e is the effective kinematic viscosity, ρ is the density, p is the pressure field and $\mathbf{g}$ is the gravitational acceleration.

Rewriting the following terms as: $\beta = \frac{1}{\rho}$ and $\mathbf{g} = \nabla(\mathbf{g} \bullet \mathbf{x})$,
and decomposing the pressure into its hydrostatic and dynamic parts:

$$p = p_d + \frac{\mathbf{g} \bullet \mathbf{x}}{\beta} \tag{5.3}$$

the moment equation has the final form:

$$\frac{\partial \mathbf{u}}{\partial t} + \nabla \bullet (\mathbf{u}\mathbf{u}) - \nabla \bullet (\nu_e \nabla \mathbf{u}) = -\beta \nabla p_d \tag{5.4}$$

5.2.2 Free Surface Modelling

For the free surface flows, the interface capturing is treated with re-distanced LS (Level Set) transport equation derived from PF (Phase Field) equation (Vukčević et al., 2016a), which unites the unboundedness of the signed distance function of the LS method and preserves the hyperbolic tangent profile of PF method (Sun and Beckermann, 2007). The final form of the Level Set transport equation derived from (Sun and Beckermann, 2007) is:

$$\frac{\partial \psi}{\partial t} + \mathbf{u} \bullet \nabla \psi = b\left(\nabla \bullet (\nabla \psi) + \frac{\sqrt{2}}{\epsilon}\left(1 - |\nabla \phi|^2\right)\tanh\left(\frac{\psi}{\epsilon\sqrt{2}}\right) - \nabla \bullet \left(\frac{\nabla \phi}{|\nabla \phi|}\right)\right) \tag{5.5}$$

where: ψ is the signed distance function of LS method, b is diffusion coefficient, ϵ is a measure of the width of the hyperbolic tangent profile of PF method. The numerical value of the parameter b is determined with the Courant-Friedrichs-Lewy (CFL) condition (Sun and Beckermann, 2007). The left side represents advection of the distance field ψ. On the right side the first term takes into account the diffusion effect, the second models the curvature-driven motion of the interface and the third one counteracts the second. Introducing new variables as described in (Vukčević, 2016), the level set transport equation can be written in a more suitable form for discretisation as:

$$\frac{\partial \psi}{\partial t} + \nabla \bullet (\mathbf{c}\psi) - \psi\nabla \bullet \mathbf{c} - b\nabla \bullet (\nabla \psi) = b\frac{\sqrt{2}}{\epsilon}\tanh\left(\frac{\psi}{\epsilon\sqrt{2}}\right) \tag{5.6}$$

5.2.3 Implicit Treatment of Free Surface Jump Conditions

Following Vukčević et al. (2017), both air and water fluids may be considered incompressible and the approximated jump conditions on the interface are treated with the GFM (Bo and Grove (2014), Huang et al. (2007)) which overcomes numerical errors found in the conventional method by imposing interface kinematic and dynamic boundary conditions, and accounts for the discontinuous density field.

The kinematic and dynamic interface boundary conditions are:

- Density jump across the interface:
  $[\rho] = \rho^- - \rho^+$
  where $[\cdot]$ is the jump at the interface between air (-) and water (+) fluids.

- Kinematic boundary condition stating that the velocity field is continuous across the interface:
  $[\mathbf{u}] = \mathbf{u}^- - \mathbf{u}^+$

- Dynamic boundary condition that is divided in:

  - Tangential stress which defines the effective kinematic viscosity continuous across the interface; neglecting the gradient of surface tension coefficient and assuming that the tangential velocity gradient is continuous across the free surface; from the tangential stress balance derives the continuity of the velocity gradient (Vukčević, 2016)
    $[\nu_e] = 0 \rightarrow [\nabla \mathbf{u}] = 0$

  - Normal stress, which defines continuous the pressure across the interface, neglecting the surface tension, and defines a jump for the dynamic pressure (from pressure decomposition), proportional to the density jump:
    $[p] = 0$ and $[p_d] = -\left[\frac{1}{\beta}\right] \mathbf{g} \bullet \mathbf{x}$

- Dynamic pressure gradient which is continuous across the interface due to the continuous of velocity field, velocity gradient and kinematic viscosity, derived by momentum equation jump at free surface:
  $[\beta \nabla p_d] = 0$

5.2.4 Wave Modelling

Wave modelling is introduced with a double decomposition method: a solution decomposition, to introduce the wave field, achieved with the Spectral Wave Explicit Navier-Stokes Equations (SWENSE) method (Vukčević et al., 2016a) and a domain decomposition, to reduce the wave reflection, based on the implicit relaxation zone approach (Jasak et al., 2015). The SWENSE method, (Ferrant et al., 2002) (Ducrozet et al., 2014), decomposes the fields in incident and perturbed components, with the idea to capture features of the free surface, with a potential flow incident arbitrary field, and superimpose non-linear, two phase, turbulent effects by extending the incident component to a full Navier-Stokes model via the perturbed component.

The governing equations therefore are decomposed as follows. The decomposed continuity equation is:

$$\nabla \bullet \mathbf{u}_P = \nabla \mathbf{u}_I \tag{5.7}$$

47

Even if $\nabla \bullet \mathbf{u}_I$ is zero in potential flow, the term is kept because there is no guarantee it vanishes in a numerical framework.

The momentum equation is decomposed in:

$$\frac{\partial \mathbf{u}_P}{\partial t} + \nabla \bullet (\mathbf{u}\mathbf{u}_P) - \nabla \bullet (\nu_e \nabla \mathbf{u}_P) = -\frac{\partial \mathbf{u}_I}{\partial t} - \nabla \bullet (\mathbf{u}\mathbf{u}_I) + \nabla \bullet (\nu_e \nabla \mathbf{u}_I) - \beta \nabla p_d \quad (5.8)$$

The velocity is decomposed in the time derivative, in the diffusion term and only for the convected component in the convection term while the convecting component is not decomposed for time consuming. The dynamic pressure otherwise would yield two pressure equations: one for the incident and one for the perturbed field, which would separately force $\nabla \bullet \mathbf{u}_P$ and $\nabla \bullet \mathbf{u}_I$ to vanish.

The Level Set transportation equation is decomposed in:

$$\frac{\partial \psi_P}{\partial t} + \nabla \bullet (\mathbf{c}\psi_P) - \psi_P \nabla \bullet \mathbf{c} - b\nabla \bullet (\nabla \psi_P) =$$
$$\frac{\partial \psi_I}{\partial t} + \nabla \bullet (\mathbf{c}\psi_I) - \psi_I \nabla \bullet \mathbf{c} - b\nabla \bullet (\nabla \psi_I) + b\frac{\sqrt{2}}{\epsilon} \tanh\left(\frac{\psi}{\epsilon\sqrt{2}}\right) - \frac{\mathbf{u}_P}{\tau}\omega \quad (5.9)$$

As in the previous decomposition, the convecting field, $\mathbf{c}$, and the hyperbolic tangent term are not decomposed.

The wave is present in the whole computational domain explicitly, instead of prescribing wave boundary conditions at far field boundaries.

To prevent wave relaxation, which can cause errors in CFD calculated results, an implicit relaxation zones approach (Jasak et al., 2015) is used to force a general perturbed field, (χ_P), to vanish in the far-field boundaries. The approach consists in introducing three terms: a general transport operator, $\mathcal{T}(\chi_P)$, that is defined by the total transport equation, acting on the perturbed field (χ_P), and is function of the incident and perturbed component; a Relaxation zone operator, $\mathcal{R}(\chi_P) = \frac{\chi_P}{\tau}$, which imposes the perturbed field to be zero at the boundary; and a weight field, w, exponential function equal to 1 at the far field and reducing to 0 in the interior domain near the area of interest. The weighted combination of transport and relaxation equation yields:

$$(1 - w)\mathcal{T}(\chi_P) + w\mathcal{R}(\chi_P) = 0 \quad (5.10)$$

At the far field, where $w = 1$, $\mathcal{R}(\chi_P) = 0$ and the perturbed component vanishes, leaving only the incident prescribed field. In the interior domain, where $w = 0$, the $\mathcal{T}(\chi_P) = 0$ and the total CFD solution is obtained by solving the transport equation of incident and perturbed fields. In between, where $0 < w < 1$, a blending region is defined where the perturbed component is forced to vanish with w weight function.

The governing equation are therefore decomposed as following, continuity, momentum and Level Set equation:

$$(1 - w)(\nabla \bullet \mathbf{u}_P - \nabla \bullet \mathbf{u}_I) = 0 \quad (5.11)$$

$$(1 - w)\left(\frac{\partial \mathbf{u}_P}{\partial t} + \nabla \bullet (\mathbf{u}\mathbf{u}_P) - \nabla \bullet (\nu_e \nabla \mathbf{u}_P)\right) =$$
$$-(1 - w)\left(\frac{\partial \mathbf{u}_I}{\partial t} - \nabla \bullet (\mathbf{u}\mathbf{u}_I) + \nabla \bullet (\nu_e \nabla \mathbf{u}_I) - \beta \nabla p_d\right) - w\frac{\mathbf{u}_P}{\tau} \quad (5.12)$$

$$(1-w)\left(\frac{\partial\psi_P}{\partial t}+\nabla\bullet(\mathbf{c}\psi_P)-\psi_P\nabla\bullet\mathbf{c}-b\nabla\bullet(\nabla\psi_P)\right)=$$

$$-(1-w)\left(\frac{\partial\psi_I}{\partial t}+\nabla\bullet(\mathbf{c}\psi_I)-\psi_I\nabla\bullet\mathbf{c}-b\nabla\bullet(\nabla\psi_I)+b\frac{\sqrt{2}}{\epsilon}\tanh\left(\frac{\psi}{\epsilon\sqrt{2}}\right)\right)-\frac{\psi_P}{\tau}w$$

$$(5.13)$$

The sink term $w/\tau\mathbf{u}_P$ forces the perturbed field to vanish when $w=1$

5.2.5 Finite Volume Method

The partial non linear differential equations governing the fluid flow are discretised into a corresponding system of algebraic equations using a second-order accurate Finite Volume Method (VFM) for arbitrary polyhedral grids. The discretisation is made in two steps: solution domain and equation discretisation. The solution domain discretisation is divided in time, using a time step, and in space using control volumes (cells). For full description and details refer to Jasak (1996). For the equation discretisation the Finite volume method requires that the governing equations in integral form are satisfied over the control volume around the centre point P. Moreover indicating with $\{\}^i$ and $\{\}^e$ the implicit and explicit FV discretisation, the momentum equation is written as:

$$(1-w)\left(\{\frac{\partial\mathbf{u}_P}{\partial t}\}^i+\{\nabla\bullet(\mathbf{u}\mathbf{u}_P)\}^i-\{\nabla\bullet(\nu_e\nabla\mathbf{u}_P)\}^i\right)=-\{\frac{w}{\tau}\mathbf{u}_P\}^i+$$

$$-(1-w)\left(\{\frac{\partial\mathbf{u}_I}{\partial t}\}^e+\{\nabla\bullet(\mathbf{u}\mathbf{u}_I)\}^e-\{\nabla\bullet(\nu_e\nabla\mathbf{u}_I)\}^e\right)$$

$$(5.14)$$

where the time derivative, convection and diffusion terms of the perturbed field are discretised implicitly and the convection term is linearized to avoid non linearities as in Versteeg (2007). Following Jasak (1996) for FVM discretisation and in particular Vukčević (2016) for the domain and solution decomposition, the linear algebraic equation for the discretised momentum equation is:

$$a_P\mathbf{u}_{P,P}+\sum_f a_N\mathbf{u}_{N,P}=\mathbf{b_u} \tag{5.15}$$

$$a_P\mathbf{u}_{P,P}=\mathbf{H}(\mathbf{u}_{N,P})-\beta\nabla p_d \tag{5.16}$$

$$a_P\mathbf{u}_{P,P}=\mathbf{H}(\mathbf{u}_{N,P})-\sum_f \mathbf{s}_f\bullet(\beta p_d)_f \tag{5.17}$$

$$\mathbf{H}(\mathbf{u}_{N,P})=-\sum_f a_N\mathbf{u}_{N,P}=\mathbf{b_u} \tag{5.18}$$

where: $\mathbf{u}_{P,P}$ is the value of the perturbed velocity field in the center of the cell P, $\mathbf{u}_{N,P}$ is the value of perturbed velocity field in the neighbouring cells N of the control volume, $a_{P,P}$ and $a_{N,P}$ are the diagonal and off diagonal terms of the coefficient matrix for the equation of the control volume V_P, $\mathbf{b}_u$ represents the combined source term arising from: old step contributions, possible correction of convective and diffusion terms of perturbed

field, explicit dynamic pressure gradient and incident flow field terms (time derivative, convection and diffusion). $\sum$ denotes the sum over all neighbouring faces cell, implying interpolation from cell-centred values to face-centred values (by GFM), denoted by index f, and $\mathbf{s}_f$ represents the surface area vector. The discretised pressure equation, derived from pressure-velocity coupling algorithm, as described in Vukčević (2016) after Jasak (1996) referred to Patankar and Spalding (1972), is:

$$\sum_f \mathbf{s}_f \bullet \left[\left(\frac{1}{a_P} \right) (\beta)_{f_\Gamma} (\nabla p_d)_{f_\Gamma} \right] = \sum_f \mathbf{s}_f \bullet \left(\frac{\mathbf{H}(\mathbf{u}_{N,P})}{(a_P)_f} + \mathbf{u}_{f,I} \right)_f \qquad (5.19)$$

where $\mathbf{u}_{f,I}$ represents the explicit incident velocity field and $(\beta)_{f_\Gamma}$ the face-interpolated inverse density field of the two fluid mixture. The index f denotes the value interpolated from cell-centred values to face-centred values (by GFM). And the total volumetric face flux is given by equation:

$$F = \mathbf{s}_f \bullet (\mathbf{u}_{f,P} + \mathbf{u}_{f,I}) = \mathbf{s}_f \left[\frac{\mathbf{H}(\mathbf{u}_{N,P})}{(a_P)_f} - \left(\frac{1}{a_P} \right)_f \right) (\beta)_{f_\Gamma} (\nabla p_d)_{f_\Gamma} + \mathbf{u}_{f,I} \right] \qquad (5.20)$$

The discretised Level Set equation is:

$$(1-w) \left(\{ \frac{\partial \psi_P}{\partial t} \}^i + \{ \nabla \bullet (\mathbf{c}\psi_P) \}^i - \{ \psi_P \nabla \bullet \mathbf{c} \}^i - \{ b \nabla \bullet (\nabla \psi_P) \}^i \right)^i = -\{ \frac{\psi_P}{\tau} w \}^i +$$

$$-(1-w) \left(\{ \frac{\partial \psi_I}{\partial t} \}^e + \{ \nabla \bullet (\mathbf{c}\psi_I) \}^e - \{ \psi_I \nabla \bullet \mathbf{c} \}^e - \{ b \nabla \bullet (\nabla \psi_I) \}^e + \{ b \frac{\sqrt{2}}{\epsilon} \tanh \left(\frac{\psi}{\epsilon \sqrt{2}} \right) \}^e \right)$$

$$(5.21)$$

In the discretised governing equations, the terms related to incident fields are evaluated with numerical approach, mapping the incident wave on the numerical grid and discretising the mathematical operators in the underlying numerical framework.

5.3 Physical Modelling

5.3.1 Rigid Body Motions

The rigid body motion equations are introduced along with the governing flow equations to describe ship motions. As described in Gatin et al. (2019), the coupling of the rigid body motion equations and the fluid flow is performed using an enhanced approach: i.e. the rigid body motion equations are solved once per pressure corrector step and a geometric method (Muller and Terze, 2016) is used for integration of rigid body motion equations.

5.3.2 Wave Theory

The free surface elevation of the regular wave field is described using a flow model with linear wave theory on an infinite domain. The linear solution is extended to incorporate the weakly non-linear effects, yielding higher order Stokes theories (Dean and Dalrymple, 2002).

5.3.3 Propeller Action Modelling: Actuator Disk Patch

In order to perform self-propulsion simulations, in case the detailed geometry of the propeller is not available, a propeller model of a simplified actuator disc can be used. This model lowers the mesh generation and simulation time but still achieves acceptable accuracy in results (Seb, 2017). This propeller model is based on the assumption of a thin infinite blade and the disk is actually a cylindrical interface with the same diameter as the model propeller (Krasilnikov, 2013) (Seb, 2017). The circular surface of the actuator disk is defined by the following parameters: location of propeller plane, direction of the propeller axis, inner radius R_H (equal to the hub radius) and outer radius R_P (equal to the propeller radius) (Jasak et al., 2018) (Bakica et al., 2019). The inflow and outflow propellers' regions are defined by 2 cylinders having radius equal to propeller radius and thickness containing at least 1 cell mesh. To reproduce thrust and torque values, the pressure boundary condition is defined to produce the desired pressure jump and the velocity condition is set to add a swirl (Seb, 2017). Following Goldstein distribution (Goldstein, 1929), the pressure jump, Δp, and the tangential velocity jump, Δu_t, are defined as:

$$\Delta p = A_X r^* \sqrt{1 - r^*} \tag{5.22}$$

$$\Delta u_t = A_\theta \frac{r * \sqrt{1 - r*}}{r * (1 - r_h^|) + r_h^|} \tag{5.23}$$

where r^* is the normalized disk radius defined as:

$$r^* = \frac{r^| - r_h^|}{1 - r_h^|} \tag{5.24}$$

$$r^| = \frac{r}{R_P} \tag{5.25}$$

$$r_h^| = \frac{R_H}{R_P} \tag{5.26}$$

$$r = R_H + r^*(R_P - R_H) \tag{5.27}$$

and the functions A_X and A_θ, derived in Seb (2017), are defined as:

$$A_X = \frac{105}{8} \frac{T(J)}{\pi(R_P - R_H)(3R_H + 4R_P)} \tag{5.28}$$

$$A_\theta = \frac{105}{8} \frac{Q(J)}{\rho \pi u_X R_P(R_P - R_H)(3R_H + 4R_P)} \tag{5.29}$$

where u_X is the axial speed at the propeller plane.
$T(J)$ and $Q(J)$ are the thrust and torque values obtained from the open water test curves. The advanced speed is calculated with an axial velocity correction in order to properly compute inflow velocity on the propeller plane, as described in Jasak et al. (2018) and Bakica et al. (2019).

$$V_A = V_{D,CFD} - \frac{T}{2\rho A_D V_{D,CFD}} \tag{5.30}$$

The second term in the r.h.s. accounts for the velocity correction, where A_D, is the actuator disk surface and $V_{D,CFD}$, is the axial speed at the propeller plane evaluated from CFD computations, taking into account the flow accelerations due to the actuator disk theory.

5.4   Segregated Solution Algorithm

The governing equations, momentum, pressure, LS and the rigid body equations are solved following a segregated solution algorithm using PIMPLE solver. PIMPLE is composed of an outer loop called Semi-Implicit Method for Pressure Linked Equations (SIMPLE) (Patankar and Spalding, 1972), which starts solving the motion equations, moves the rigid mesh and evaluates the incident fields with the potential wave theory, and an inner loop called Pressure-Implicit with Splitting of Operators (PISO) (Issa, 1986), which predicts the perturbed velocity field and solves the dynamic pressure, through pressure-velocity coupling. For each time instance of boundary condition updates, the pressure jump of the actuator disk is added to the current value of the pressure field on the chosen actuator disk faces. Coupling between the body motion and the actuator disk is fully resolved by recalculating the thrust direction axis and actuator disk faces position after each mesh motion update.

The used Linear equation solvers are the preconditioned Krylov subspace linear system (Saad, 2003), in particular, the Conjugate Gradient for symmetric pressure equations and Bi-Conjugate stabilised BICGStab for the other equations (van der Vorst, 2003).

Chapter 6

Test Case Application

6.1 Systematic Serie D Description

The study on surf-riding occurrence has been performed on the Systematic Series D (Kracht and Jacobsen, 1992), originated from a semi-displacement, transom stern, twin-screw, round-bilge hull form, initially made by the German yard Howaldtswerke-Deutsche Werft. The Systematic Series D was developed with the necessity of having resistance and power predictions on a shorter and wider ship as this was a trend of corvette and frigate ship design during the 1990s. The D-Series has seven models derived from a parent hull form, D1, in two different ways:

- by linear distortion of y- and z-coordinates proportional to given scales to obtain hulls D2-D4;

- by alteration of the sectional area curve to create the second parent hull form D5, from which by linear distortion of y- and z-coordinates proportional other two hulls were obtained, D6 and D7.

The body plan of parent hull form D1 is shown in Figure 6.1 and the body plans of all seven hulls are represented in Figure 6.2.
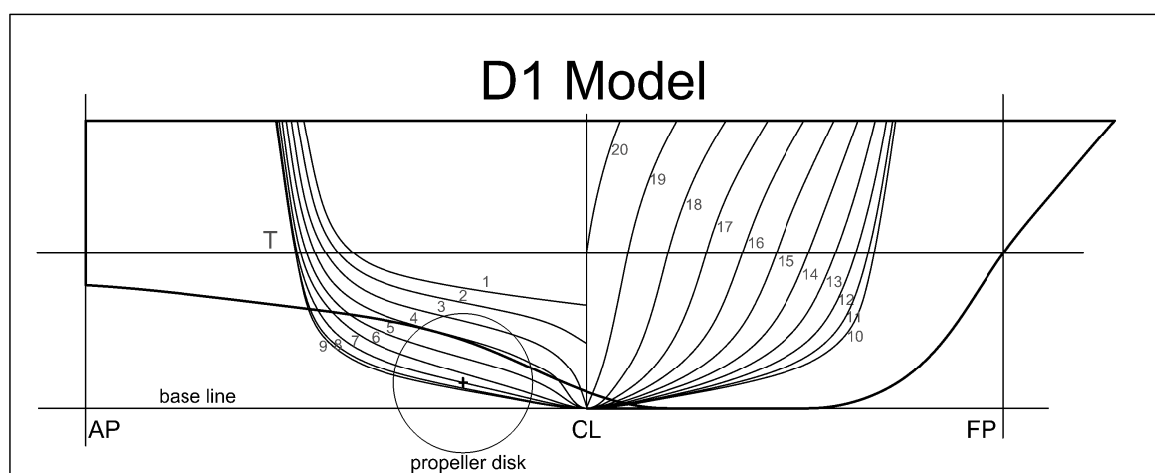

Figure 6.1: Nondimensional cross-section lines of the parent hull form D1 with in between distance of $L_{PP}/20$.
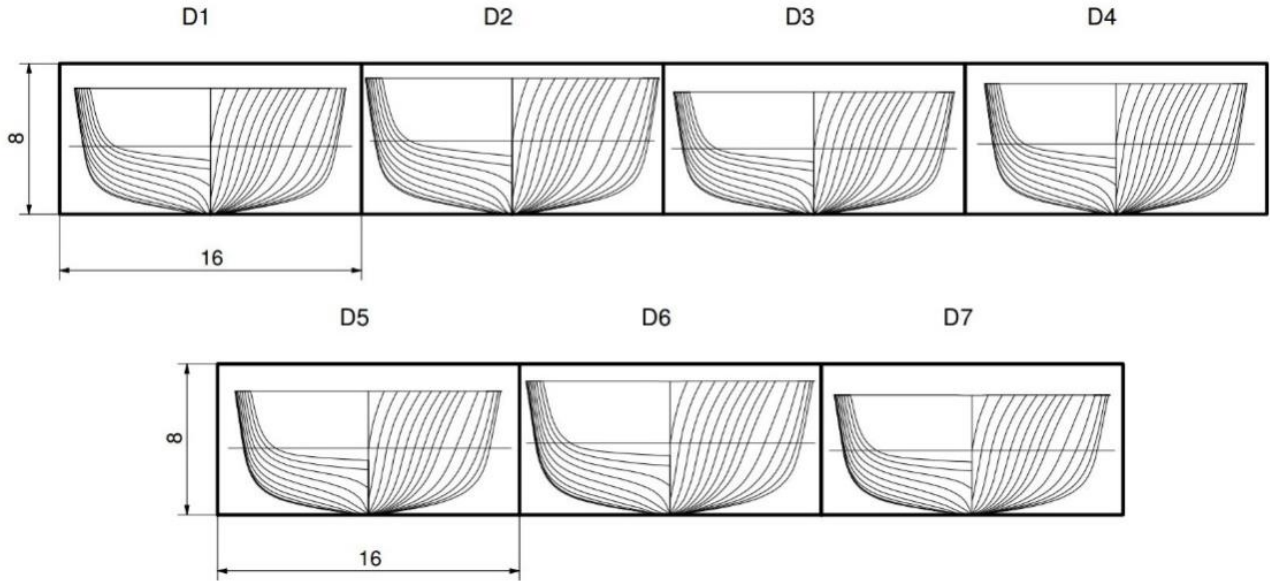
Figure 6.2: Body plans of the D Systematic Series hulls.

The resistance tests were performed at three different drafts, which were fixed so that the displacement volume, at each secondary draft, corresponded to the next higher or lower volumetric coefficient, C_V. A suitable change of C_V was $\Delta C_V = \pm 5 \cdot 10^{-4}$. The three main parameters of the series are: prismatic coefficient, C_P, equal to 0.620 and 0.646, beam to draft ratio B/T equal to 3.500, 3.750 and 4.000 and volumetric coefficient $10^3\, C_V$ equal to 3.000 and 3.500.

Resistance and propulsion tests have been performed in calm water only. The test program in speed range of Froude's number from 0.15 to 0.80 covered:

1. resistance tests with bare hull with all models from D1 to D7 at three drafts resulting in the residual resistance coefficients;

2. with models D1, D3, D5, D7 at draft T2:

   - resistance tests with appendages,

   - self-propulsion or speed variation tests,

   - load variation tests at some constant speeds executed during propulsion tests at various speeds, yielded propulsion factors which are more realistic than those determined from separately performed resistance and propulsion tests.

From the models' resistance coefficients C_{TM}, C_{RM}, C_{FM}, the total ship resistance R_{TS} including appendages has been calculated by Froude method as reported in Kracht and Jacobsen (1992). A full scale ship calm water resistance and thrust have been obtained, reporting all data to 90 m length ship, i.e. ship-model scale $\lambda = 15$.

For a design speed of 25 kn and $L_{PP} = 90$ m, the Froude number is equal to $Fn = 0.433$. In order to obtain the rate of revolution n_S and thrust T_S at full scale, the model values, n_M and T_M, obtained from the D-Series self-propulsion EFD tests, were scaled directly by ITTC'57 method.

For the thrust deduction coefficient t_p and wake fraction w_p, the equations indicated by the Authors are respectively:

$$b_T(Fn) = -1.0 - 0.443 \, Fn \exp\left(\frac{Fn}{Fn_0}\right)$$

$$t_p = 1.0 + 1/(b_T(Fn))$$

$$w_P = 1 - (J_{KT} n_M D_M)/v_M$$

The Systematic series parameters, reported to scaled ships (Kracht and Jacobsen, 1992) are given in Table 6.1.

Table 6.1: D-Systematic Series - ships main dimensions.

MODEL	L	B	T	L/B	B/T	C_B	C_P	Δ	D_P
	(m)	(m)	(m)	(-)	(-)	(-)	(-)	(t)	(m)
D1	90	13.500	3.600	6.6666	3.7500	0.50	0.62	2243.623	3.215
D2	90	14.581	3.888	6.1725	3.7500	0.50	0.62	2617.197	3.215
D3	90	13.943	3.486	6.4548	4.0000	0.50	0.62	2243.697	3.215
D4	90	13.043	3.726	6.9004	3.5000	0.50	0.62	2243.744	3.215
D5	90	13.225	3.527	6.8052	3.7500	0.52	0.65	2239.289	3.215
D6	90	14.285	3.809	6.3004	3.7500	0.52	0.65	2612.496	3.215
D7	90	13.659	3.415	6.5891	4.0000	0.52	0.65	2239.293	3.215

For each model, $D1 - D7$, the values of total resistance, R_{TS}, number of revolutions, n_S and thrust T_S, in the range of $Fn = 0.15 \div 0.75$, are given in Appendix in Tables 11.1, 11.2 and 11.3. For each of the seven models at draft $T2$, the curves for the total resistance are shown in Figure 6.3. Models D2 and D6 are wider and about 10% heavier than others so their resistance is also significantly greater for the Froude number range greater than $Fn = 0.4$. At $Fn = 0.3$, where Level 1 distinguishes vulnerability, the resistance curve of all hull forms are very close.

To find the polynomial expressions for the measured resistance, function of the ship speed, the resistance curves have been fitted with a 5th order polynomial, as suggested by SDC3/INF10 (2015). From the open water test results, (all models have been equipped with the same propellers), the $K_T(J)$ curve has been fitted with a 3rd order polynomial, as suggested by SDC3/INF10 (2015).

An example of resistance and thrust coefficient fitting curves is given for D1 hull in Figure 6.4, and the obtained polynomial coefficients $r_0 \div r_5$ and $k_0 \div k_2$ are reported in Table 6.2.
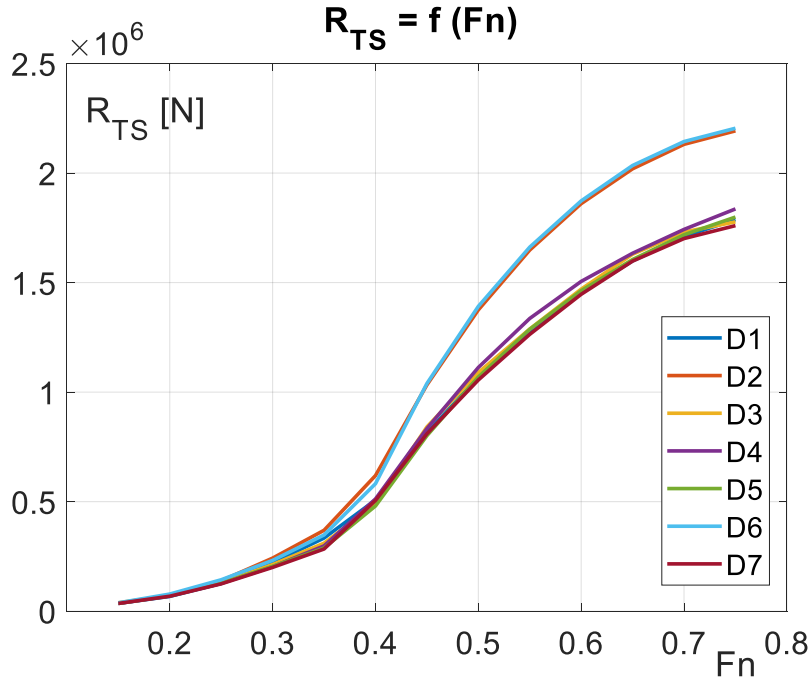
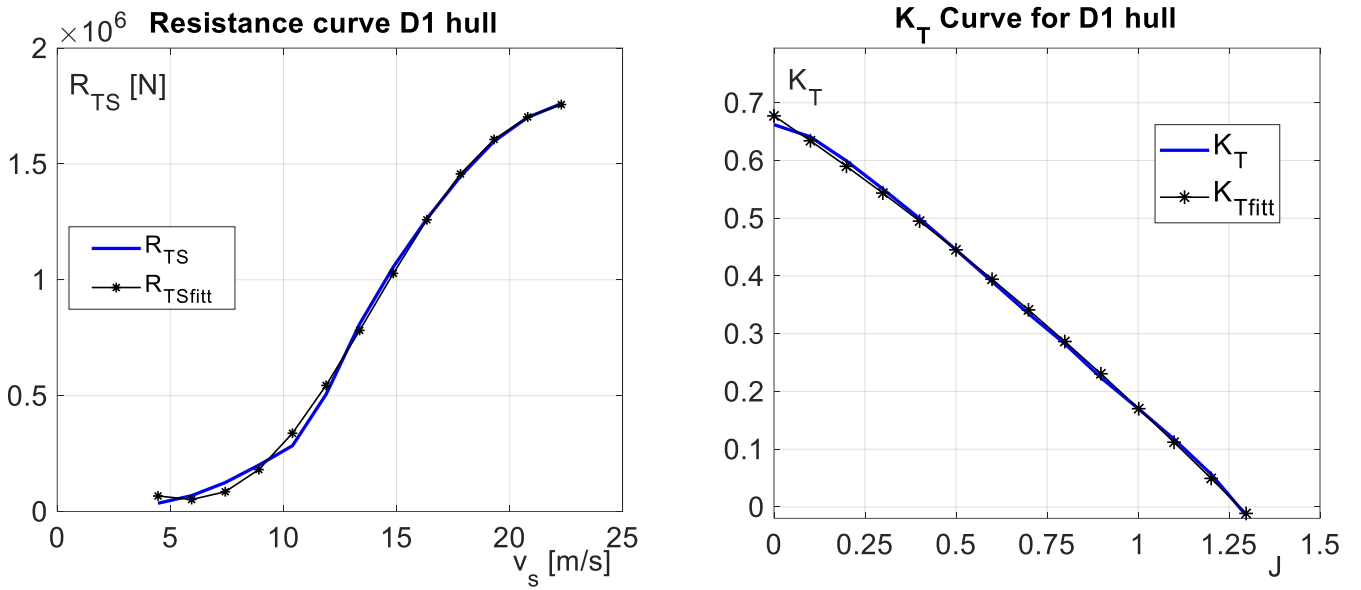Figure 6.3: Resistance curves for hulls D1 to D7.

Figure 6.4: Resistance and K_T curves and fittings for D1 hull form.

Table 6.2: D1 hull full scale resistance and thrust coefficients from fitting curves.

r_0	0	k_0	0.677
r_1	126890.9	k_1	-0.422
r_2	-46622.51	k_2	-0.084
r_3	5918.15		
r_4	-262.09		
r_5	3.86		

6.2 IMO Level 1 and 2 Applications

By applying the IMO criterion for surf-riding/broaching failure mode, the Series D has been found vulnerable to Level 1 as the criterion is simply not satisfied: the design speed at 25 knots corresponds to a Froude number of 0.433, which is considerably greater than 0.3, upper limit of the criterion; and the ship length is less than 200 m, lower limit.

Level 2 vulnerability assessment, following the procedures of IMO SDC2/WP4 (2015) and SDC3/WP5 (2016) implemented in the Matlab ® code, has been performed for all seven models at draft condition T2. Loading condition, resistance and thrust data used in the calculations refer to the values reported in Section 6.1. At service speed the Index C value for all the hull forms has been found greater than 0.005, therefore neither of them pass Level 2.

A further investigation on the maximum allowable Froude number complying with Level 2 criterion has been done in a range of Froude number going from 0.3 to 0.433 for two cases, linear and non linear wave celerity. During the development of the SDC regulations and problem resolution for the 2nd level of the surf-riding criterion, the wave celerity formulation has been long discussed and changed in time. Until 2015 (SDC3/INF10, 2015), IMO documents included two formulas to assess the wave celerity: a linear celerity, as define in Equation (2.9), depending only on the wave number, and a non-linear wave celerity, as defined in Equation (6.1), depending on the wave number and amplitude. After 2016 (SDC3/WP5, 2016) the IMO group agreed to use the linear wave celerity for the 2nd level assessment.

The non linear wave celerity is evaluated with the following formula:

$$c_i = \sqrt{\frac{g}{k_i}} \sqrt{1 + \left(k_i \frac{H_{ij}}{2} \right)^2} \tag{6.1}$$

The Index C values are reported in Figures 6.5 and 6.6 for linear and non linear wave celerity respectively.

It can be seen that all hull forms, except D2 and D6, pass Level 2 performed with linear wave celerity at a Froude number slightly higher than 0.3, limit for Level 1. With nonlinear wave celerity all the hulls exceed $Fn = 0.3$ and the limiting speeds increase, making this approach less conservative

A "ranking list among the hull forms" defines the hulls D2 and D6 as worst, since they have the lowest speed limit in passing the criterion, while D7, with the highest limit, has "the best" hull form for the surf-riding occurrence. This surf-riding vulnerability rank list reflects the resistance curve properties of the 7 hulls shown in Figure 6.3, where it can be seen that D2 has the highest resistance curve and D7 has the lowest resistance curve.
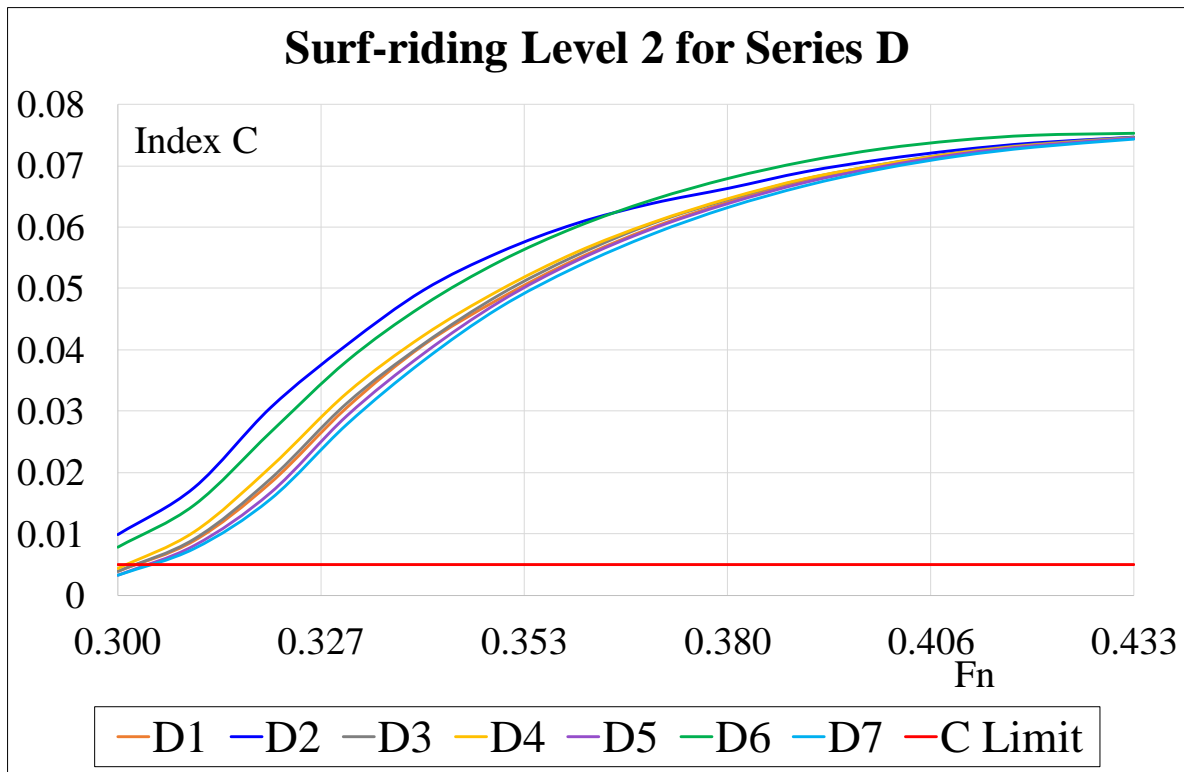
Figure 6.5: Level 2 evaluation of Index C for all 7 hulls with linear wave celerity in the range of Froude numbers of $0.3 \div 0.433$.
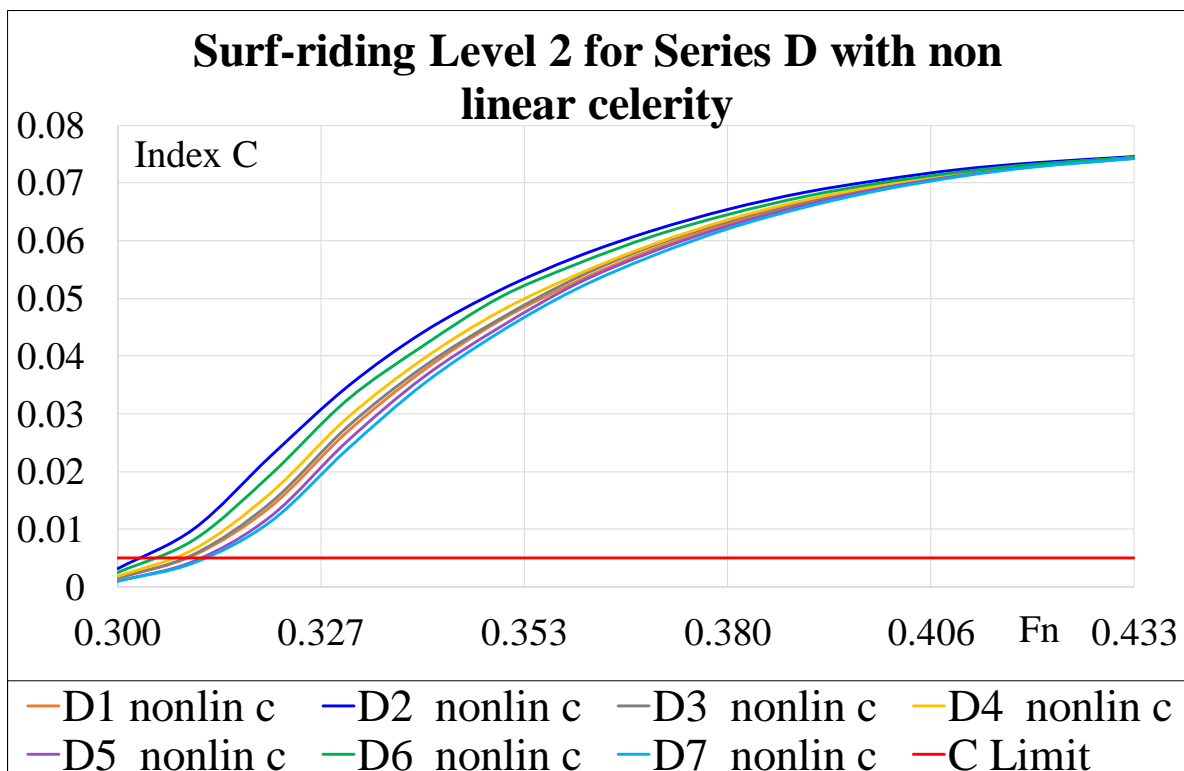

Figure 6.6: Level 2 evaluation of Index C for all 7 hulls with nonlinear wave celerity in the range of Froude numbers of $0.3 \div 0.433$.

6.2.1 Diffraction Effect

The formulation of the wave induced force has been long discussed in IMO documents. In early documents (SDC2/INF10, 2014) the wave surge force was formulated by considering only the Froude-Krylov component and the effect of the diffraction component was considered by means of an empirical correction factor, μ_x. Later on, in IMO SDC3/WP5 (2016) the diffraction effect was neglected. In IMO SDC4/5/4 (2016) it has been proposed that, for wave surge force predictions, a 3-D panel method can be used as an alternative method to the current strip-based model.

In the view of these discussions and following the works of Feng et al. 2015, 2017, additional calculations have been performed to assess the Index C values including the diffraction component. The hull tested are: D1 parent hull, D7 with the best performance hull for the lowest value of Index C, and hull D4 with the parameters and Index C value in the middle of range. The surging forces, including both diffraction and Froude-Krylov component, have been calculated using a 3-D panel method by the commercial linear potential theory software HydroSTAR®, by Bureau Veritas.

HydroSTAR is a 3-D diffraction/radiation potential theory software based on the Green Function for wave-body interactions and it provides a complete solution of 1st and 2nd order wave loads. The wave excitation loads for incoming waves are obtained by integrating the dynamic pressure on the vessel up to the still waterline.

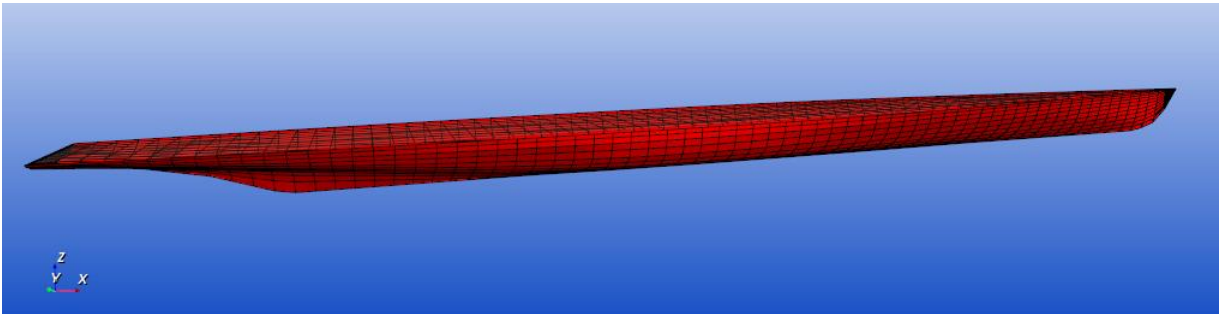The hull geometry representation in HydroSTAR for the parent model D1 is shown in Figure 6.7.

Figure 6.7: D1 hull form below waterline from HydroSTAR.

HydroSTAR calculations have been set for different ship speeds corresponding to $Fn = 0.3 \div 0.35$. For each Froude number case, 81 wave frequencies have been considered, corresponding to the wavelength to ship length ratio, $\lambda/L = 1 \div 3$, as defined by r_i in Level 2.

The calculated values of the surging forces, for each ship speed case, are shown in Figure 6.8 in non-dimensional form and as function of the wave to ship lengths. The non-dimensional form is obtained by dividing the force by the density, ρ, the gravitational acceleration, g, the wave amplitude, A, the ship length, L, and breadth, B.

Having observed that surf-riding Level 2 assessment is verified for Froude values around $Fn = 0.3$, and since the curve values are very close, in the range $Fn = 0.3 \div 0.35$, the values of the surging forces corresponding to curve Fn=0.3 have been introduced in the IMO formulation to evaluate the diffraction effect.

Figure 6.9 represents the nondimensional surge forces calculated with HydroSTAR for $\lambda/L = 1 \div 3$ at Froude $Fn = 0.3$ for hulls D1, D4 and D7.
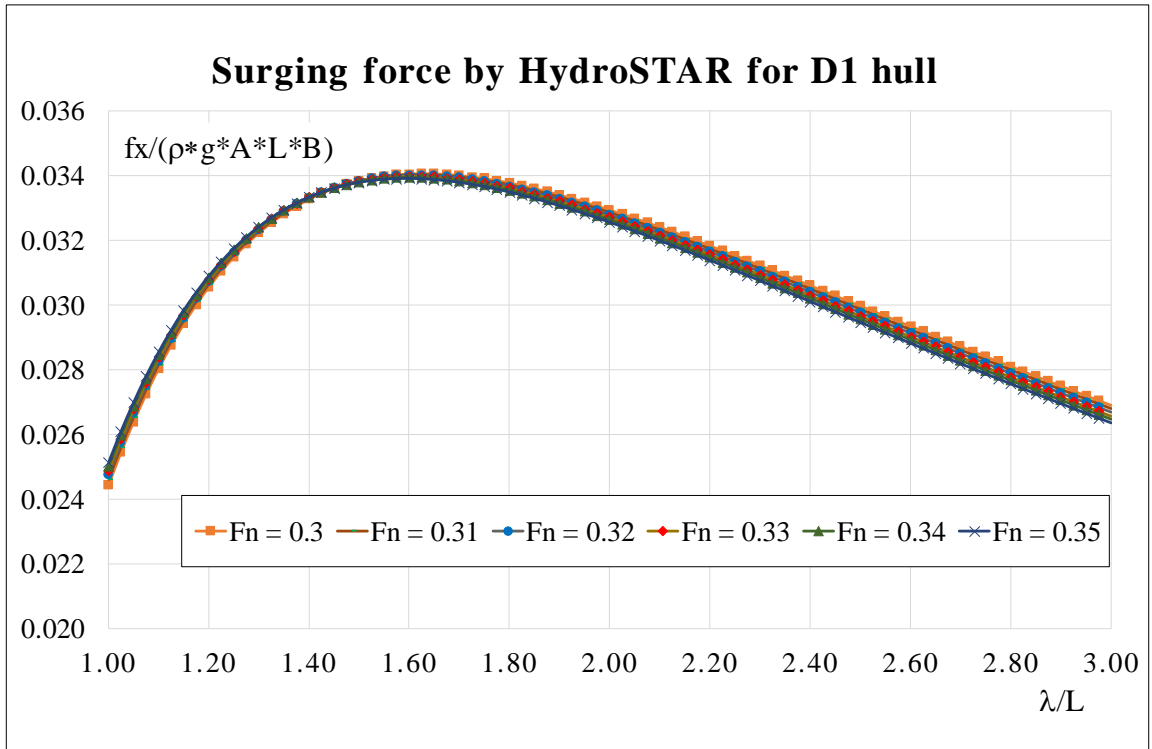
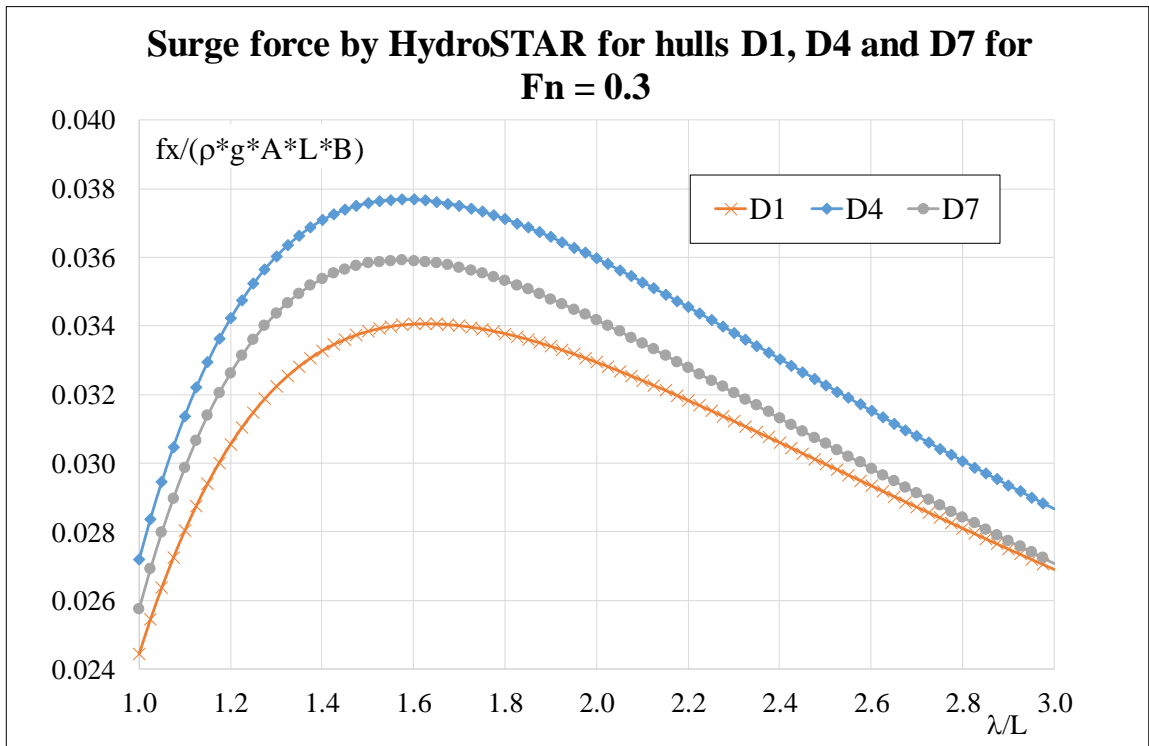Figure 6.8: D1 Surging forces, calculated by HydroSTAR.

Figure 6.9: Comparison of surge forces calculated by HydroSTAR for D1, D4 and D7 hulls.

The value of the surge force, f_x, computed in HydroSTAR is calculated for a unitary wave amplitude, therefore to obtain the amplitude of the wave surging force, f_{ij}, required for Level 2 IMO procedure, given by Equation (2.18), the surge force value is

multiplied by the wave amplitude, corresponding to one half of wave height obtained for each combination of wave steepness, $s_j = H_{ij}/\lambda_i$, and wavelength to ship length ratio, $r_i = \lambda_i/L$:

$$f_{ij} = f_{xi} \cdot (H_{ij}/2)$$

Figures 6.10, 6.11 and 6.12 show the Index C values for the hulls D1, D4 and D7 for 3 cases:

- with linear wave celerity;

- with non linear wave celerity (nonlin c);

- with linear wave celerity and diffraction effect (lin c + diffr).

Figure 6.13 represents the comparison of the Index C values considering linear celerity with and without diffraction effect for hulls D1, D4 and D7.

From all the diagrams it can be seen that for all the three hull forms the linear celerity effect gives a lower Froude number limit, and therefore this case is more conservative, while including the diffraction effect allows a higher speed limit for the ship to be considered not vulnerable to surf-riding Level 2 criterion.
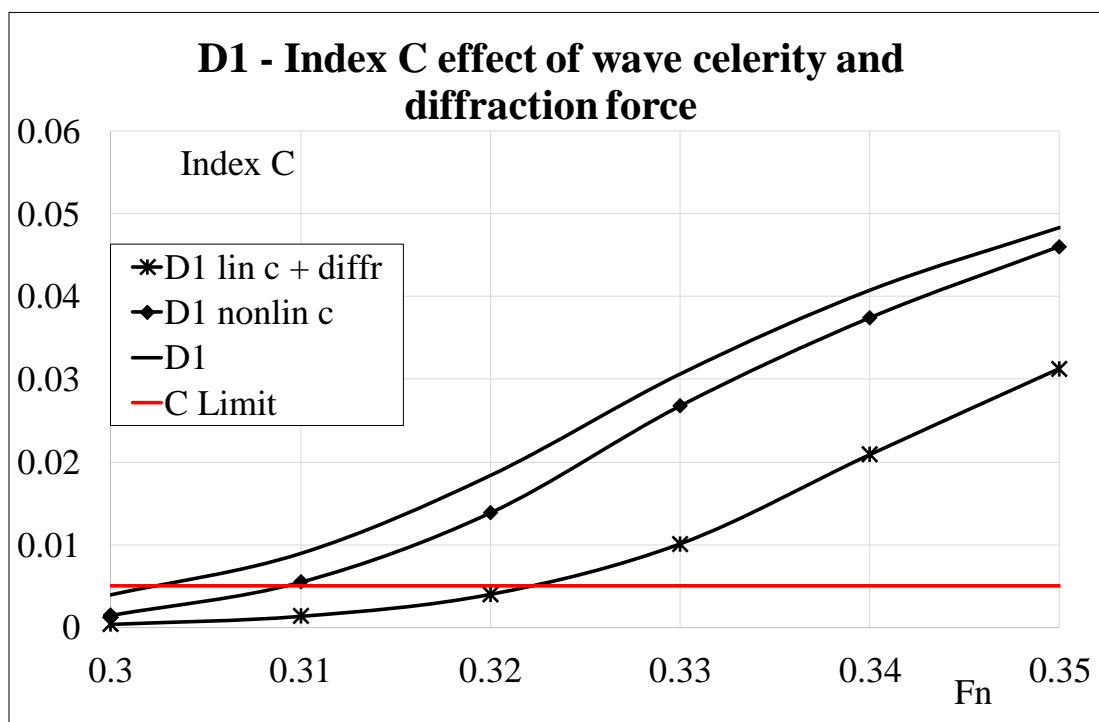

Figure 6.10: Index C value for linear and nonlinear celerity and with diffraction effect (linear celerity case) for hull D1.
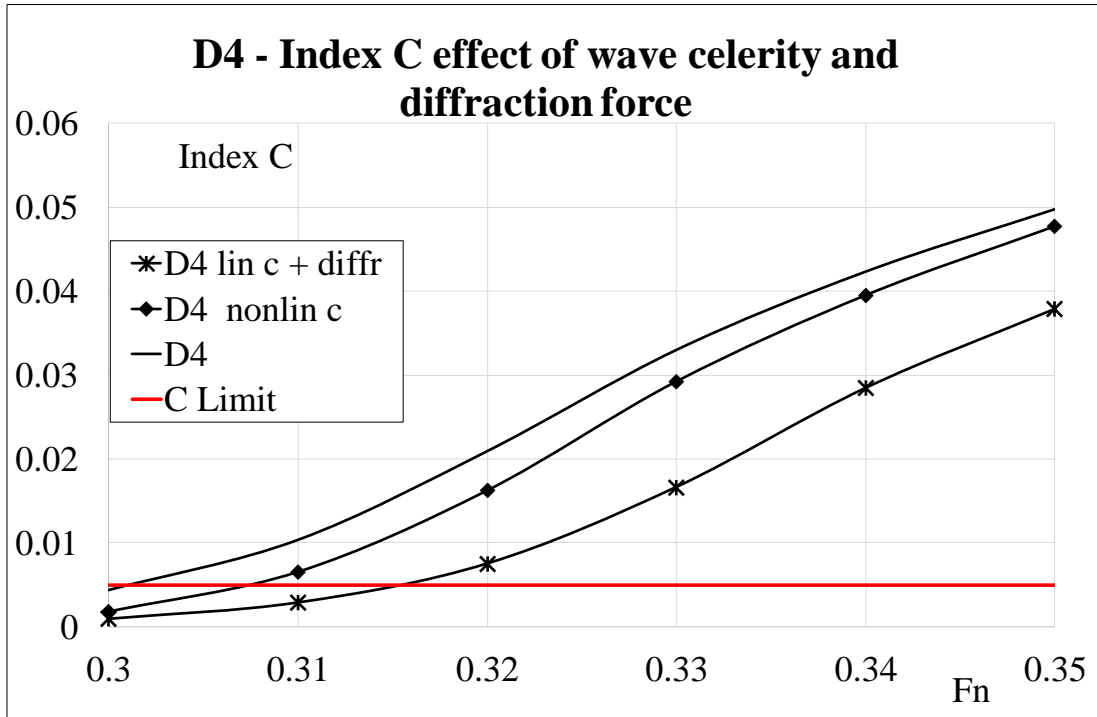
61

Figure 6.11: Index C value for linear and nonlinear celerity and with diffraction effect (linear celerity case) for hull D4.
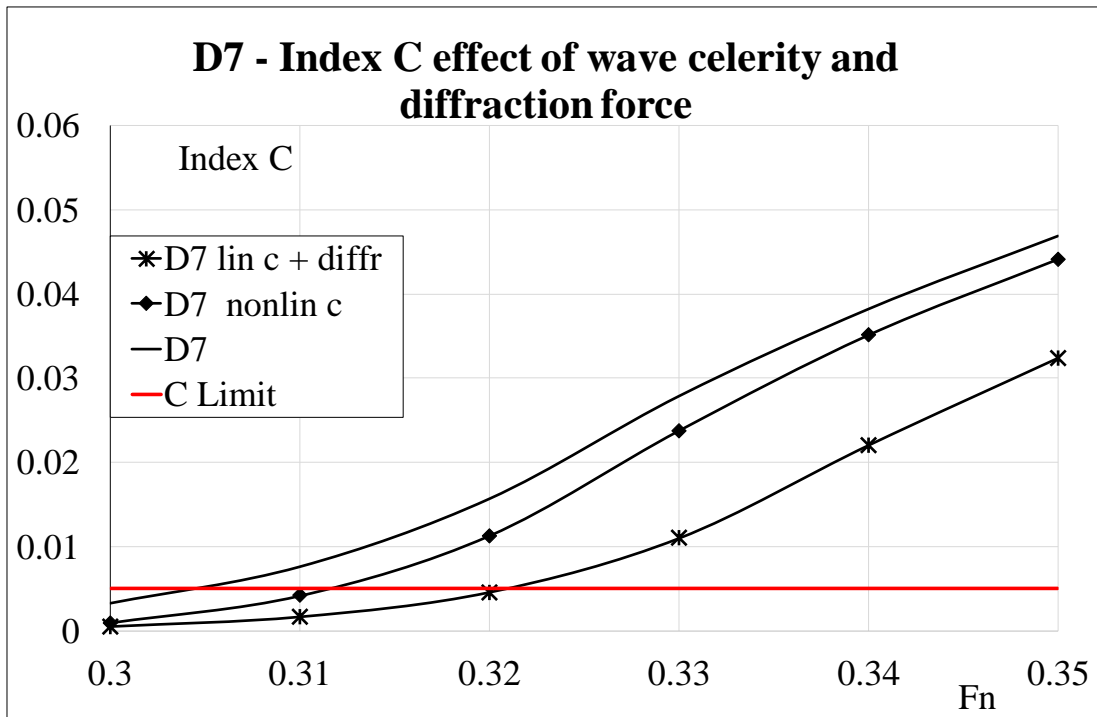

Figure 6.12: Index C value for linear and nonlinear celerity and with diffraction effect (linear celerity case) for hull D7.
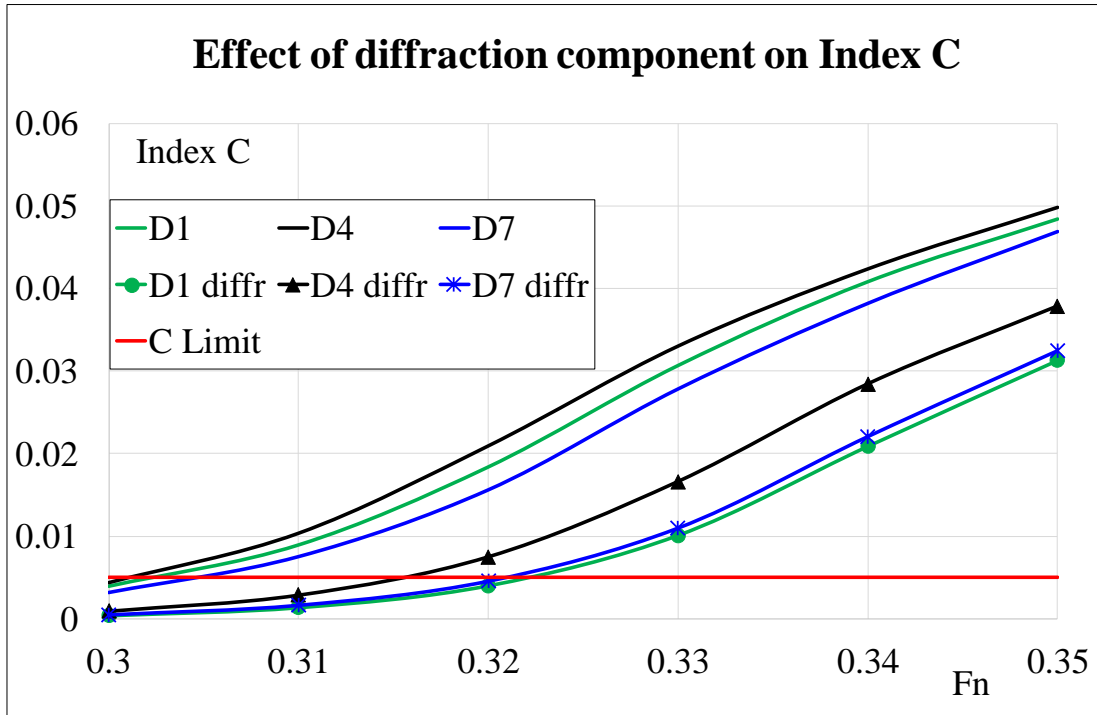
Figure 6.13: Index C value with linear celerity with and without diffraction effect for hulls D1, D4 and D7.

6.3 1-DOF Application

The 1-DOF surge mathematical model described and validated in Section 3 has been performed for D1 hull form of the Series D, whose main dimensions and experimental tests data are described in Section 6.1.

Surf-riding 2nd threshold limits are identified by numerical simulations of the 1-DOF surge motion equation throughout the phase plane analysis, as described in Section 3.1.2, imposing a fixed wave length, λ, and a fixed number of revolutions, n, in order to reach the corresponding ship speed in calm water conditions, and varying the wave steepness, H/λ.

Surf-riding limits are found, in terms of wave steepness for different Froude numbers and wave to ship lengths, for two cases, with and without diffraction effect, as shown in Figure 6.14. The Froude number range goes from 0.3, equal to the first limit defined by the IMO criterion, to 0.433, equal to the service speed. Following IMO guidelines, the chosen wave to ship lengths go from $\lambda/L = 1 \div 3$.
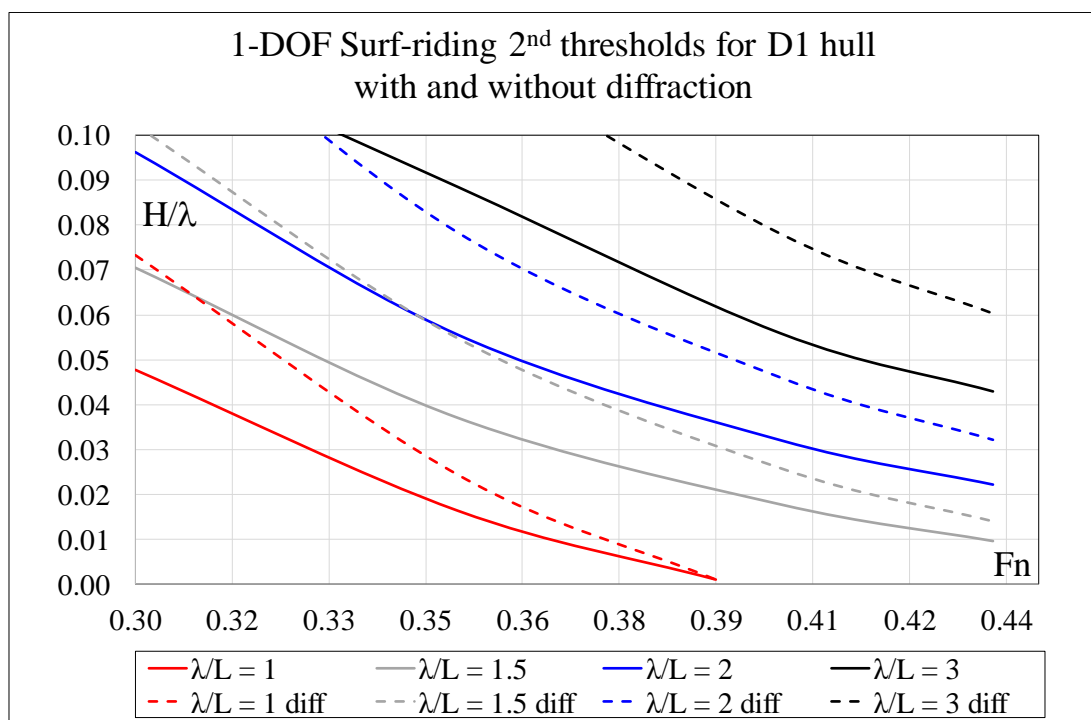

Figure 6.14: 1-DOF surf-riding limits with and without diffraction for D1 hull.

For the cases without diffraction effect, the wave excitation has been determined with the strip theory considering only the linear Froude-Krylov component, as described in IMO SDC3/WP5 (2016). In the other case, the wave excitation has been obtained by Hydrostar ® software, including both Froude-Krylov and diffraction components, as described in Section 6.2.1. Figure 6.15 shows the small difference in magnitudes, about 0-1%, of the Froude Krylov forces calculated by the two approaches, IMO and Hydrostar.
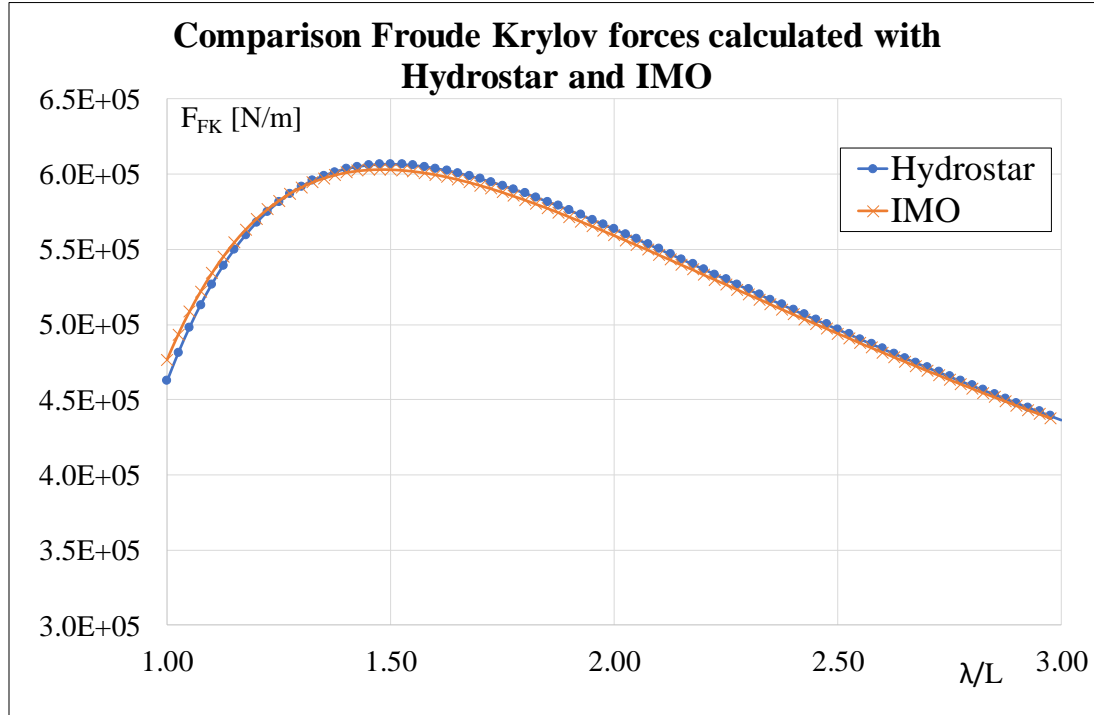
Figure 6.15: Difference in magnitudes of Froude Krylov forces calculated by IMO approach and Hydrostar.

From Figure 6.14 it can be noticed that for $\lambda/L = 1$ no surf-riding limit can been found for $Fn \geq 0.4$, since at this Froude number the ship is faster than the wave and the only possible phenomenon is wave blocking. Moreover, including the diffraction component, the surf-riding limits are higher, that is the ship experiences surf-riding for higher wave heights. The difference between the case with and without diffraction is lower for decreasing wave steepness, when the diffraction effect plays a smaller role, and for increasing Froude numbers, when the ship speed reaches wave celerity and surf-riding is more likely to occur no matter what approximation is made.

6.3.1 Comparison with Level 2 IMO Criterion

The comparison of the two approaches used to evaluate surf-riding occurrence, Melnikov's method within Level 2 and 1-DOF phase plan analysis, has been done in the following way. The values of the critical number of revolutions have been calculated for a set of combinations of wave lengths and heights by Melnikov's method, following the procedure as in Level 2 (SDC7/WP6, 2020). The number of revolutions obtained, corresponding to surf-riding 2nd threshold, are then used as input parameter in the 1-DOF model, for the corresponding sea state condition, and surf-riding thresholds have been identified by phase plane analysis to check whether the 1-DOF approach resulted in a more or less conservative requirement than Melnikov's method.

The wave cases range has been chosen following IMO procedure: wave to ship lengths, λ/L, go from 1 to 3, with a step 0.05, and wave steepness, H/λ go from 0.03 to 0.15 with a step of 0.0048. The critical number or revolutions, calculated by Melnikov's method, and the corresponding motion observed with 1-DOF are shown in Figure 6.16.

sj = H/λ	Ncr										
0.03	2.7	3.24	3.78	4.32	4.86	5.4	5.94	6.48	7.02	7.56	8.1
0.0396	3.564	4.2768	4.9896	5.7024	6.4152	7.128	7.8408	8.5536	9.2664	9.9792	10.692
0.0492	4.428	5.3136	6.1992	7.0848	7.9704	8.856	9.7416	10.627	11.513	12.398	13.284
0.0588	5.292	6.3504	7.4088	8.4672	9.5256	10.584	11.642	12.701	13.759	14.818	15.876
0.0684	6.156	7.3872	8.6184	9.8496	11.081	12.312	13.543	14.774	16.006	17.237	18.468
0.078	7.02	8.424	9.828	11.232	12.636	14.04	15.444	16.848	18.252	19.656	21.06
0.0876	7.884	9.4608	11.038	12.614	14.191	15.768	17.345	18.922	20.498	22.075	23.652
0.0972	8.748	10.498	12.247	13.997	15.746	17.496	19.246	20.995	22.745	24.494	26.244
0.1068	9.612	11.534	13.457	15.379	17.302	19.224	21.146	23.069	24.991	26.914	28.836
0.1164	10.476	12.571	14.666	16.762	18.857	20.952	23.047	25.142	27.238	29.333	31.428
0.126	11.34	13.608	15.876	18.144	20.412	22.68	24.948	27.216	29.484	31.752	34.02
0.1356	12.204	14.645	17.086	19.526	21.967	24.408	26.849	29.29	31.73	34.171	36.612
0.1452	13.068	15.682	18.295	20.909	23.522	26.136	28.75	31.363	33.977	36.59	39.204
ri = λ/L	1	1.2	1.4	1.6	1.8	2	2.2	2.4	2.6	2.8	3
λ	90	108	126	144	162	180	198	216	234	252	270

Color Legend
No fixed points
Between 1st and 2nd surf-riding threshold

Figure 6.16: Comparison Level 2 and 1-DOF approach.

It can be noticed that with the critical number of revolutions used in 1-DOF approach the observed motions are: surge when no fixed points are found, or surf-riding occurrence between the 1st and 2nd thresholds. It can be concluded that 1-DOF approach can predict less conservative surf-riding limits.

6.4 6-DOF Potential Flow Theory Application

The 6-DOF potential flow theory allows simulations of surf-riding phenomenon up to broaching-to instability. The assumptions on the manoeuvring model do not concern surf-riding developments, but they will affect the development of broaching instability.

The time domain simulations have been set up for regular sinusoidal waves, defined by length and steepness, and have been started by fixing an initial Froude number, Fn_{int}, that set the propellers' number of revolutions and the initial encounter frequency for the calculation of radiation and diffraction forces. The ship's velocity and dynamic motions were the variables that changed in time.

The simulations have been performed on the D1 hull form for sailing and wave conditions close to the ones in which surf-riding was detected by the 1-DOF approach. A first series of results and comparison between the two methods is reported in Acanfora et al. (2019). Each simulations ran for about 1000-3000 seconds in physical time and lasted no more than few minutes of calculation time.

From the analysis of forces, ship speed and ship motions variations the following conditions were observed:

- surge motion, when forces and ship speed oscillated in time and the yaw angle had small variations;

- surf-riding occurrence, when forces and ship speed tended to constant values;

- broaching occurrence, when large variations were observed for the yaw angle.

Figure 6.17 shows time domain simulations of the difference between thrust and resistance, X_{prop}-$X_{resistance}$, and Froude Krylov forces, F_{FK}, Figure 6.18 shows the ship speed, u, variations, and Figure 6.19 reports the yaw angle, ψ, changes in time, for a wave case of period $T = 7.5$ s and height $H = 1.5$ m and initial Froude number of $Fn = 0.35$, corresponding to the propeller's number of revolution $n = 3.073$ rps. This case features the dynamic equilibrium of surging, where all forces oscillate in time.
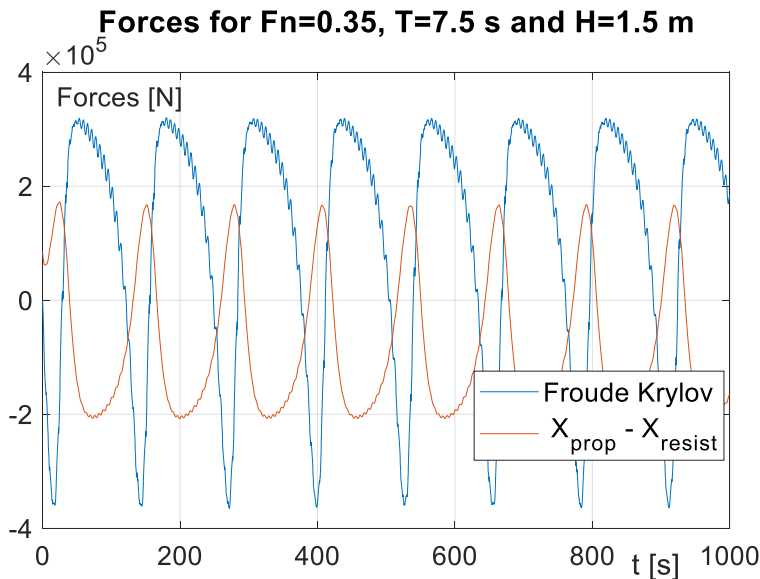

Figure 6.17: $X_{prop} - X_{resistance}$ and Froude Krylov time domain simulations for $Fn = 0.35$, $T = 7.5$ s and $H = 1.5$ m – surge motion observed.
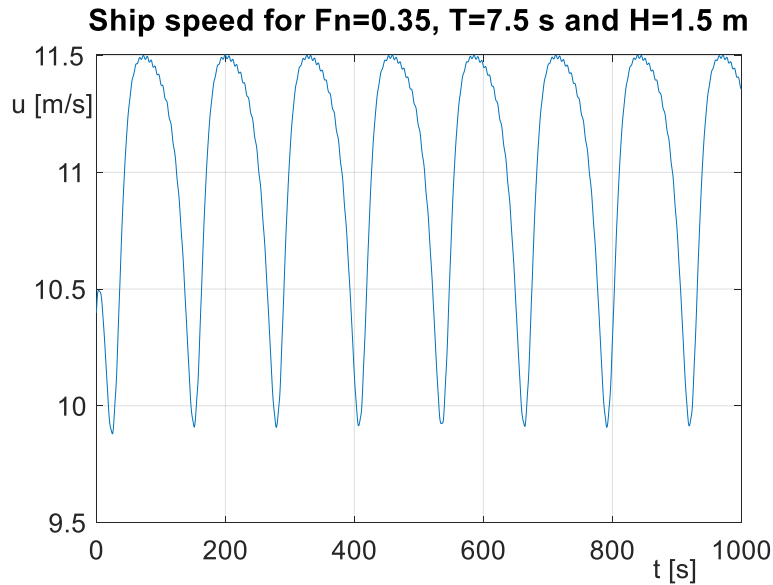
Figure 6.18: Ship speed time domain simulations for $Fn = 0.35$, $T = 7.5$ s and $H = 1.5$ m – surge motion observed.
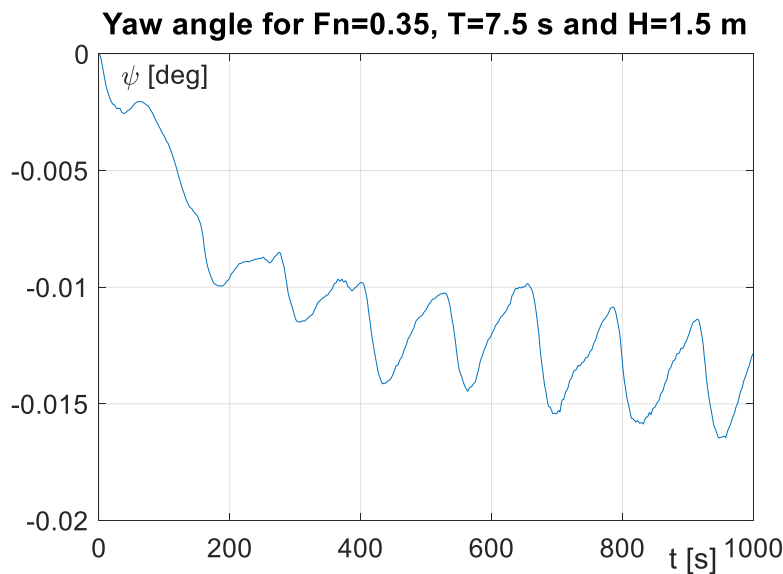

Figure 6.19: Yaw angle time domain simulations for $Fn = 0.35$, $T = 7.5$ s and $H = 1.5$ m – surge motion observed.

Figures 6.20, 6.21 and 6.22 show time domain simulation resulting values for a wave of the same period, $T = 7.5$ s and increased height to $H = 2.5$ m, and for the same initial Froude number $Fn = 0.35$. It can be observed that, after initial oscillations, the forces, ship speed and yaw angle remain constant, identifying a surf-riding equilibrium. Around 500 s, the yaw angle increases and generates an instability that has been identified as broaching phenomena.
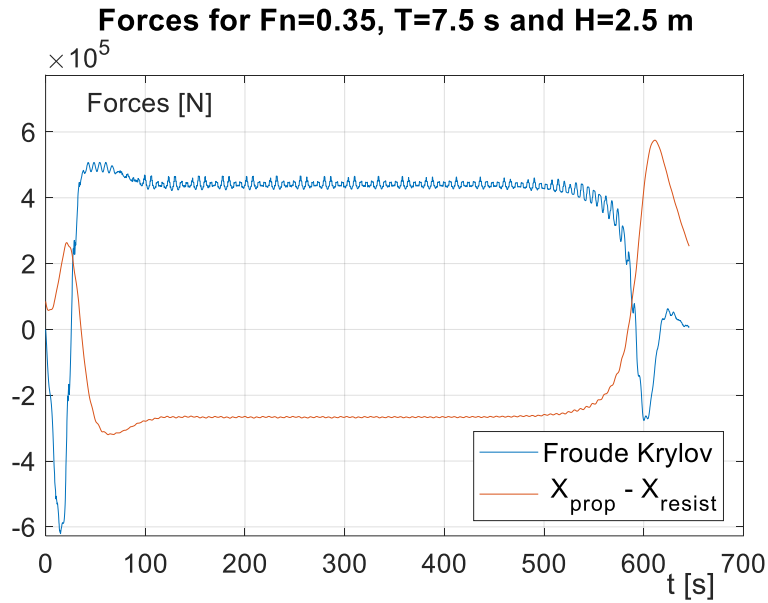
68

Figure 6.20: $X_{prop} - X_{resistance}$ and Froude Krylov time domain simulations for $Fn = 0.35$, $T = 7.5$ s and $H = 2.5$ m – surf-riding and broaching observed
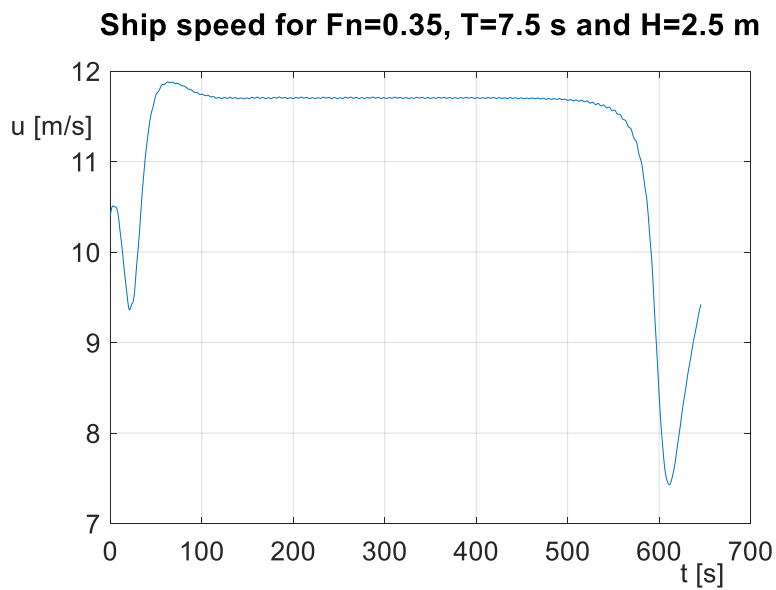

Figure 6.21: Ship speed time domain simulations for $Fn = 0.35$, $T = 7.5$ s and $H = 2.5$ m – surf-riding and broaching observed
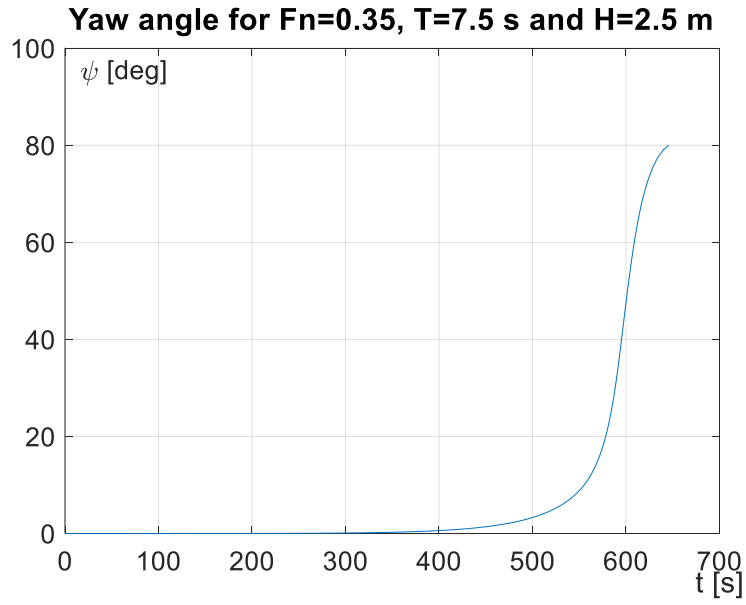
Figure 6.22: Yaw angle time domain simulations for $Fn = 0.35$, $T = 7.5$ s and $H = 2.5$ m – surf-riding and broaching observed

6.5 CFD Simulations by Naval Hydro Pack of Open-FOAM

The aim of performing CFD simulations is to define surf-riding limits for ship operability with a more direct and less conservative approach, taking into account force changes in wave conditions, neglected in 1-DOF methodology which is based on approximations of calm water forces.

3-DOF CFD simulations, for a self-propelled ship sailing in regular following sea, free in surge, heave and pitch motion, have been performed for D1 full-scale ship, with 90 m length. Full scale has been chosen to directly compare the maximum allowable wave height obtained by CFD and 1-DOF results against IMO guidelines on SGISC for Direct Stability Assessment and Operational Measures. To reduce computational effort and using the flow symmetry for the considered degrees of freedom, only half of the domain has been meshed in the simulations, but the resulting forces are reported for the full ship. The main results obtained have been presented for the first time in Begovic et al. (2020).

6.5.1 Grid Generation and Case Set-up

An unstructured polyhedral FVM grid has been used to mesh the bare hull and the hub geometries of the full scaled D1 ship. Calculations have been performed with the bare hull geometry because detailed geometries of the rudder, propeller and shaft brackets were not available, therefore for a fair comparison only EFD bare hull results were used. The only appendage geometry considered is an approximated hub to avoid numerical errors for back flow in the propeller disk.

The coordinate system used has the origin at the intersection of aft perpendicular, free surface and ship symmetry plane at time zero, as shown in Figure 6.23. The x axis is positive towards the bow, the z positive upwards and the y positive to port side, and the system translates with a constant forward speed.

The CFD domain has been meshed with dimensions of about 1.5 L_{PP} for the inlet, 4.5 L_{PP} for the outlet, 2.5 L_{PP} for the bottom and 3 L_{PP} for the side boundaries, as shown in Figure 6.24.
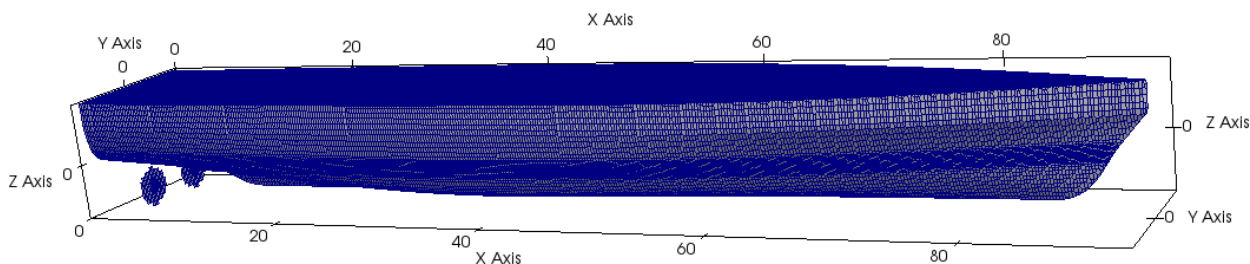

Figure 6.23: Reference system on D1 mesh domain.
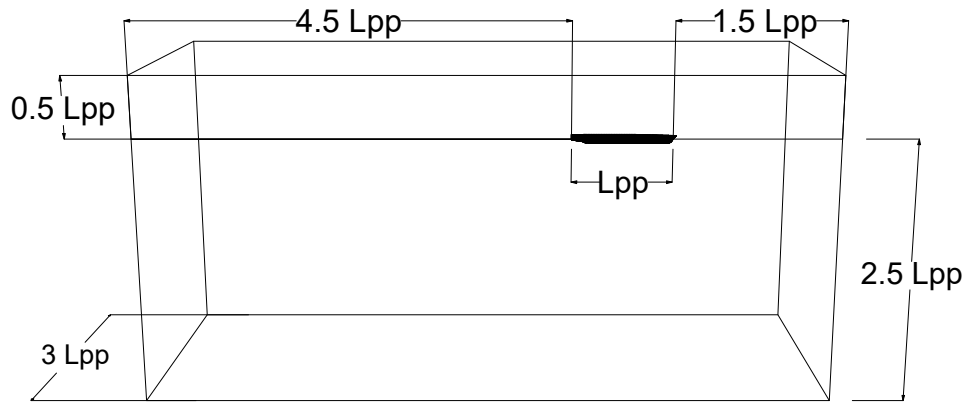
Figure 6.24: Bounding box and dimensions for CFD domain definition.

Five additional refinement boxes, as shown in Figure 6.25, have been added to provide sufficient resolution around the hull surface and in the relaxation zones imposing an adequate thickness with respect to the wave length.

Two hull geometries have been meshed, the first one corresponding to the body plan reported in Kracht and Jacobsen (1992), for resistance EFD tests, and the second with a higher deck to avoid green water phenomenon when run following wave simulations. Figure 6.26 shows the first mesh generated for hull, hub and actuator disk, and Figure 6.27 represents the hull with the extended free board. The total domain of the mesh accounts for 1 166 333 cells for the first case and 1 626 516 cells for the second case.

Figure 6.25: Mesh refinement boxes.

Figure 6.26: D1 mesh for calm water resistance simulations.

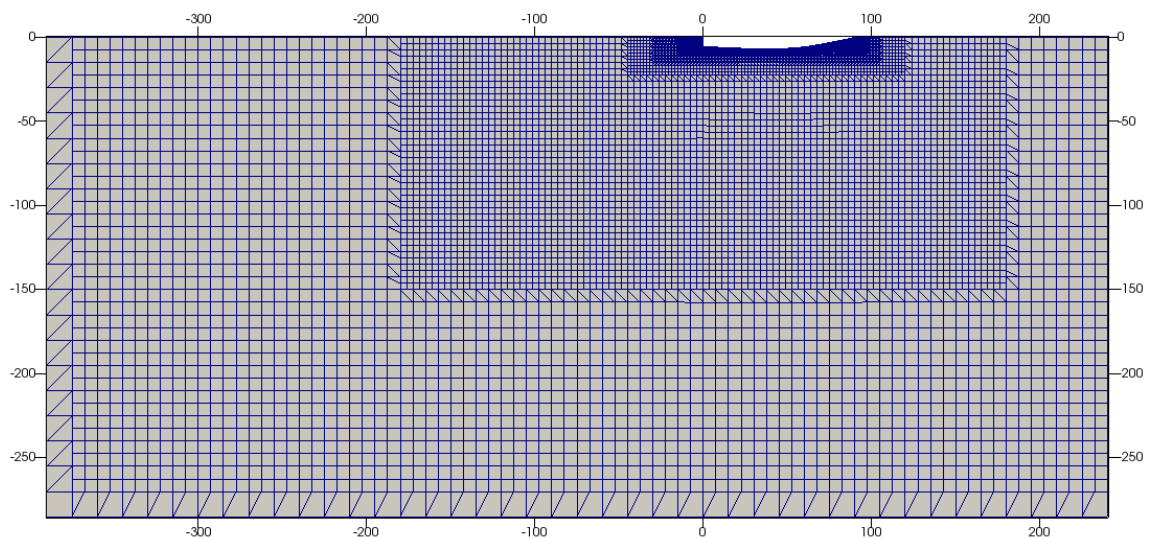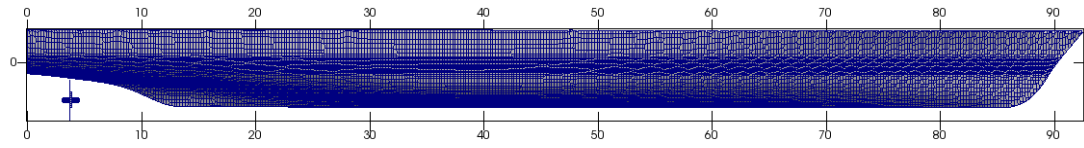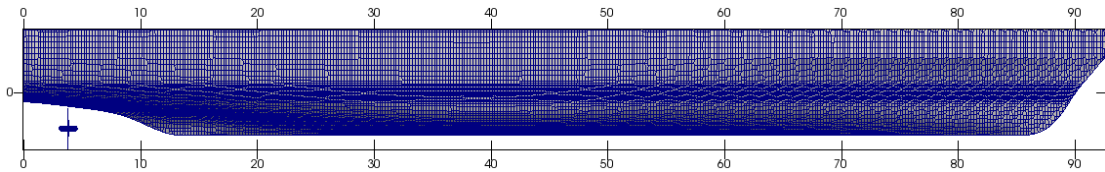Figure 6.27: D1 mesh with the extended freeboard for following waves simulations.

For wave modelling, the relaxation zone thickness have been set to about 1 to 2 wave lengths for the inlet and side boundaries, and about 2.5 to 4 wave lengths for the outlet boundary, depending on the wavelengths chosen for the simulation cases.

The relaxation zone parameter used is equal to the time step and the blending function is the exponential one reported in Jasak et al. (2015). The calculated values of the reflection coefficient (Perić et al., 2018) go from 0.001704919, corresponding to the shortest wave and thickest relaxation zone, to 0.237066911 corresponding to the longest wave and thinnest relaxation zone.

Figure 6.28 shows two types of refinements made, around the waterline for wave height and around the hull for longitudinal diffusion. A refinement region around the waterline, of about 1.8 m height, has been meshed in order to have at least 15 cells per wave height for the lowest wave and up to 24 cells for the highest wave. Refinements for the longitudinal wave diffusion have been applied in order to have from about 20 cells per wave length, for the shortest wave, up to 30 cells, for the longest wave in the outer refinement region zone, and from 320 up to 480 cell in the inner refinement region near the hull. In the figure the black line represents the free surface of the wave profile.
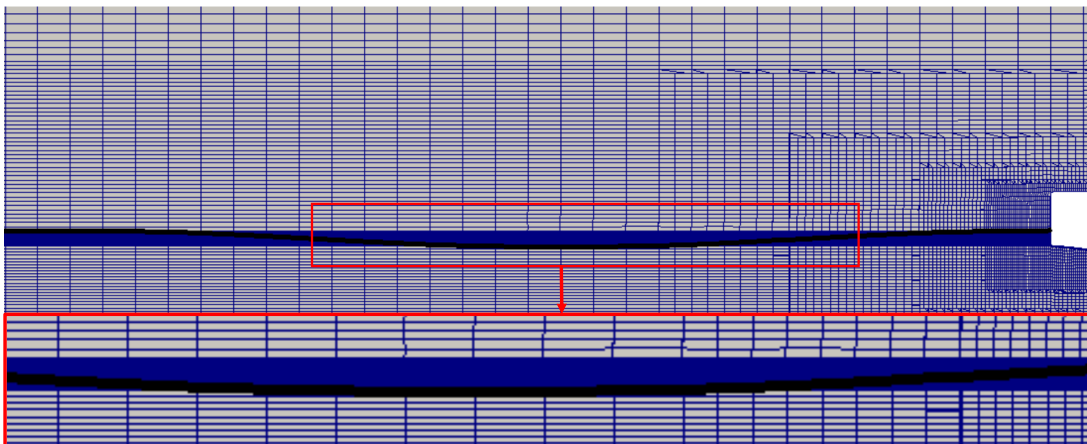

Figure 6.28: Mesh refinements: around waterline and for longitudinal diffusion, where the black curve represents free surface.

With the unstructured grid and for small motion simulation cases, (considering only the surf-riding phenomenon and excluding the capsizing event) in this work a body fitted grid with rigid displacement deformation has been used instead of the overset mesh, which has been used in CFDShip Iowa (Carrica et al., 2008).

The turbulent model used is the $k - \omega$ SST with the values listed in Table 6.3.

Table 6.3: Initial and inlet fluid flow properties used in the CFD simulations.

Turbulence properties			
Freestream velocity	**V**	11.883	m/s
Turbulence kinetic energy	k	0.084752	m^2/s^2
Specific turbulence dissipation	ω	8475.1935	1/s
Turbulence intensity	$\mathbf{T_u}$	2	%
Kinematic viscosity	ν	$1.00E-06$	m^2/s

In a first attempt for fast and steady simulations, as for calm water resistance and self-propulsion, adjustable time step was considered based on fixed Courant number equal to 20. For transient simulations in surf-riding conditions, Courant number has been set to 10. Although a time step sensitivity study has not been conducted, the large time steps has been proved to achieve acceptable results as reported in the works of Jasak et al. (2018), for full scale self-propulsion simulations, and in Vukčević and Jasak (2015) for seakeeping simulations.

For the PIMPLE algorithms, each number of the inner and outer loops has been set to 4.

The code validation and verification has been extensively reported in Gatin et al. (2015b) for calm water resistance calculations, in Vukčević et al. (2016b) for wave propagation, in Jasak et al. (2018) for self-propulsion cases and in Gatin et al. (2017) for grid sensitivity in seakeeping simulations.

The validation of the CFD case set up has been conducted for full scale calm water resistance comparing the results with EFD data, available from the publication of Kracht and Jacobsen (1992).

The calculations for bare hull steady state resistance, R_{HS}, have been performed with free heave (sinkage) and pitch (trim) motions and fixed surge motion, with no wave generation, and have been conducted for 4 different speeds, in a range of Froude number from 0.3 to 0.45. Table 6.4 and Figures 6.29, 6.30 and 6.31 report the comparison between CFD results and EFD results for bare hull full scale resistance, trim and sinkage calculations. The comparison shows the following results: the relative errors for resistance are about 1-4 % ; trim values differences are ranging from -0.02 to 0.06 degrees; sinkage differences go from -0.045 to -0.002 meters. This is in line with the validation studies for the Naval Hydro Pack (Gatin et al., 2015a).

Table 6.4: Calm water resistance comparison between CFD and EFD results.

	RESISTANCE			TRIM			SINKAGE		
FN	**CFD**	**EFD**	**Rel Er**	**CFD**	**EFD**	**diff**	**CFD**	**EFD**	**diff**
-	N	N	-	deg	deg	deg	m	m	m
0.3	173480	179276	3.2%	-0.08	-0.07	-0.01	-0.218	-0.219	-0.002
0.35	266368	257118	-3.6%	-0.07	-0.13	0.06	-0.297	-0.252	-0.045
0.4	461385	465826	1.0%	0.28	0.24	0.04	-0.402	-0.432	-0.03
0.45	723005	754591	4.2%	0.86	0.88	-0.02	-0.486	-0.501	-0.015
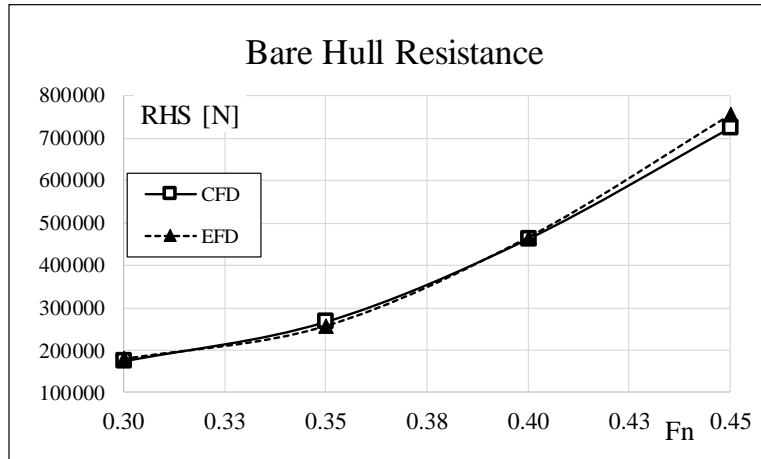
Figure 6.29: Comparison of CFD and EFD calm water bare hull resistance, RHS [N], for Froude number range of Fn=0.3-0.45.
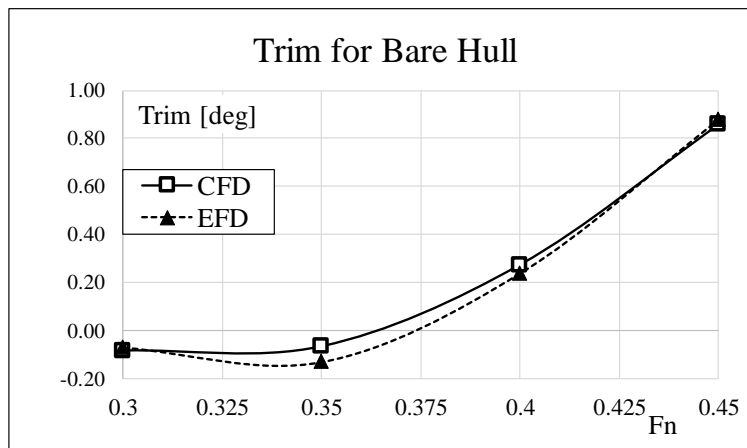
Figure 6.30: Comparison of CFD and EFD trim [deg] variations.
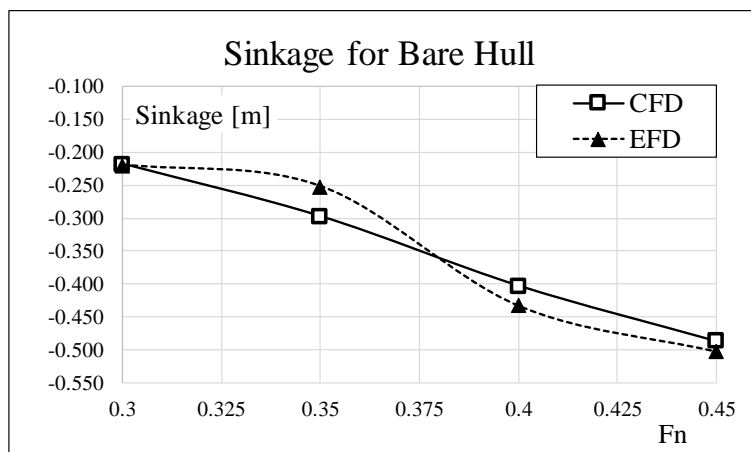
Figure 6.31: Comparison of CFD and EFD sinkage [m] variations.

In order to predict the number of revolution needed to reach each ship speed, the propeller controller of the actuator disk is set up to achieve zero residual forces (that is zero difference between resistance and thrust).

To compare the trend and order of magnitude, CFD bare hull resulting number of revolutions are represented together with the EFD ones referring to the appended hull, which is the only self-propulsion data available, as shown in Figure 6.32. The trend of the two curves is qualitatively similar but not quantitatively. The observed difference is due to the major resistance of the EFD appended hull case and it has been considered acceptable to validate the numerical set up.

The obtained values of number of revolutions have been used to perform simulations in waves to predict surging or surf-riding tendency, imposing the fixed number of revolutions corresponding to the desired value of Fn in calm water.

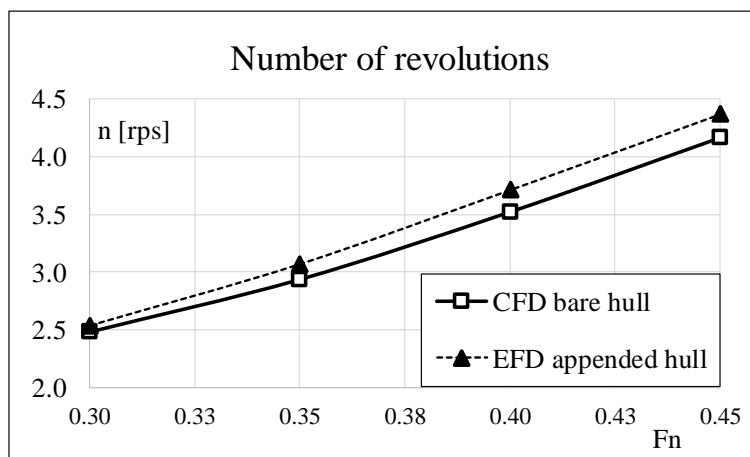Figure 6.32: Comparison of CFD bare hull and EFD appended hull number of revolutions, n [rps].

6.5.2 Calculation Results

After testing and validating the numerical set up in calm water, D1 hull behaviour in regular waves has been tested in different operational conditions and for various wave characteristics, to investigate whether the ship will be caught by the wave, leading to surf-riding phenomenon or whether she will remain in safe surging motion.

Although an extensive grid study is not performed due to the limited availability of time and computational resources, the set ups follow the basic grid study, reported by (Gatin et al., 2017) and, in a first attempt, are considered sufficient to validate the present simulations in waves.

Since CFD simulations are time consuming, the test cases have been carefully chosen following IMO recommendations, (SDC6/WP6, 2019), and surf-riding limits obtained by 1-DOF model approach.

From the 1-DOF approach, results have been obtained for the combination of four Froude numbers, equal to 0.3, 0.35, 0.4 and 0.433 (corresponding to ship speed of 8.913, 10.398, 11.883 and 12.864 m/s) and four wavelength to ship length values, equal to 0.75, 1, 1.25 and 1.565 (corresponding to wave celerity of 10.264, 11.852, 13.251 and 14.827 m/s). Through the phase plane analysis, surf-riding limits have been found in terms of wave heights.

1-DOF surf-riding limits have been performed for the loading case corresponding to draft T2, the resistance coefficients considered referred to the bare hull experimental tests and the number of revolutions set for each Fn case has been taken equal to the value obtained by CFD simulations.

Table 6.5 reports the first (lower) wave height value at which the ship experienced surf-riding phenomenon over the 2nd threshold by 1-DOF approach. The non reported limit values refer to cases in which the ship speed was greater than wave celerity and the only possible phenomenon could be wave blocking. Although wave blocking limits could be easily found with the same 1-DOF procedure used for the surf-riding ones, the study is focused only on the most dangerous phenomenon of surf-riding and wave blocking limits are set aside.

Table 6.5: Wave heights values at which the 2nd threshold of surf-riding occurs.

	H [m] Limits for 1-DOF			
	$\lambda/L = 0.75$ $\lambda[m] = 67.5$ $T[s] = 6.576$	$\lambda/L = 1$ $\lambda = 90$ $T = 7.594$	$\lambda/L = 1.25$ $\lambda = 112.5$ $T = 8.49$	$\lambda/L = 1.565$ $\lambda = 140.9$ $T = 9.5$
Fn = 0.30	3.07	4.29	6.62	10.40
Fn = 0.35	-	1.70	3.41	6.00
Fn = 0.40	-	-	1.56	3.10
Fn = 0.433	-	-	-	1.80

CFD simulations have been conducted for some of the 1-DOF cases. The wave to ship lengths have been set by imposing an initial wave period and the Froude number case by fixing the number of revolutions corresponding to the Fn in calm water conditions. For each wave length-Froude number case, the simulations have been performed starting with a value of wave height close to the limit one for which the ship experienced surf-riding by 1-DOF approach. From CFD simulations, analysing the ship speed variations and the wave celerity, oscillating surging or converging surf-riding motions can be observed. If surging motion was observed then a new simulation with increased wave height was performed until surf-riding phenomenon occurred. The simulations have been performed for about 200 or 300 seconds of physical time for surging conditions and 60-150 seconds for surf-riding conditions in full scale. Surging simulations have been performed for longer time in order to observe at least 2 or 3 wave encounter periods, and since the tested cases had wave frequency close to zero, the wave encounter periods were high. Surf-riding phenomenon instead could be observed in less time.

Table 6.6 reports the values of wave heights set in CFD simulations for each wave length and ship speed case, and the corresponding observed motion: surging (surge) or surf-riding (SURF).

Table 6.6: Observed motion, surging (surg) or surf-riding (SURF), in CFD simulation for different wave and speed conditions, defining surf-riding limits in terms of wave height.

	H [m] CFD			
	$\lambda/L = 0.75$	$\lambda/L = 1$	$\lambda/L = 1.25$	$\lambda/L = 1.565$
Fn = 0.3	surge -› 3, 4.5, 5.5	-	-	-
Fn = 0.35	-	surge -›1.8, 3 SURF-› 3.5, 4	surge -› 3.5, 4.5 (ph π) SURF-› 4.5 (ph 0), 5.5	-
Fn = 0.4	-	-	surge -› 1.5, 2 SURF-› 3, 3.5, 4	-
Fn = 0.433	-	-	-	surge -› 2.5 SURF-› H 3.5

The averaged values of y^+ of the first layer from the solid walls were about 5870 around the hull patch, and 1328 around the hub, for case $\lambda/L = 1, Fn = 0.35$ and $H = 3.5m$, and about 8481 around the hull patch and 1279 around the hub patch, for case $\lambda/L = 1.25, Fn = 0.4$ and $H = 3.5m$.

The 1-DOF calculations were performed on a standard notebook with 4 cores and processor Intel Core i7-77ooHQ CPU @ 2.80GHz, and the CPU time was around few second. All CFD simulations were ran in parallel using 4 cores computer with Intel Core i7-4820K CPU @ 3.70GHz, and the CPU time reached up to 5 or 6 days for each wave case.

Figure 6.33 shows a CFD simulation of D1 hull surf-riding at Froude number equal to $Fn = 0.35$ in sea conditions with wave to ship length equal to $\lambda/L = 1$ and steepness equal to $H/\lambda = 1/22.5$, which corresponds to wave height equal to $H = 4m$.
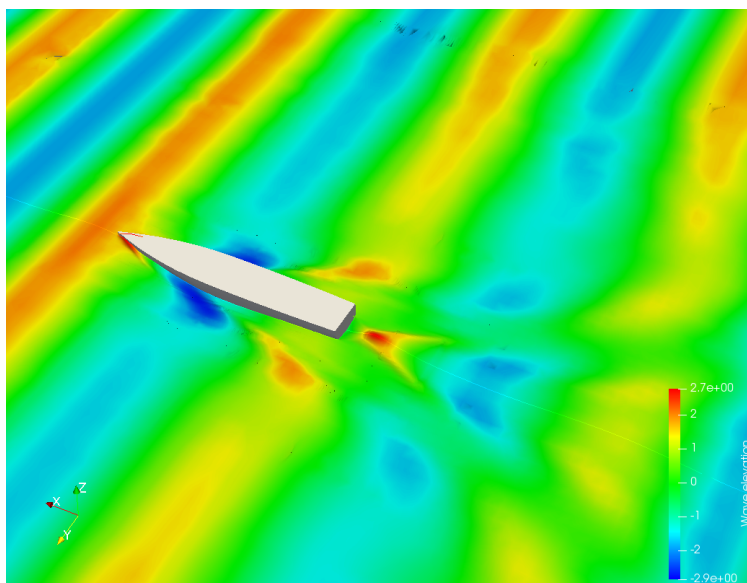

Figure 6.33: CFD simulation of D1 ship surf-riding in wave conditions $\lambda/L = 1$ and H = 4m for Fn = 0.35 case.

From CFD simulations, surf-riding occurrence has been identified by analysing the ship speed variations, compared with wave celerity, and the phase plane transitions for a fixed number of revolutions, a fixed wave length and for increasing wave heights, as shown in Figures 6.34 and 6.35.

The cases with fixed $\lambda/L = 1$ and number of revolutions set to obtain $Fn = 0.35$ and increasing wave height are shown in Figure 6.34. Figure 6.34 a) reports the ship speed variations compared to the wave celerity value in time domain simulations. When ship speeds are lower than wave celerity the surging condition was identified, as in the first 2 diagrams (where $H/\lambda = 1/50$ and $H/\lambda = 1/30$) and for increasing wave height when the ship speed reaches the wave celerity the surf-riding phenomenon was observed, as in the last two figures (for $H/\lambda = 1/25.7$ and $H/\lambda = 1/22.5$).

In Figure 6.34 b) surge motion and surge velocity are analysed in the phase plane diagram. It can be seen that in surging conditions, displacement and velocity oscillate, while in surf-riding conditions, they tend to the equilibrium point (fixed point).

In Figure 6.35 the same analysis for surf riding occurrence is done for case with fixed $\lambda/L = 1.25$ and number of revolutions set to obtain $Fn = 0.4$ in calm water.
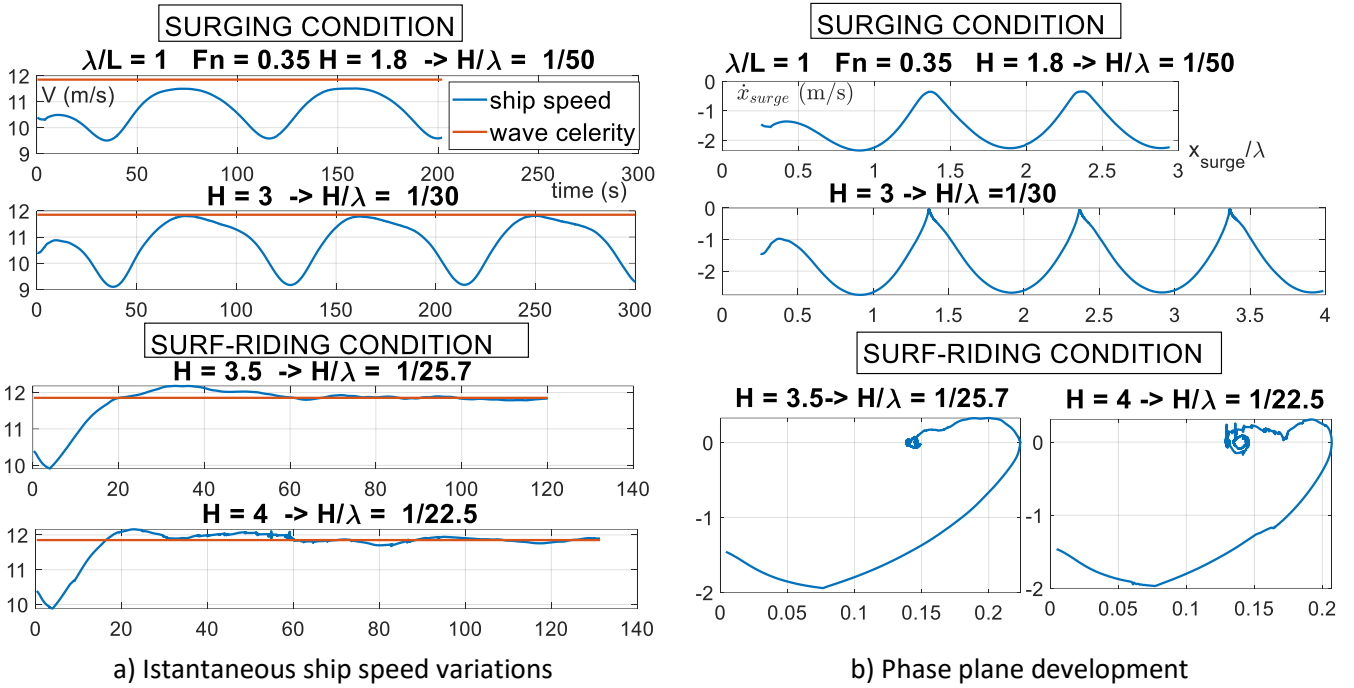
Figure 6.34: Surging to surf-riding transition for case $\lambda/L = 1$, $Fn = 0.35$ with increasing wave heights.
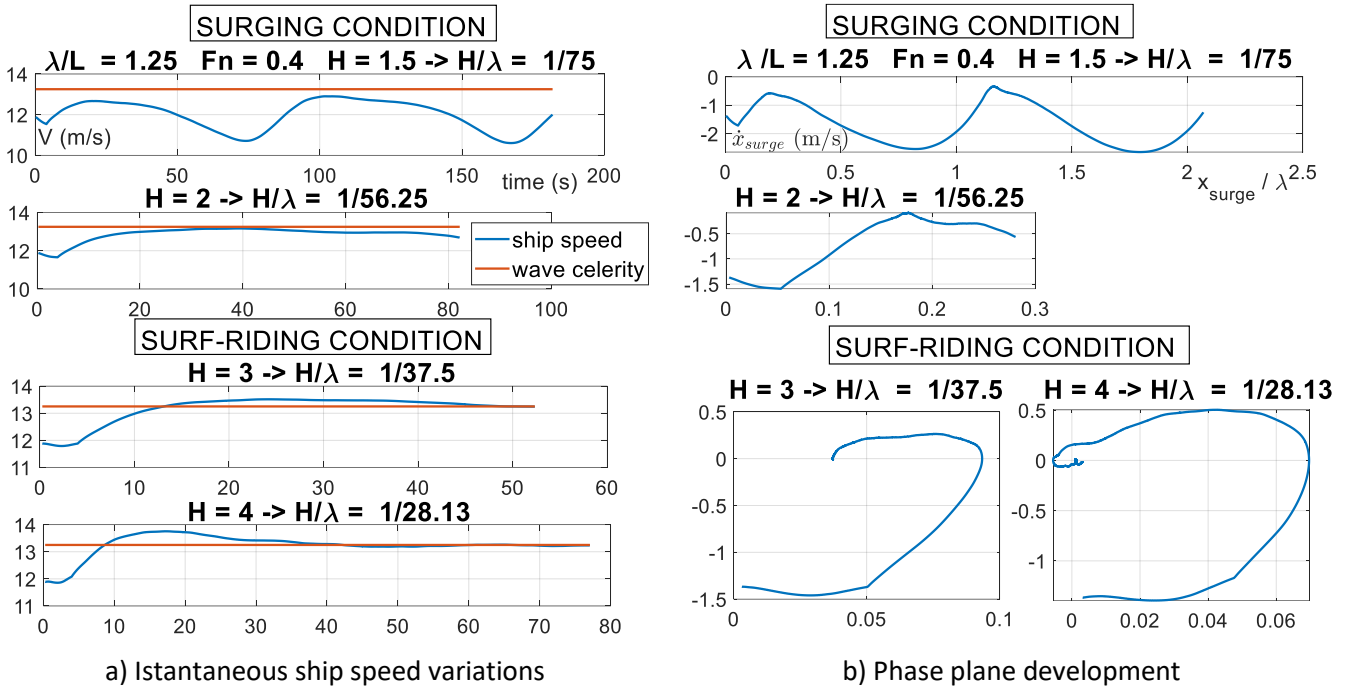
Figure 6.35: Surging to surf-riding transition for case $\lambda/L = 1.25$, $Fn = 0.4$ with increasing wave heights.

In CFD simulation for wave cases $\lambda/L = 0.75$ the ship never experienced surf-riding phenomenon up to wave height equal to 5.5 m ($H/\lambda = 1/12$). This can be due to the increased resistance at bow for waves shorter than ship length when the wave crest is around stern, and therefore the forces balance will lead to surge motion. The dynamic

pressure distributions on the hull for wave height of 4 m and wave to ship lengths equal to 0.75, 1 and 1.25 are shown respectively in Figures 6.36, 6.37 and 6.38, where the black curve represents the free surface. Cases of $\lambda/L = 1$ and 1.25 are shown for a time instant when the ship reaches surf-riding equilibrium, therefore the wave crest is around the stern. For case $\lambda/L = 0.75$, since the ship never goes in surf-riding, the time instance represented is also chosen when the wave crest is around the stern position. It can be noticed that shorter the wave, greater is the zone of high pressures on the bow, and longer the wave higher the pressure at the stern position.
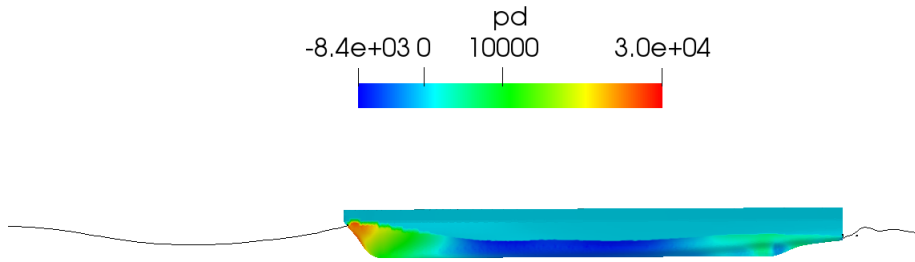
Figure 6.36: Dynamic pressure distribution for case $\lambda/L = 0.75$, $Fn = 0.3$ and $H = 4$ m.
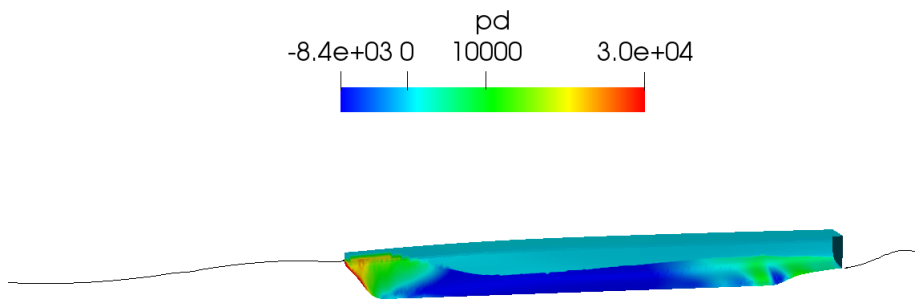
Figure 6.37: Dynamic pressure distribution for case $\lambda/L = 1$, $Fn = 0.35$ and $H = 4$ m.
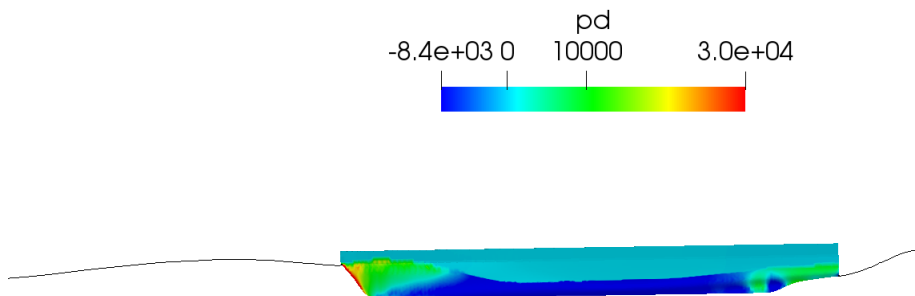
Figure 6.38: Dynamic pressure distribution for case $\lambda/L = 1.25$, $Fn = 0.4$ and $H = 4$ m.

The dynamic equilibrium in CFD simulations is given by Equation 6.2 :

$$M\ddot{x} + F_{TOT\ X} - T = 0 \tag{6.2}$$

where:

$M\ddot{x}$ is the inertia force;

$F_{TOT\ X}$ is the total force in the X direction which includes the hull resistance in waves R_{TW}, the wave force F_{WX}, and added mass force, $M_X\ddot{x}$, as described in Equation 6.3:

$$F_{TOT\ X} = M_X\ddot{x} + R_{TW} + F_{WX} \tag{6.3}$$

T is the thrust force obtained by the propeller actuator disk.

The $F_{TOT\ X}$ and T forces calculated in waves for cases $\lambda/L = 1$ and $Fn = 0.35$, and $\lambda/L = 1.25$ and $Fn = 0.4$, are reported in Figures 6.39 and 6.40 respectively.

The forces are reported together with the relative position between the wave crest and the ship stern.

For lower wave heights, the forces and relative crest position oscillating in time indicate surging conditions. For higher waves the forces and the relative crest position remain constant and defining surf-riding occurrence.
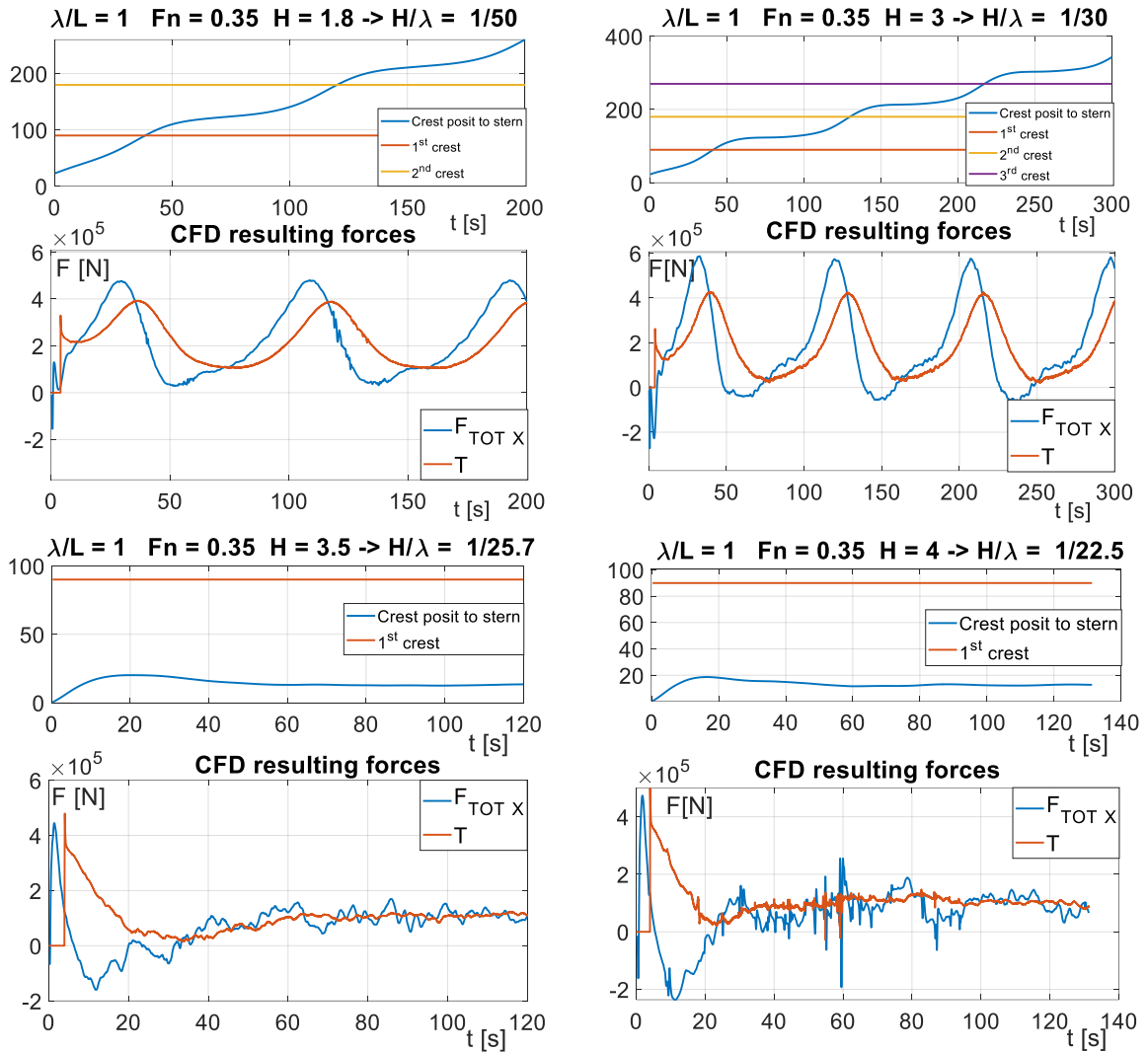
Figure 6.39: CFD calculated forces: F_X and thrust for $\lambda/L = 1$ and $Fn = 0.35$, for increasing wave heights.
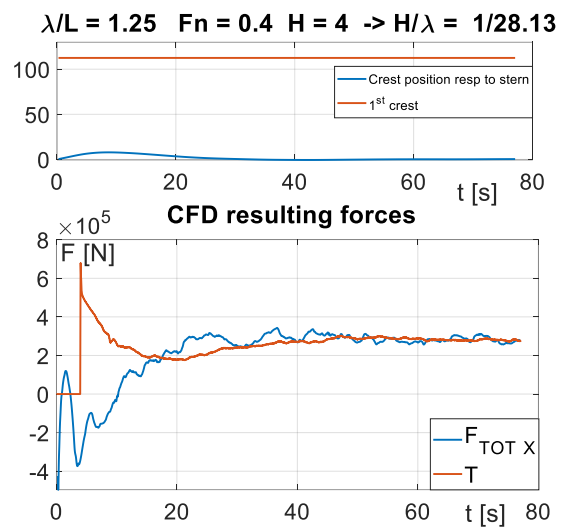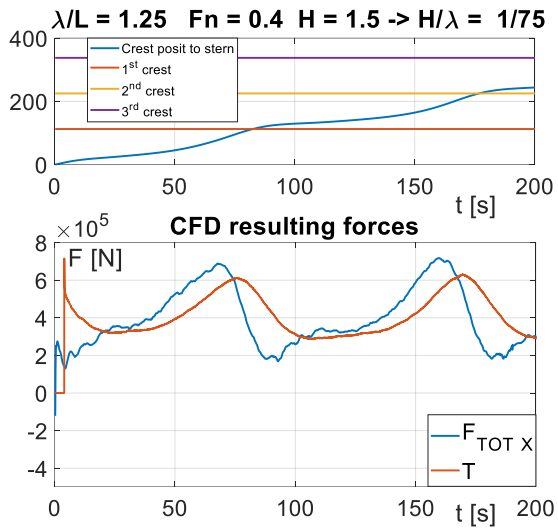
Figure 6.40: CFD calculated forces: Total Force in X direction, $F_{TOT\ X}$, and thrust, T, for $\lambda/L = 1.25$ and $Fn = 0.4$, for increasing wave heights.

Chapter 7

Possible Improvements for 1-DOF Methodology

7.1 Evaluation of Resistance and Thrust Tendencies in Waves: Comparison Between 1-DOF and CFD Approaches

A qualitative and quantitative comparison has been made between 1-DOF and CFD forces to analyse the differences between the two approaches.

For a direct comparison of resistance, knowing the CFD forces decomposition, as in Equation (6.2), and the 1-DOF force decomposition, as in Equation (3.3), the resistance in waves calculated by CFD can be obtained by the following decomposition:

$$R_{TW} = F_{TOT\ X} - M_X\ddot{x} - F_{WX} \qquad (7.1)$$

where the wave force, F_{WX}, including both Froude Krylov and diffraction component, is obtained by Hydrostar calculations.

Therefore, the total resistance in waves, obtained by Equation (7.1), and the thrust evaluated with CFD simulations are compared with the respective forces, resistance R_{CW} and thrust T_{CW}, calculated with calm water 1-DOF approach considering the ship speed variations defined by $u = \dot{x} - c$, where the surge displacement, x, has been obtained directly from CFD resulting motions.

All the forces have been plotted together with the relative wave crest position referred to ship stern.

From the analysis of Figure 7.1 for wave case $\lambda/L = 1$ and increasing wave heights, it can be seen how calm water approximations, considering the diffraction effect in the wave force, are very close to the forces calculated by CFD simulations in both surging and surf-riding cases.

The difference in thrust may be attributed to the different propeller inflow velocity, since the wave field velocity is taken into consideration only in CFD calculations. When the wave crest is around the stern position, the thrust evaluated by CFD is greater because the actual inflow velocity at the propeller is less than the ship speed, since on wave crest the wave field velocity is opposite to the ship speed. When the crest is around amidships and the trough is around the propeller, the inflow velocity is increased, since wave field and ship speed have the same directions, and therefore the thrust is lower compared to 1-DOF.

The resistance differences may be attributed to the variations of the wetted surface and wave force changes under the actual wave profile considered only in the CFD simulations, since diffraction and Froude-Krylov components are calculated under calm water profile in the 1-DOF approach.

Moreover, from Figures 7.1 and 7.3 it can be noticed that when the wave crest is around the stern position, in which surf-riding normally occurs, the resistance calculated with 1-DOF approach is lower than the one obtained by CFD. Therefore 1-DOF resistance values are underestimated, especially in the described relative position between ship and wave, so making surf-riding more likely to occur.

Figure 7.1: Resistance and Thrust trends and differences with CFD and 1-DOF approach for $\lambda/L = 1$ and $Fn = 0.35$ in surging and surf-riding condition.

Figure 7.2 reports the forces comparison for wave case $\lambda/L = 1.25$ in surging and surf-riding condition. Although resistance values are similar in both approaches for the surging case, in surf-riding condition the CFD resistance obtained from the force decomposition is underestimated. This difference may be due to the actual wave profile neglected in the wave force calculations performed by Hydrostar.

Figure 7.3 reports the forces comparison for wave case $\lambda/L = 0.75$ in the only surging condition, since no surf-riding phenomenon has been detected up to 5.5 m wave height. It can be observed that when the wave crest is around the stern, the difference between the decomposed CFD resistance and the calculated 1-DOF one is increasing according to increasing wave heights. The underestimation of the 1-DOF resistance makes surf-riding less likely to occur.
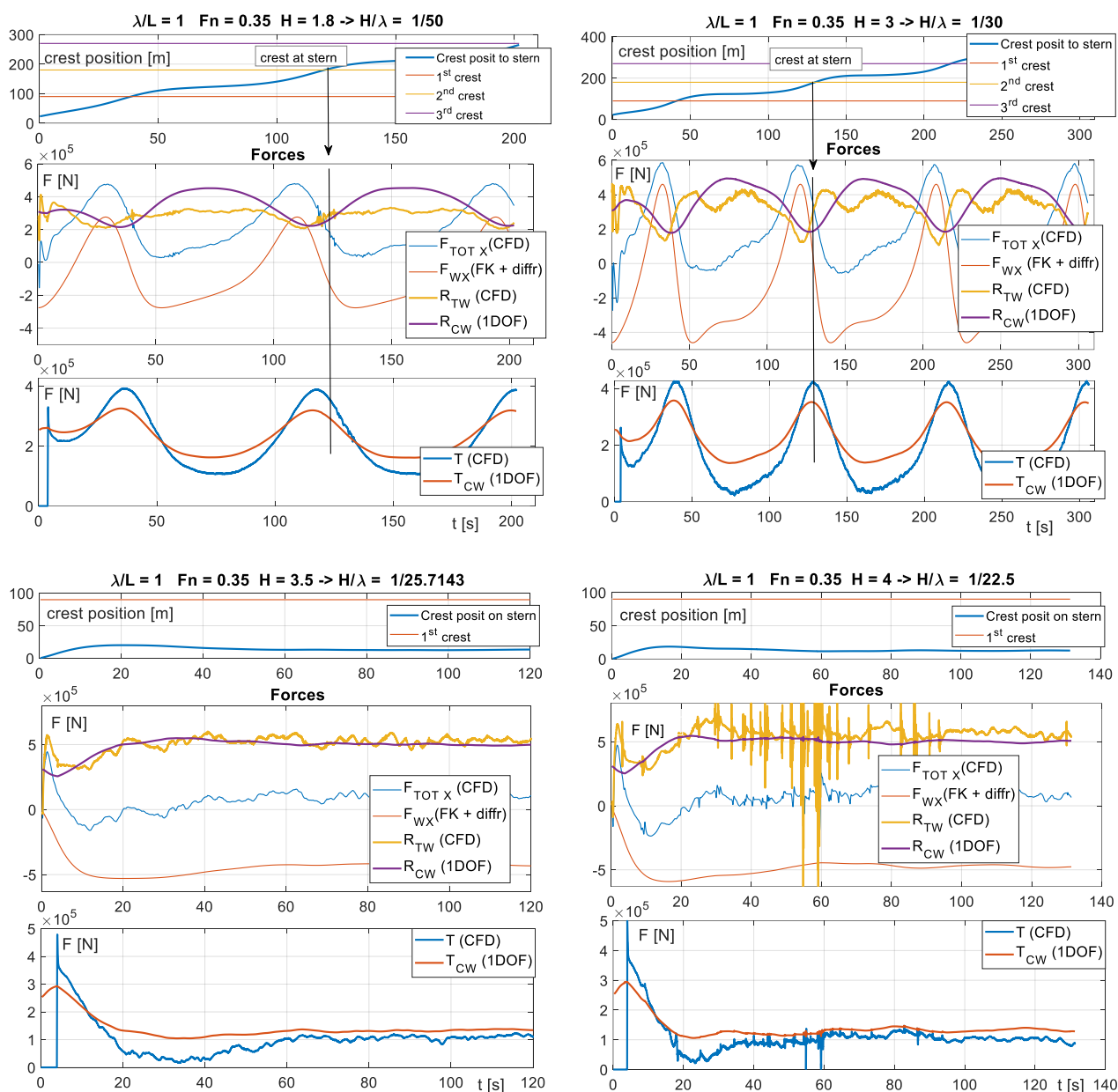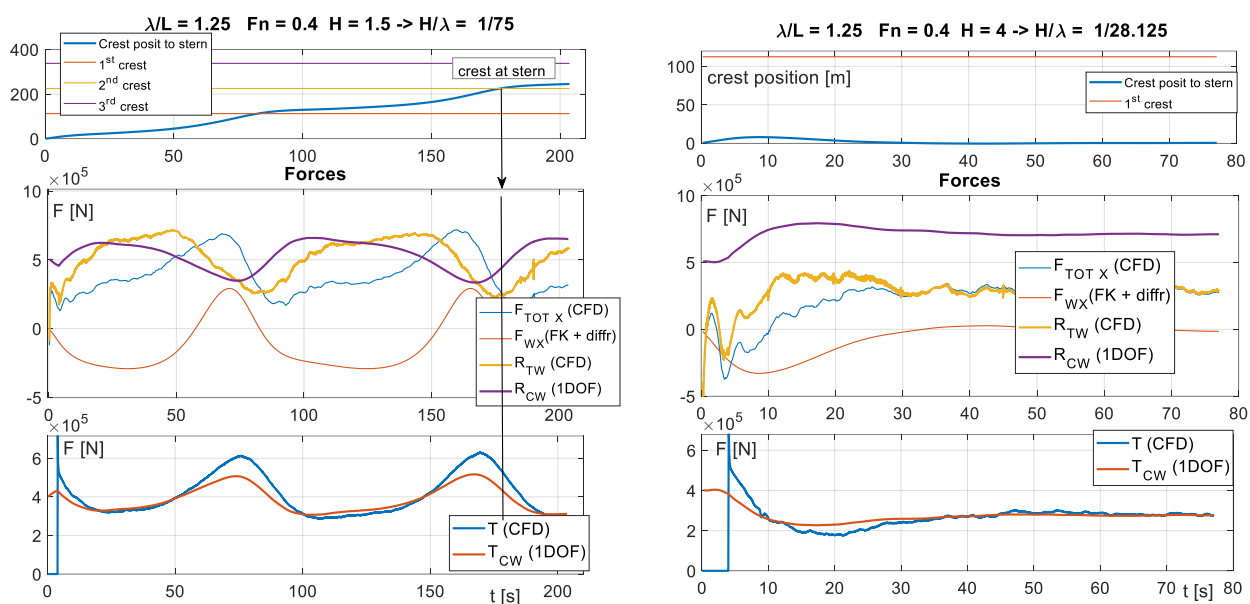

Figure 7.2: Resistance and Thrust trends and differences with CFD and 1-DOF approach for $\lambda/L = 1.25$ and $Fn = 0.4$ in surging and surf-riding condition.
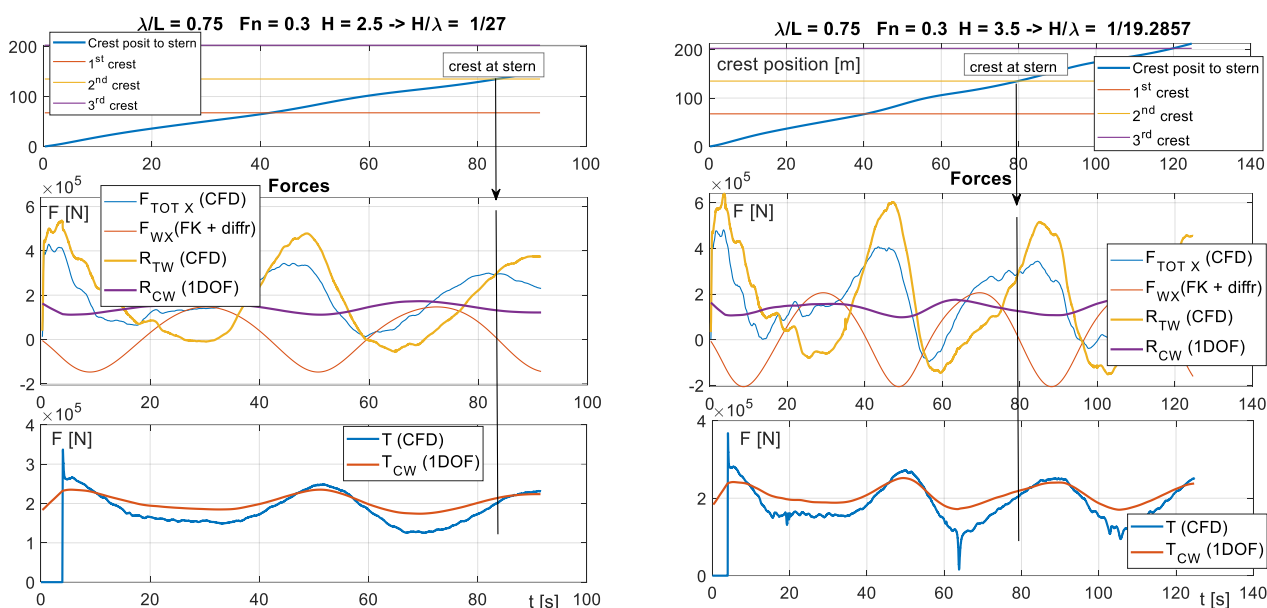

Figure 7.3: Resistance and Thrust trends and differences with CFD and 1-DOF approach for $\lambda/L = 0.75$ and $Fn = 0.3$ in Surging conditions.

7.2 Wave Particle Contributions

Having analysed the forces calculated with CFD simulations, a part of the differences has been attributed to the wave field influence on the ship speed which is not included in the 1-DOF model.

The modifications of the surge mathematical model that take into account the effect of wave particle velocity in resistance and thrust calculations have been done by Umeda (1984) Hashimoto et al. (2004), and Spyrou (2006).

Considering the reference systems described in Section 3, the wave potential can be written in fixed to earth or fixed to ship reference systems respectively as:

$$\phi = cAe^{-kz}\sin(\omega t - kX) = cAe^{-kz}\sin(\omega_e t - kx) \tag{7.2}$$

where: X is the distance of ship trough from fixed to Earth reference system, A is the wave amplitude, k is the wave number, ω is the wave frequency and ω_e is the wave encounter frequency.

Therefore wave velocity in x direction, in fixed to ship coordinate systems, is expressed as:

$$u_x = \frac{\partial \phi}{\partial x} = -cAke^{-kz}\cos(\omega_e t - kx) \tag{7.3}$$

This wave velocity component in surge direction can be added to the ship speed considered in the calculation of calm water resistance and to the propeller inflow velocity used to evaluate thrust. The influence of the wave field will therefore be proportional to wave heights and non-negligible for higher waves.

An approximated semi-empirical formula, that takes into account the wave field influence, can be added to the still-water value of ship speed, used to calculate the resistance, by defining a wave particle velocity averaged on the ship length, L. Following Spyrou (2006) this correction formula can be expressed as:

$$
\begin{aligned}
\overline{u}_w &= \frac{1}{L}\int_{-L/2}^{L/2}\frac{\partial \phi}{\partial x}(x, x_s)\,dx_s = -\frac{1}{L}\int_{-L/2}^{L/2}cAke^{-kz}\cos k(x + x_s)\,dx_s = \\
&= -\frac{cAke^{-kz}}{L}\int_{-L/2}^{L/2}[\cos kx \cos kx_s - \sin kx \sin kx_s]\,dx_s = \\
&= -\frac{cAke^{-kz}}{L}\cos kx \int_{-L/2}^{L/2}\cos kx_s dx_s = -\frac{cAke^{-kz}}{kL}\cos kx\; 2\sin k\frac{L}{2} = \\
&= -\frac{cAke^{-k(\overline{d}/2)}\sin\left(\frac{\pi L}{\lambda}\right)}{\frac{\pi L}{\lambda}}\cos kx = -a\cos kx
\end{aligned}
\tag{7.4}
$$

where: x is the distance of the wave trough from ship center of gravity, x_s is the distance of each ship section from center of gravity and $\overline{d}/2$ is the averaged local draft for ship length. Since the wave velocity is averaged in space along the ship length for each relative position of wave and ship, the time dependence is neglected.

Analysing the formula, it can be observed that for wavelengths equal to ship lengths the averaged speed on the total hull will be zero, therefore the wave fields influences the ship speed only if the wave length is different from the ship length.

The influence of the wave particle velocity on the inflow velocity of the propeller can be considered by adding to ship speed an approximated contribution of the horizontal wave particle velocity averaged on the propeller disk. Since the propeller is positioned at about L/2 from G, the relative position between wave trough and propeller is $\left(x + \frac{L}{2}\right)$. Moreover the propeller feels the wave particles moving with a relative velocity between ship and wave, $c - u = -\dot{x}$, therefore the correction formula, following Spyrou (2006), can be expressed as:

$$
\begin{aligned}
\overline{u}_w^p &= -\frac{1}{D_P} \int_{z_0}^{z_0+D_P} Ak(c-u)e^{-kz} \cos\left[k\left(x+\frac{L}{2}\right)\right] \, dz = \\
&= -\frac{1}{D_P} Ak(c-u) \cos\left[k\left(x+\frac{L}{2}\right)\right] \int_{z_0}^{z_0+D_P} e^{-kz} dz = \\
&= -\frac{1}{D_P} Ak(c-u) \cos\left[k\left(x+\frac{L}{2}\right)\right] \left(-\frac{1}{k}\right) e^{-kz_0} \left(e^{-kD_P} - 1\right) = \\
&= \frac{1}{D_P} A \, e^{-kz_0} \left(1 - e^{-kD_P}\right) \cos\left[k\left(x+\frac{L}{2}\right)\right] \dot{x} = b \cos\left[k\left(x+\frac{L}{2}\right)\right] \dot{x}
\end{aligned}
$$

(7.5)

where: z_0 is propeller's submergence and D_P is the propeller's diameter.

Adding these fluctuating parts of velocity in the resistance and thrust formulas, neglecting the smaller second-order and higher terms and expressing the ship speed as sum of wave celerity and surge velocity, $u = c + x$, the new formulations for resistance and thrust become:

$$
\begin{aligned}
R =& r_1(u + \overline{u}_w) + r_2(u + \overline{u}_w)^2 + r_3(u + \overline{u}_w)^3 + r_4(u + \overline{u}_w)^4 + r_5(u + \overline{u}_w)^5 = \\
=& r_1 u + r_2 u^2 + r_3 u^3 + r_4 u^4 + r_5 u^5 - a(r_1 + 2r_2 u + 3r_3 u^2 + 4r_4 u^3 + 5r_5 u^4) \cos kx = \\
=& r_1(c + \dot{x}) + r_2(c + \dot{x})^2 + r_3(c + \dot{x})^3 + r_4(c + \dot{x})^4 + r_5(c + \dot{x})^5 + \\
&- a(r_1 + 2r_2(c + \dot{x}) + 3r_3(c + \dot{x})^2 + 4r_4(c + \dot{x})^3 + 5r_5(c + \dot{x})^4) = \\
=& r_1 c + r_2 c^2 + r 3_c^3 + r_4 c^4 + r_5 c^5 + \\
&+ \left(r_1 + 2r_2 c + 3r_3 c^3 + 4r_4 c^3 + 5r_5 c^4\right) \dot{x} + \\
&+ \left(r_2 + 3r_3 c + 6r_4 c^2 + 10r_5 c^3\right) \dot{x}^2 + \\
&+ \left(r_3 + 4r_5 c + 10r_5 c^2\right) \dot{x}^3 + \left(r_4 + 5r_5 c\right) \dot{x}^4 + r_5 \dot{x}^5 + \\
&- a \left(r_1 + 2r_2 c + 3r_3 c^2 + 4r_4 c^3 + 5r_5 c^4\right) \cos kx + \\
&- a \left(2r_2 + 3 \cdot 2r_3 c + 4 \cdot 3r_4 c^2 + 5 \cdot 4r_5 c^3\right) \dot{x} \cos kx + \\
&- a \left(3r_3 + 4 \cdot 3r_4 c + 5 \cdot 6r_5 c^2\right) \dot{x}^2 \cos kx + \\
&- a \left(4r_4 + 5 \cdot 4r_5 c\right) \dot{x}^3 \cos kx - a \left(5r_5\right) \dot{x}^4 \cos kx
\end{aligned}
$$

(7.6)

$$T = N_P \left\{ \tau_0 n^2 + \tau_1 (u + \overline{u}_w^p) n + \tau_2 (u + \overline{u}_w^p)^2 \right\} =$$

$$= N_P \left\{ \tau_0 n^2 + \tau_1 n \left(c + \dot{x} - b \cos \left[k \left(x + \frac{L}{2} \right) \right] \dot{x} \right) + \tau_2 \left(c + \dot{x} - b \, \cos \left[k \left(x + \frac{L}{2} \right) \right] \dot{x} \right)^2 \right\} =$$

$$= N_P \left(\tau_2 c^2 + \tau_1 nc + \tau_0 n^2 \right) + N_P \left(2\tau_2 c + \tau_1 n \right) \dot{x} - N_P \left\{ \left(2\tau_2 c + \tau_1 n \right) b \, \cos \left[k \left(x + \frac{L}{2} \right) \right] \right\} \dot{x} +$$

$$+ N_P \tau_2 \dot{x}^2 - N_P \left\{ 2\tau_2 b \, \cos \left[k \left(x + \frac{L}{2} \right) \right] \right\}$$

<div align="right">(7.7)</div>

The wave force for regular wave can be expressed as:

$$F_X = -f_X \sin(kx^*) \tag{7.8}$$

where:

$$f_X = \rho g k \zeta_A \sqrt{F_C^2 + F_S^2} \tag{7.9}$$

where: ζ_A is the wave amplitude, F_C and F_S are the Froude Krylov component in calm water, calculated with the strip theory method (SDC3/WP5, 2016), and $x^* = x - \theta$ with $\theta = -\tan^{-1} \frac{F_C}{F_S}$.

Writing every expression of forces as function of x^*, substituting $x = x^* + \theta$ and $\dot{x}^* = \dot{x}$, and neglecting the squared or higher terms of velocity corrections, the second order nonlinear surge equation, recalling Equation (3.16), becomes:

$$\begin{aligned}
\ddot{x}^* = \frac{1}{M + M_x} \Big[& T_c - R_c - (A_1 \dot{x}^* + A_2 \dot{x}^{*2} + A_3 \dot{x}^{*3} + A_4 \dot{x}^{*4} + A_5 \dot{x}^{*5}) + \\
& - (M_0 + M_1 \dot{x}^* + M_2 \dot{x}^{*2} + M_3 \dot{x}^{*3} + M_4 \dot{x}^{*4}) \cos kx^* + \\
& - (G_0 + G_1 \dot{x}^* + G_2 \dot{x}^{*2} + G_3 \dot{x}^{*3} + G_4 \dot{x}^{*4}) \sin kx^* - f_X \sin(kx) \Big]
\end{aligned} \tag{7.10}$$

where all the coefficients are expressed as:

$$\begin{aligned}
T_C &= N_P (\tau_0 n^2 + \tau_1 nc + \tau_2 c^2) \\
R_C &= r_1 c + r_2 c^2 + r_3 c^3 + r_4 c^4 + r_5 c^5 \\
A_1 &= r_1 + 2(r_2 - N_P \tau_2) c + 3 r_3 c^2 + 4 r_4 c^3 + 5 r_5 c^4 - N_P \tau_1 n \\
A_2 &= r_2 + 3 r_3 c + 6 r_4 c^2 + 10 r_5 c^3 - N_P \tau_2 \\
A_3 &= r_3 + 4 r_4 c + 10 r_5 c^2 \\
A_3 &= r_4 + 5 r_5 c \\
A_5 &= r_5
\end{aligned} \tag{7.11}$$

$$M_0 = -a(r_1 + 2r_2c + 3r_3c^2 + 4r_4c^3 + 5r_5c^4)\cos k\theta$$

$$M_1 = -a(2r_2 + 3\cdot 2r_3c + 4\cdot 3r_4c^2 + 5\cdot 4r_5c^3)\cos k\theta + N_P(2\tau_2c + \tau_1 n)b\cos\left[k\left(\theta + \frac{L}{2}\right)\right]$$

$$M_2 = -a(3r_3 + 4\cdot 3r_4c + 5\cdot 6r_5c^2\cos k\theta + N_P(2\tau_2c)b\cos\left[k\left(\theta + \frac{L}{2}\right)\right]$$

$$M_3 = -a(4r_4 + 5\cdot 4r_5c)\cos k\theta$$

$$M_4 = -a(5r_5)\cos k\theta$$

$$G_0 = a(r_1 + 2r_2c + 3r_3c^2 + 4r_4c^3 + 5r_5c^4)\sin k\theta$$

$$G_1 = a(2r_2 + 3\cdot 2r_3c + 4\cdot 3r_4c^2 + 5\cdot 4r_5c^3)\sin k\theta + N_P(2\tau_2c + \tau_1 n)b\sin\left[k\left(\theta + \frac{L}{2}\right)\right]$$

$$G_2 = a(3r_3 + 4\cdot 3r_4c + 5\cdot 6r_5c^2\sin k\theta + N_P(2\tau_2c)b\sin\left[k\left(\theta + \frac{L}{2}\right)\right]$$

$$G_3 = a(4r_4 + 5\cdot 4r_5c)\sin k\theta$$

$$G_4 = a(5r_5)\sin k\theta$$

$$(7.12)$$

The surge equation has been studied with the nonlinear dynamics procedure as described in Section 3.1.1.

Equation (7.10), transformed in a 1st order system of equations and equal to zero, becomes:

$$T_C - R_C = (G_0 + f_X)\sin kx^* + M_0 \cos ks^* = B\sin(kx^* + \phi) \tag{7.13}$$

where:
$B = \sqrt{(G_0 + f_X)^2 + M_0^2}$ and $\phi = tan^{-1}\frac{M_0}{G_0 + f_X}$.

The fixed points are then defined as:

$$
\begin{aligned}
y_1 &= \left[\sin^{-1}\left(\frac{T_C - R_C}{B}\right) - \tan^{-1}\left(\frac{M_0}{G_0 + f_X}\right)\right]\frac{1}{k} \\
y_2 &= \left[-\sin^{-1}\left(\frac{T_C - R_C}{B}\right) - \tan^{-1}\left(\frac{M_0}{G_0 + f_X}\right) + k\frac{\lambda}{2}\right]\frac{1}{k}
\end{aligned}
\tag{7.14}
$$

Solving Equation (7.10) with Runge-Kutta method, and plotting the solutions of surge displacement and velocity in a phase plane diagram, the surf-riding 2nd thresholds have been found.

7.3 Comparison of Surf-riding Limits with and without Wave Particle Velocity Corrections

To evaluate the contribution of wave field particle velocities, surf-riding 2nd thresholds have been defined for hull D1 in terms of wave steepness by performing the 1-DOF approach with and without the semi-empirical correction formulas taking into account the wave field influence, as shown in Figure 7.4. The comparison has been performed for a wave to ship length range from 1 to 3, as recommended by IMO, and for a Froude number range from 0.3, IMO 1st level limit, to 0.4.
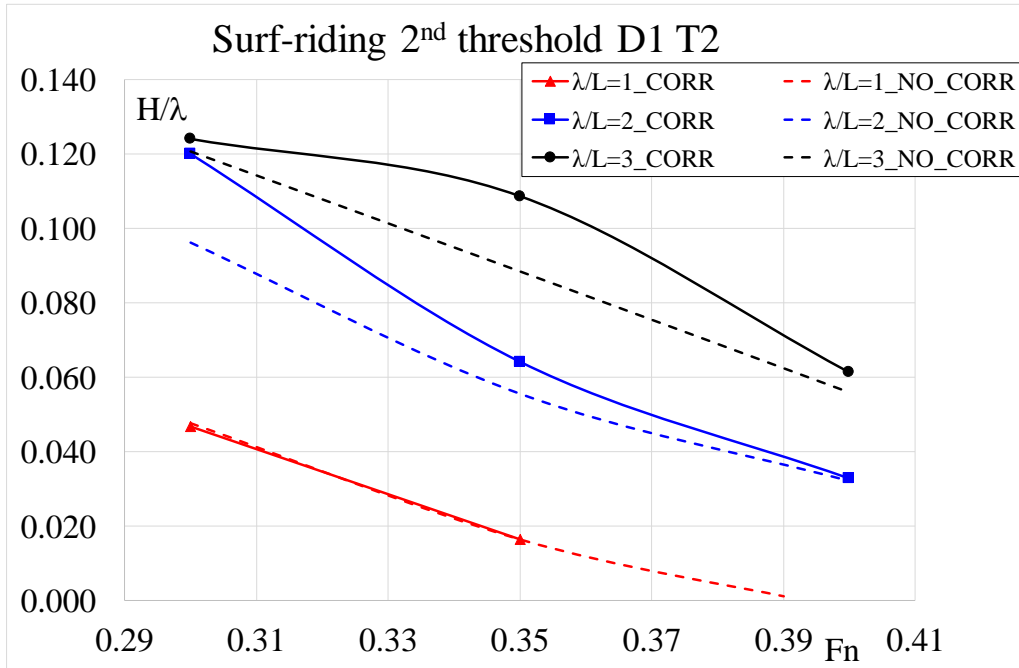
Figure 7.4: Comparison of surf-riding 2nd thresholds for 1-DOF approach with and without wave field correction.

The curves delimit the maximum wave steepness over which surf-riding occurs under any initial conditions (over 2nd threshold). As expected, analysing Equation (7.4), for wave lengths equal to the ship length, the a value goes to zero and the only contribution of the b value is not big enough to show differences between the two methods. While for wave lengths greater than ship lengths, the difference between the two approaches is significant for low Froude numbers and tends to reduce for higher ones. Overall it can be noticed how minor contributions do not help avoiding surf-riding phenomenon when the ship speed increases and the wave steepness decreases, conditions in which surf-riding becomes inevitable.

Chapter 8

Comparison between Different Numerical Approaches

8.1 Surf-riding Occurrence Comparison

Three different numerical methods, 1-DOF bifurcation analysis, 6-DOF potential theory, and CFD simulations, have been performed on the D1 hull to compare surf-riding occurrences in a Froude number range from 0.3 (limit defined for Level 1) to 0.433 (corresponding to the service speed).

Surf-riding and wave blocking limits have been first found by performing 1-DOF approach with and without the diffraction effect and the wave field influence. From the phase plane analysis, described in Section 3.1.2, different conditions have been identified for each sea state, combination of wave period and height, as follows:

1. no fixed points in wave blocking condition, when no equilibrium points exist and only surge motion is possible;

2. condition between 1st and 2nd wave blocking thresholds when both surging and wave blocking phenomena may occur;

3. over the 2nd threshold in wave blocking condition when only wave blocking may occur;

4. over the 2nd threshold in surf-riding condition when only surf-riding may occur;

5. between 1st and 2nd surf-riding thresholds when both surging and surf-riding phenomena may occur;

6. no fixed points in surf-riding condition, when no equilibrium points exist, and the only surge motion is possible.

The results are presented in the range of wave heights and wave periods from the Global Wave Statistic (Hogben et al., 1986), i.e. $Tz = 3.5 \div 13.5$ s $Hs = 0.5 \div 14.5$ m.

The limits have been searched for cases with and without the correction formulas regarding the wave field contributions, as described in Section 7, but no significant differences are found for the considered intervals of wave heights and periods.

The 6-DOF potential theory approach, described in Section 4, has been used to evaluate surf-riding occurrence around the limits found by 1-DOF approach. The simulations

were performed until wave height value around the moulded depth, about 6.5 m, over which the simulations were no more reliable due to the initial assumptions.

From the analysis of forces, ship speed and ship motions variations the following conditions were observed:

- **SAFE** $\rightarrow$ surge motion: forces and ship speed oscillations in time and small yaw angle variations;

- **SAFE*** $\rightarrow$ surge motion with transient yaw angle of 20 degrees;

- **UNSAFE** $\rightarrow$ surf-riding occurrence: constant forces and ship speed, and large yaw angle variations;

- **UNSAFE*** $\rightarrow$ surf-riding occurrence only for certain wave phases.

The comparison of 1-DOF and 6-DOF results are shown in Figure 8.1 for Froude numbers 0.3, 0.35, 0.4 and 0.433.

The wave length similar to the ship length is highlighted in yellow, while the wave celerity, c, range in which the ship speed case falls is highlighted in light blue.

It can be observed that for wave heights lower than 6.5 m the results obtained with potential theory simulations are in line with the ones obtained the 1-DOF diffraction one. The exceptions are: when the wave to ship lengths are greater than 1 the 6-DOF resulted less conservative and when the wave to ship lengths are smaller than 1 more the 1-DOF was found less conservative.

D1 hull motions with 1-DOF and 6-DOF approach

Fn = 0.30   v = 8.913 [m/s]   n = 2.533 [rps]

T [s]	3.5	4.5	5.5	6.5	7.5	8.5	9.5	10.5	11.5	12.5	13.5
λ [m]	19.1	31.6	47.2	65.9	87.8	112.8	140.9	172.1	206.4	243.9	284.5
c [m/s]	5.5	7.0	8.6	10.1	11.7	13.3	14.8	16.4	17.9	19.5	21.1
ω [rad/s]	1.80	1.40	1.14	0.97	0.84	0.74	0.66	0.60	0.55	0.50	0.47
λ/L	0.21	0.35	0.52	0.73	0.98	1.25	1.57	1.91	2.29	2.71	3.16

Fn = 0.35   v = 10.398 [m/s]   n = 3.073 [rps]

T [s]	3.5	4.5	5.5	6.5	7.5	8.5	9.5	10.5	11.5	12.5	13.5
λ [m]	19.1	31.6	47.2	65.9	87.8	112.8	140.9	172.1	206.4	243.9	284.5
c [m/s]	5.5	7.0	8.6	10.1	11.7	13.3	14.8	16.4	17.9	19.5	21.1

Fn = 0.40   v = 11.883 [m/s]   n=3.708 [rps]

T [s]	3.5	4.5	5.5	6.5	7.5	8.5	9.5	10.5	11.5	12.5	13.5
λ [m]	19.1	31.6	47.2	65.9	87.8	112.8	140.9	172.1	206.4	243.9	284.5
c [m/s]	5.5	7.0	8.6	10.1	11.7	13.3	14.8	16.4	17.9	19.5	21.1

Fn = 0.433   v=12.864 [m/s]   n=4.142 [rps]

T [s]	3.5	4.5	5.5	6.5	7.5	8.5	9.5	10.5	11.5	12.5	13.5
λ [m]	19.1	31.6	47.2	65.9	87.8	112.8	140.9	172.1	206.4	243.9	284.5
c [m/s]	5.5	7.0	8.6	10.1	11.7	13.3	14.8	16.4	17.9	19.5	21.1

LEGEND 1-DOF
- No fixed points in wave blocking condition
- between 1st-2nd threshold in wave blocking condition
- over 2nd threshold in wave blocking condition
- over 2nd threshold in surf-riding condition
- between 1st-2nd threshold in surf-riding condition
- No fixed points in surf-riding condition

LEGEND 6-DOF
- SAFE : surging
- SAFE* : surging with larghe yaw
- FAIL : surf-riding
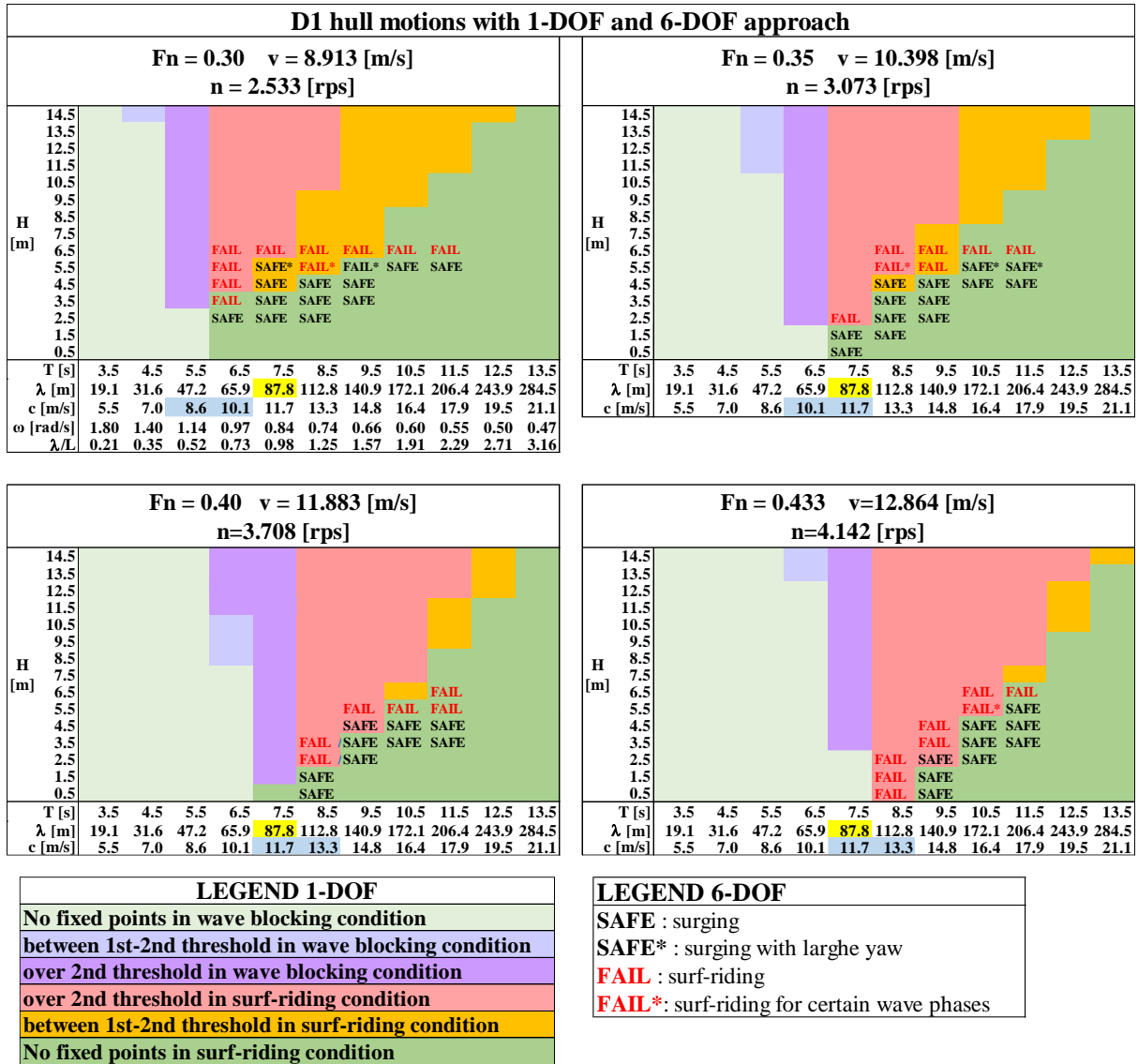- FAIL* : surf-riding for certain wave phases

Figure 8.1: D1 ship motions resulting from 1-DOF and 6-DOF approach

CFD simulations, as described in Section 6.5, have been performed for bare hull and, for each wave case and Froude number, surge or surf-riding motions have been observed analysing forces and speed variations, as reported in Table 6.6.

The results of the three methods cannot be directly compared, since 1-DOF bifurcation analysis defined precise surf-riding limits for the 1st and 2nd thresholds, while CFD and potential theory simulations allow to observe whether the surf-riding phenomenon will occur for specific environmental, operational and initial conditions without being able to define surf-riding limits.

As such, the only certain information from the simulations, ran for one loading condition and one wave case, is that:

- if surf-riding phenomenon is observed at least once, the considered sea state and sailing and loading condition falls above surf-riding first threshold;

- if surging phenomenon is observed at least once, the considered sea state and sailing and loading condition falls below surf-riding second threshold;

Surf-riding limits defined by 1-DOF approach and surge or surf-riding motions observed with potential theory (PT) and CFD approaches are reported for each combination of wave period and height in Figures 8.2, 8.3, 8.4 and 8.5, for Fn = 0.3, 0.35, 0.4, 0.433 respectively. The lines for 1-DOF thresholds in these figures were constructed following the results obtained from Figure 8.1.

Surf-riding limits for 1-DOF approach are reported in terms of maximum allowable wave height at which surf-riding occurs, and the curves represent the 2nd threshold evaluated by simple 1-DOF model, and the 1st and 2nd thresholds evaluated with the diffraction included (1-DOF diffr). The diffraction component has been included by evaluating the wave surging force with the 3-D panel method Hydrostar software as described in Section 6.2.1. The wave surging force has been calculated for ship speed and wave frequency corresponding to the Froude number and wave to ship length case respectively reported in the figures.

For Fn=0.3 no surf-riding phenomenon was observed in CFD simulations up to wave heights 5.5 m, as already discussed in Section 6.5.2.
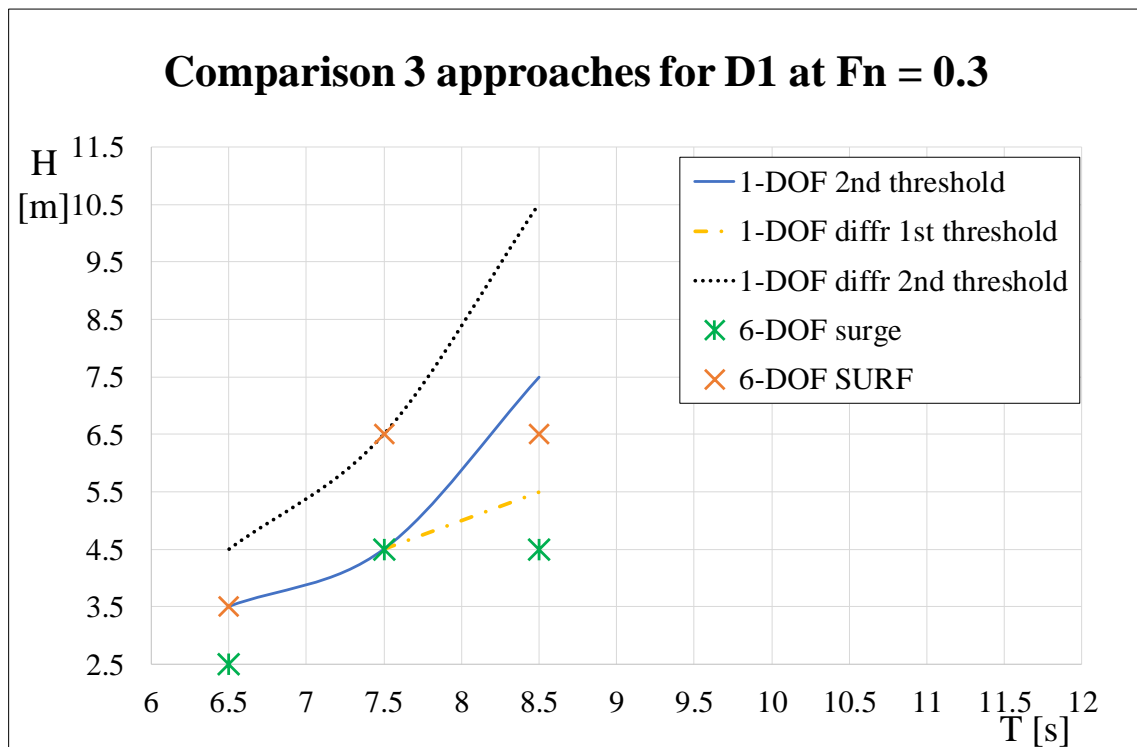

Figure 8.2: Comparison of D1 hull surf-riding limits by 1-DOF with motions observed by 6-DOF PT and 3-DOF CFD simulations for $Fn = 0.3$
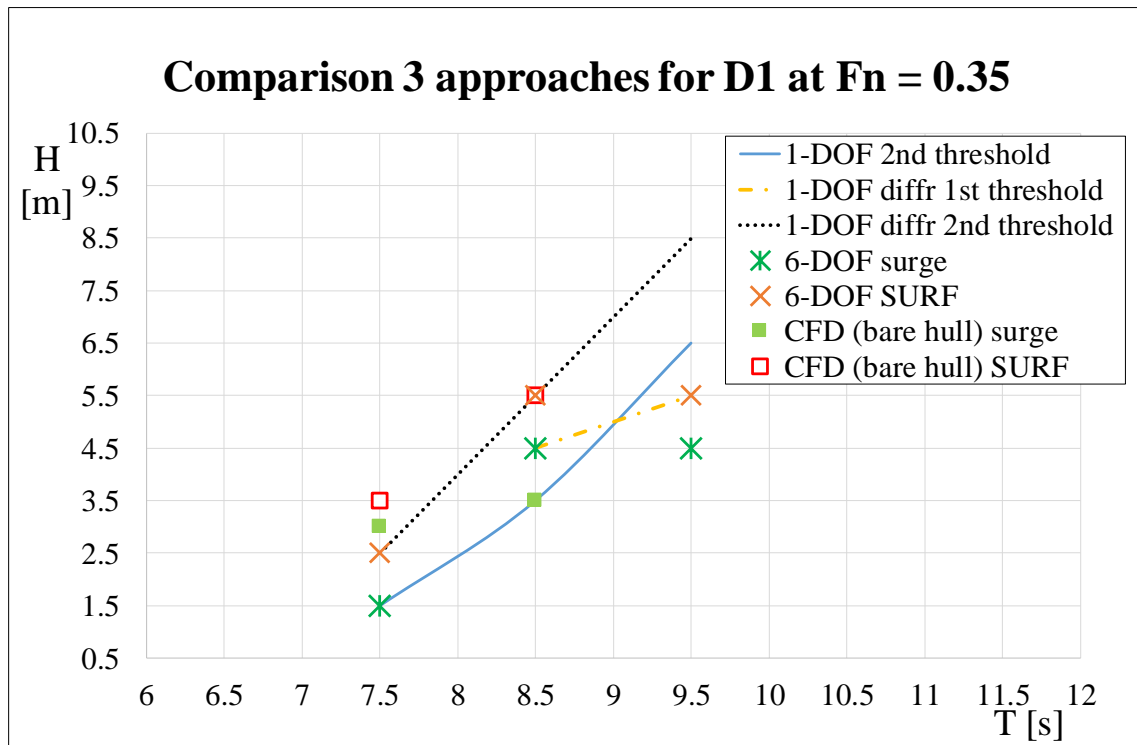
Figure 8.3: Comparison of D1 hull surf-riding limits by 1-DOF with motions observed by 6-DOF PT and 3-DOF CFD simulations for $Fn = 0.35$
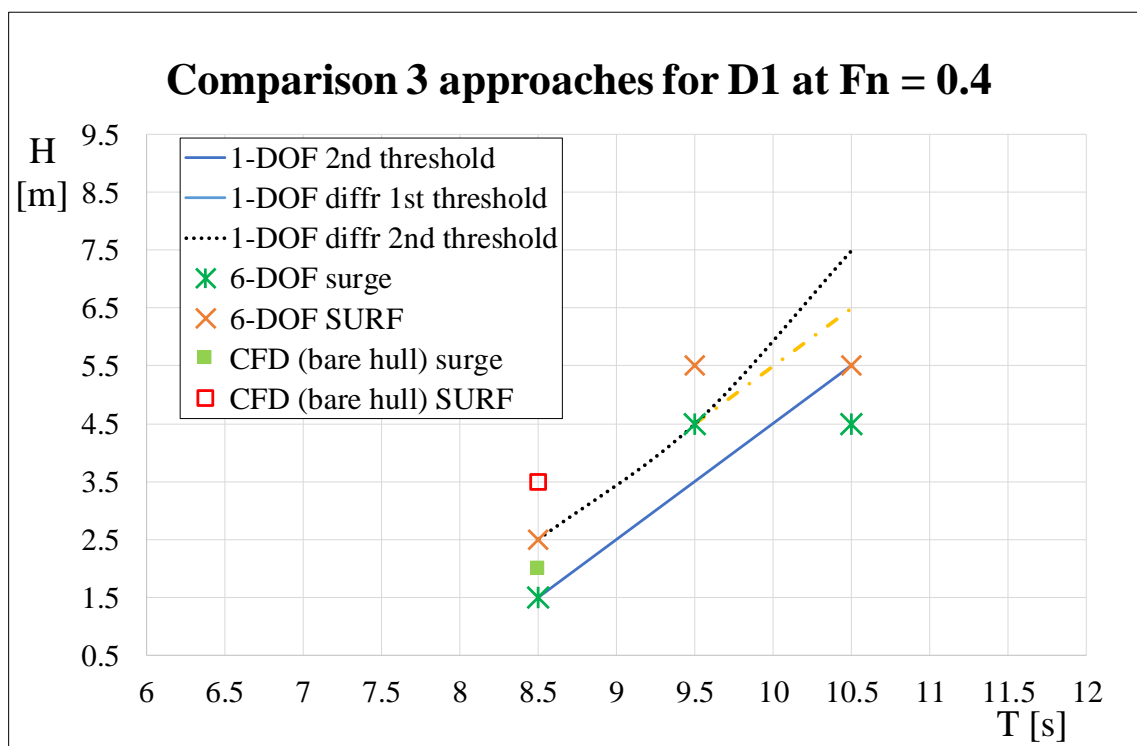

Figure 8.4: Comparison of D1 hull surf-riding limits by 1-DOF with motions observed by 6-DOF PT and 3-DOF CFD simulations for $Fn = 0.4$
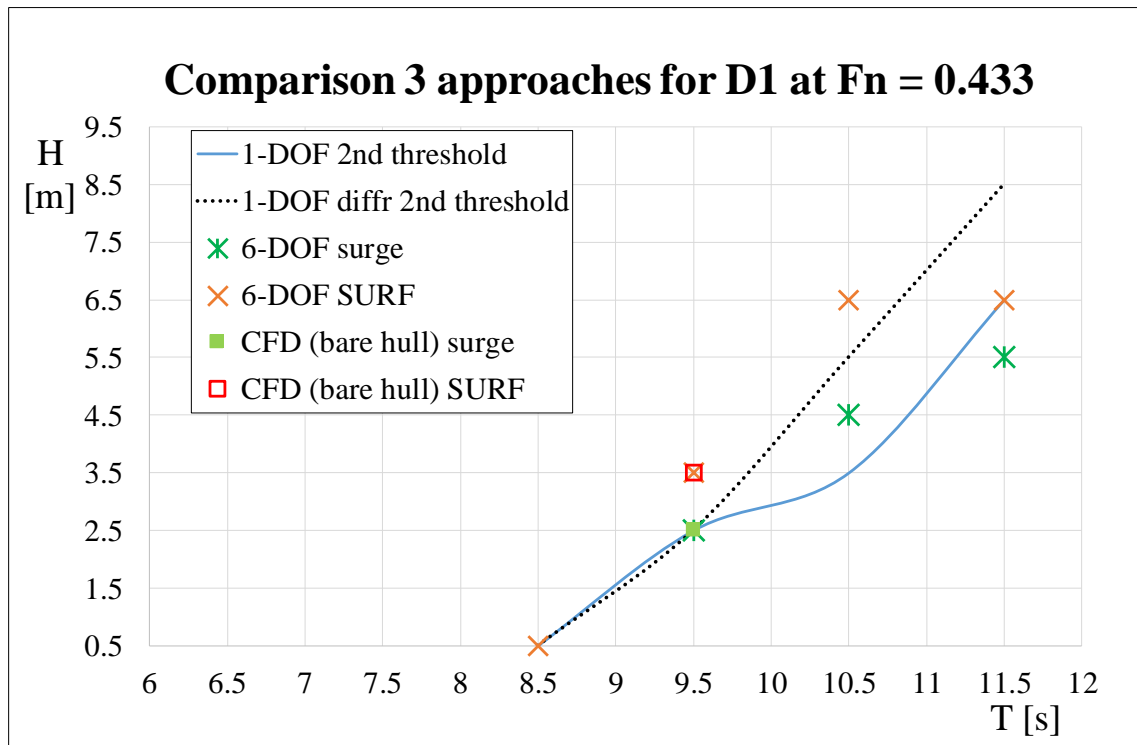
Figure 8.5: Comparison of D1 hull surf-riding limits by 1-DOF with motions observed by 6-DOF PT and 3-DOF CFD simulations for $Fn = 0.433$

Having in mind that CFD simulations have been performed for bare hull, over all results show that CFD approach predicts surf-riding motions for wave heights higher or equal than the ones observed by the PT one, but is far more time consuming. Including the diffraction effect in the 1 DOF approach, the limiting wave heights are closer to values for which surf-riding is observed with PT and CFD.

Chapter 9

IMO Operational Measures

9.1 Guidelines

When the ship is found vulnerable to one or more criteria, the substantial change of ship design to avoid the phenomena can be prohibitive for both ship designers and owners because it may increase the costs of construction and/or operation. Therefore, an alternative solution is to provide Operational Measures (OM) to avoid dangerous situations. The application of OM can reduce the likelihood of stability failure; nevertheless a loading condition for which too many situations should be avoided to achieve the required safety level should not be considered as acceptable.

IMO guidelines, (SDC7/WP6, 2020) define two types of Operational Measures, as shown in the flowchart in Figure 9.1:

- Operational Limitations (OL)

- Operational Guidance (OG)

The Operational Limitations define the limits on a ship's operation in a considered loading condition and are divided in:

- Operational Limitations related to areas or routes and seasons that permit operations in specific operational areas or routes and seasons.

- Operational Limitations related to maximum significant wave heights that permit operation in conditions up to a maximum significant wave height.

The preparation of the Operational Limitations follows the design assessments of Level 1 (L1) or 2 (L2) or Direct Stability Assessment (DSA). For the limitations related to areas or routes and seasons the assessments are performed with a MODIFIED environmental condition, based on the wave scatter table for a SPECIFIC route, area and seasons.
For the limitations related to maximum significant wave height, the assessments are performed with the SPECIFIC environmental condition based on the wave scatter table, for SPECIFIC area, route and season, limited to a selected significant wave height, defining a limited wave scatter diagram. The limited wave scatter diagram therefore cuts out all sea state in which the ship will not operate. The limited wave scatter diagram will be normalized or not according to the fact that the ship is thought to operate all the time and change route to avoid the cut out seas states, or it is to remain safe in port during the dangerous sea states, whose probability of occurrence is then reduced to calm

water condition. The normalization is done by considering the sum of the probabilities of occurrence of the limited wave scatter diagram equal to the total probability of occurrence.

The Operational Guidance defines the sailing conditions, defined as the combination of ship speeds and headings, not recommended or to be avoided in each sea state considered. The OG defines a set of operative information that support the master during the navigation in dangerous sea states.

The preparation of the Operational Guidance is based on 3 approaches: probabilistic, deterministic and simplified motion criteria, as described in Figure 9.1.

The probabilistic and deterministic approaches provide accurate and detailed recommendations for the ship forward speed and course in each sea state but require model tests or numerical methods of high accuracy. Therefore, simpler conservative approaches may be used to develop Operational Guidance for acceptable forward speed and course when it is deemed practicable.

The simplified approach for the surf-riding/broaching criterion defines either of the two following speed limits:

- the nominal speed equal or greater than $0.94 \cdot L^{1/2}$ (from Level 1 formulation) should be avoided for waves with lengths, calculated on mean wave period, greater than $80\% L$ and with significant wave height higher than $4\% L$ and heading angle less than 45 degrees;

- the critical nominal ship speed provided by the Level 2 vulnerability criteria or above should be avoided in following to beam wave directions in sea states for which $c_{HT} > 0.005$, where:

$$c_{HT}(H_s, T_z) = \sum_{i=1}^{N_\lambda} \sum_{j=1}^{N_a} w_{ij} C2_{ij} \qquad (9.1)$$

where w_{ij} and $C2_{ij}$ are calculated at Level 2 including the diffraction component in the wave force calculations.

For the calculation of the critical nominal ship speed, the reference formula reported in IMO (SDC7/WP6, 2020) is confusing, since the Froude number corresponds to the speed chosen for the calculation of Level 2 and its value corresponding to $c_{HT} = 0.005$ is the critical one.

Any simple conservative estimation for the sailing conditions that should be avoided in each relevant sea state, can be used if they are shown to provide a superior safety level compared to the design assessment requirements.

It is worth to underline that the Operational Limitations are performed considering a long term probability index, therefore it does not mean that the ship will always operate in safe conditions below the selected significant wave height but that the probability of occurring of surf-riding failure mode is sufficiently low. Therefore the crew must always operate with prudent seamanship. Instead, the simplified Operational Guidance is based on the short term index, therefore the sea state, for which the index is below the limit, is considered as safe condition for the ship to operate in.

The Operational Measures can be combined applying, for example, the Operational Limitations up to a certain significant wave height and the Operational Guidance for greater significant wave heights. While Operational Limitations related to areas or routes

do not require specific planning, the Operational Limitations related to maximum wave height and the Operational Guidance need a weather forecast available on board for planning.

The application of the Operational Limitations related to maximum significant wave height or Operational Guidance can reduce the stability failure rate to any low level. However, if too many sailing conditions in too many sea states should be avoided for a certain loading condition, such loading condition cannot be considered as acceptable in practical operation. Therefore a loading condition is not in compliance if the ratio of the total duration of all situations which should be avoided to the total operational time, is greater than 0.2 (SDC7/WP6, 2020). In the calculation of the ratio the probabilities of the sea states are taken according to the full wave scatter table, the wave headings are assumed uniformly distributed and the ship forward speed is assumed uniformly distributed between zero and the maximum service speed.

Many studies have been made and reported for the application of the first 2 levels, while Operational Measures performances are rare. Backalov et al. (2015) investigated Operational Limitations of river-sea ships for the dead ship condition (DSC) and excessive accelerations (EA) criteria. The OL procedure followed the Level 2 vulnerability assessment and the limits have been reported for different bilge keels, drafts and metacentric heights. The results of the analysis have been found generally in good agreement with the operational experience and lower metacentric heights had a positive effect on the behaviour of the examined vessel. A detailed description and discussion on Operational Measures is reported in Petacco and Gualeni (2020) together with an application of Operational Limitations of Ro-Ro pax ferry for pure loss of stability, dead ship condition and excessive acceleration criteria.
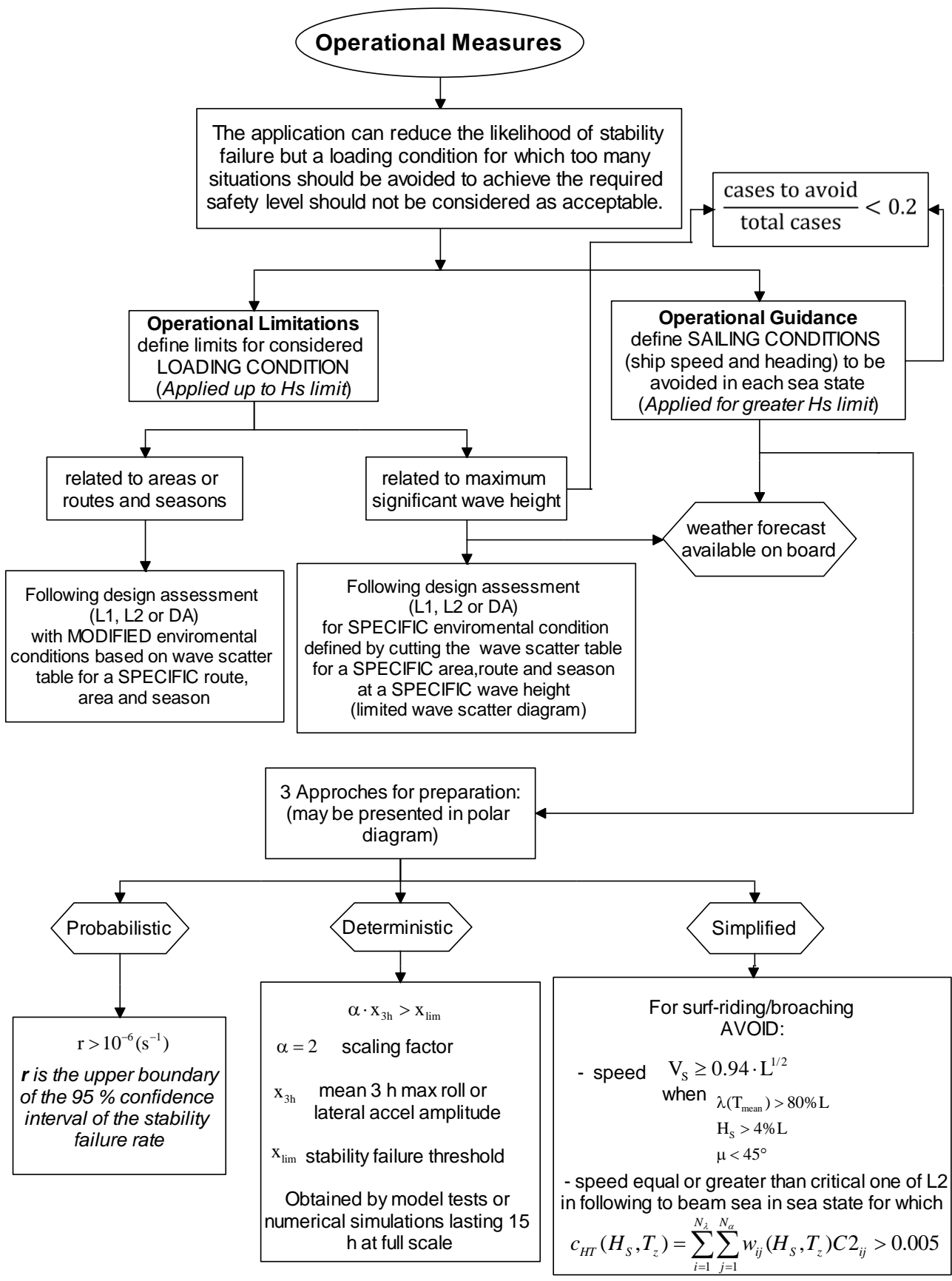
Operational Measures

The application can reduce the likelihood of stability failure but a loading condition for which too many situations should be avoided to achieve the required safety level should not be considered as acceptable.

$$\frac{\text{cases to avoid}}{\text{total cases}} < 0.2$$

Operational Limitations
define limits for considered
LOADING CONDITION
(*Applied up to Hs limit*)

Operational Guidance
define SAILING CONDITIONS
(ship speed and heading) to be
avoided in each sea state
(*Applied for greater Hs limit*)

related to areas or routes and seasons

related to maximum significant wave height

weather forecast available on board

Following design assessment
(L1, L2 or DA)
with MODIFIED enviromental
conditions based on wave scatter
table for a SPECIFIC route,
area and season

Following design assessment
(L1, L2 or DA)
for SPECIFIC enviromental condition
defined by cutting the wave scatter table
for a SPECIFIC area, route and season
at a SPECIFIC wave height
(limited wave scatter diagram)

3 Approches for preparation:
(may be presented in polar
diagram)

Probabilistic

Deterministic

Simplified

$\text{r} > 10^{-6}(\text{s}^{-1})$

r is the upper boundary of the 95 % confidence interval of the stability failure rate

$\alpha \cdot \text{x}_{3h} > \text{x}_{\lim}$

$\alpha = 2$ scaling factor

x_{3h} mean 3 h max roll or lateral accel amplitude

$\text{x}_{\lim}$ stability failure threshold

Obtained by model tests or numerical simulations lasting 15 h at full scale

For surf-riding/broaching
AVOID:

- speed $V_S \geq 0.94 \cdot L^{1/2}$
    when $\lambda(T_{mean}) > 80\%\,L$
          $H_S > 4\%\,L$
          $\mu < 45°$

- speed equal or greater than critical one of L2 in following to beam sea in sea state for which

$$c_{HT}(H_S, T_z) = \sum_{i=1}^{N_\lambda} \sum_{j=1}^{N_\alpha} w_{ij}(H_S, T_z) C2_{ij} > 0.005$$

Figure 9.1: IMO Operational Measures flow chart.

9.2 Application

Having studied the surf-riding phenomenon by different methodologies, (IMO criteria and 1-DOF assessment methods, 6-DOF potential theory and CFD approaches) the D1 hull form has been found vulnerable to surf-riding failure for wave lengths close to ship lengths and for relatively low wave heights when tested at Froude numbers corresponding to the service speed. Therefore, Operational Measures have been analysed and discussed to support operations and reduce stability failures when dangerous sea state conditions are encountered.

Considering the D-Series form as representative of an Italian corvette, the aim is to discuss Operational Limitations and Operational Guidance for a possible route in the Mediterranean Sea of the D1 ship, on a route Livorno - Barcelona, operating in AREA 26 according to the Global Wave Statistics Hogben et al. (1986).

9.2.1 Operational Limitations

Following the procedure described in the flow chart in Figure 9.1, the Operational Limitations related to areas or routes have been evaluated by performing Level 2 assessment, including the diffraction component, replacing the North Atlantic scatter diagram with the one related to AREA 26, taken from the Global Wave Statistics Hogben et al. (1986), for all wind directions and annual average, and reported in Table 9.1. The loading condition taken into consideration is the one used for Level 2 assessment.

From the performance of the OL related to areas at the service speed, corresponding to Fn=0.433, the Index C value has been found greater than the limit value 0.005, therefore the ship is found not able to operate in AREA 26 for the route considered.

At this point to comply with IMO surf-riding criterion, changes in ship design should be taken into consideration or different loading cases and speeds could be tested but the ship's operational design would change. Otherwise, there are two possible ways to make the existing ship able to operate, in the considered loading condition, in compliance with surf-riding criterion: apply Operational Limitations related to maximum wave heights, or provide Operational Guidance.

The Operational Limitations related to the maximum wave height are evaluated by performing Level 2 assessment, including the diffraction component, and replacing the North Atlantic wave scatter diagram with different limited wave scatter diagrams. The limited wave scatter diagrams are obtained by cutting the wave scatter diagram related to AREA 26 at different significant wave heights, $H_{S,LIM}$, meaning that the ship will not operate in all the cut off sea states.

Two types of situations have been considered:

- the ship operates all the time and modifies her route to avoid encountering wave heights $H_S > H_{S,LIM}$; in this case the limited scatter diagrams were normalized and the total probability of sea state occurrence which is equal to 1 corresponds to the only limited scatter diagram, since no sea state with $H > H_{S,LIM}$ are taken into consideration;

- the ship is safe in port when sea conditions are characterized by $H_S > H_{S,LIM}$, which must be avoided. In this situation the limited scatter diagrams were not normalized, since total area is taken in consideration but the probability of encountering $H_S > H_{S,LIM}$, is associated to calm water condition: H=0 m.

The Index C values obtained for the total AREA 26 and for the limited scatter diagrams of AREA 26 cut at different selected significant wave height are shown in Figure 9.2 as function of the Froude number, where curves with "N" define the situation in which the limited wave scatter diagram were normalized and without "N" if not normalized. The value of the significant wave height that defines each curve represents and includes the upper limit of the row, $H_{S,UL}$, at which the diagram has been cut excluding all the greater wave heights. As expected, the curves determined with normalized tables prove to be more conservative. From the resulting values, the OL state that the hull D1 may operate in compliance with surf-riding criterion at service speed in AREA 26 with limited significant wave height up to 3 m.

The Fn limit of Level 1 (L1) and the curves of Index C obtained by Level 2 assessment, with (L2 diffr) and without (L2) diffraction effect, are compared to the curves obtained for the OL related to AREA 26 and related to the maximum significant wave heights.

An improvement of ship speed limits can be observed passing from Level 2, through Level 2 with diffraction, and then applying the OL.
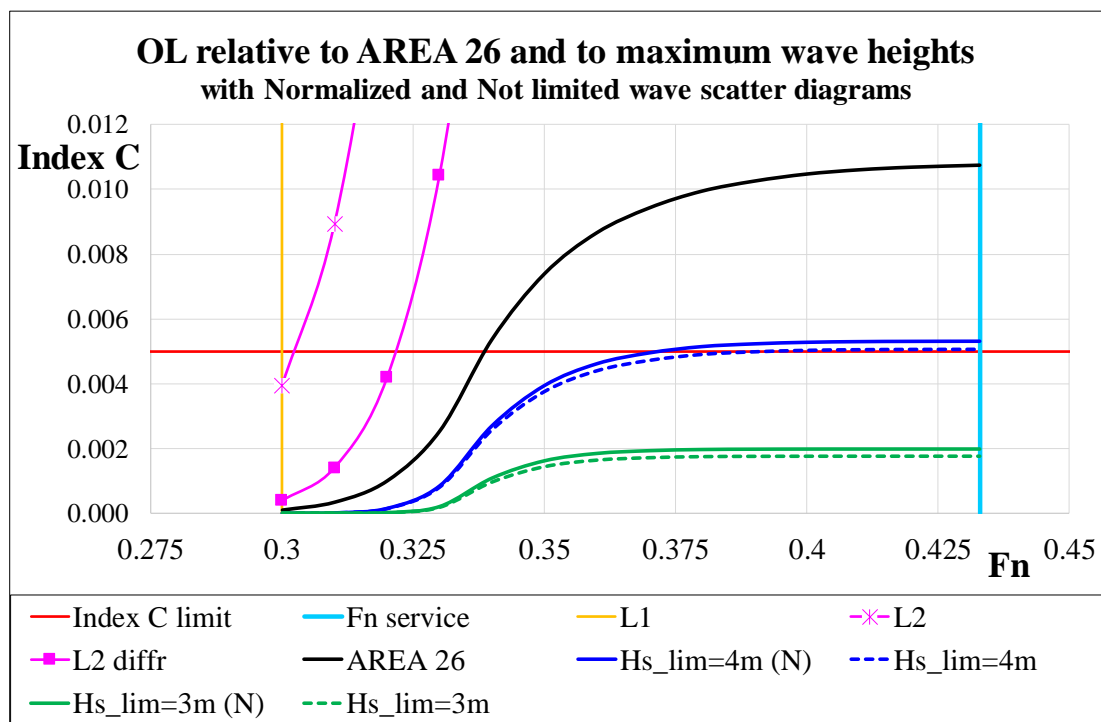
Figure 9.2: Comparison of Index C values obtained by the different methods.

The value of the maximum wave height in service speed condition, $H_S \leq 3$ m, has been checked if in accordance with the limitations of minimum allowable significant wave height to consider the loading condition acceptable, based on the calculation of the ratio between the total duration of all situations which should be avoided and the total operational time which must be greater than 0.2.

Therefore, the calculation of the total probability of all the sea states avoided when cutting the wave scatter diagram at different significant wave heights has been done and reported in Table 9.1 for AREA 26.

The values show that when cutting the diagram above the row with $H_S = 1 - 2$ m the probability of avoided cases would be greater than 0.2, therefore the maximum allowable

H_S to be in compliance with the criterion corresponds to a cut above row 2-3 avoiding all sea states with $H_S > 3$ m, for which the probability of avoided cases is < 0.2. To define a more precise limit an exact value of upper limit of significant wave height, $H_{S,UL\ (20\%)}$, having ratio equal to 0.2, has been interpolated and results equal to 2.533 m.

Table 9.1: Determination of maximum significant wave height for which the ratio between the total duration of all situations which should be avoided and the total operational time is equal to or more than 0.2.

AREA 26		Tz [s]											Prob lim to Hs	Cdf	Prob of exceeding	Hs Upper Limit
		3-4 3.5	4-5 4.5	5-6 5.5	6-7 6.5	7-8 7.5	8-9 8.5	9-10 9.5	10-11 10.5	11-12 11.5	12-13 12.5	13-14 13.5				
Hs [m]	14-15 **14.5**	0	0	0	0	0	0	0	0	0	0	0	999	1	0	15
	13-14 **13.5**	0	0	0	0	0	0	0	0	0	0	0	999	1	0	14
	12-13 **12.5**	0	0	0	0	0	0	0	0	0	0	0	999	1	0	13
	11-12 **11.5**	0	0	0	0	0	0	0	0	0	0	0	999	1	0	12
	10-11 **10.5**	0	0	0	0	0	0	0	0	0	0	0	999	1	0	11
	9-10 **9.5**	0	0	0	0	0	0	0	0	0	0	0	999	1	0	10
	8-9 **8.5**	0	0	0	0	0	0	0	0	0	0	0	999	1	0	9
	7-8 **7.5**	0	0	1	1	1	0	0	0	0	0	0	999	1	0	8
	6-7 **6.5**	0	0	1	2	1	1	0	0	0	0	0	996	0.997	0.003	7
	5-6 **5.5**	0	1	3	4	2	1	0	0	0	0	0	991	0.992	0.008	6
	4-5 **4.5**	0	3	8	9	5	2	1	0	0	0	0	980	0.981	0.019	5
	3-4 **3.5**	1	9	24	23	11	4	1	0	0	0	0	952	0.953	0.047	4
	2-3 **2.5**	3	32	66	50	20	6	1	0	0	0	0	879	0.880	0.120	3
	1-2 **1.5**	15	96	138	77	24	5	1	0	0	0	0	701	0.702	0.298	2
	0-1 **0.5**	60	140	102	35	7	1	0	0	0	0	0	345	0.345	0.655	1
													999	0.000	1.000	0

Hs,UL (20%) = 2.552

The Index C values have been represented as function of $H_{S,UL}$ of the limited scatter diagram for different Froude numbers, as in Figure 9.3. The curves have range of operability limited by the area crossed with red oblique lines, defined by the maximum allowable wave height in compliance with ratio of avoided cases $< 20\%$, as calculated above, and by the value of 0.005 over which the Index C is not in compliance with Level 2 assessment. It can be seen that by linear interpolation the marginal value of the upper limit of wave heights, $H_{S,UL}(marg)$ reaches a value around 3.8 m, which is higher than the limit found by analysing Figure 9.2.

Besides the significant improvement of Level 2 assessment performed with the diffraction effect, overall results show that the ship will have ship speed limitations in AREA 26 for wave heights higher than 3.8 m to comply with surf-riding Operational Limitation.
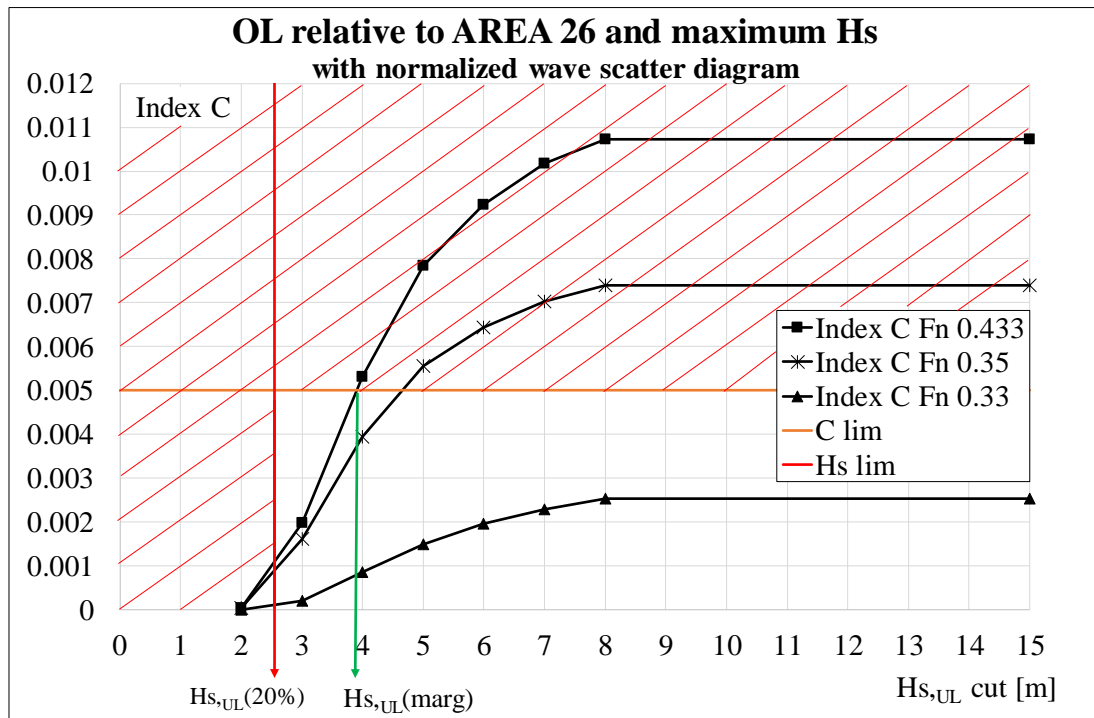
Figure 9.3: Operational Limitations relative to maximum wave height in AREA 26.

9.2.2 Operational Guidance

If the ship happens to be in dangerous sea state conditions, the Operational Guidance shall be followed, as shown in Figure 9.1.

The simplified Operational Guidance, applied on the D1 hull, states that to avoid surf-riding phenomenon when the ship encounters sea state with significant wave heights greater than 3.6 m and wave lengths greater than 72 m, corresponding to periods between 6.5 and 7 s, ship speeds higher than 8.92 m/s, corresponding to Fn ∼0.3, should be avoided.

The second simplified approach for the OG has been performed in the following way. The Index c_{HT}, as defined in Equation (9.1), has been calculated for a range of Froude number from 0 to 0.433, for average zero-crossing wave period range of $T_Z = 3.5 \div 18.5$ s and significant wave height range of $H_S = 0.5 \div 16.5$ m, as in the North Atlantic wave scatter diagram.

For each sea state, corresponding to each combination of T_Z and H_S, the interpolated value of Froude numbers, corresponding to index c_{HT} equal to 0.005, has been found and reported in Table 9.2. When $c_{HT} = 0.005$ was verified for $Fn > 0.433$, no specific value has been reported, since the service speed is the maximum value of interest.

Table 9.2: Simplified Operational Guidance indicating the critical nominal Froude number for each sea state for hull D1.

		Simplified Operational Guidance														
Critical		**Tz**														
Fn		3.5	4.5	5.5	6.5	7.5	8.5	9.5	10.5	11.5	12.5	13.5	14.5	15.5	16.5	17.5	18.5
	0.5	>0.433	>0.433	>0.433	>0.433	>0.433	>0.433	>0.433	>0.433	>0.433	>0.433	>0.433	>0.433	>0.433	>0.433	>0.433	>0.433
	1.5	>0.433	>0.433	>0.433	>0.433	>0.433	>0.433	>0.433	>0.433	>0.433	>0.433	>0.433	>0.433	>0.433	>0.433	>0.433	>0.433
	2.5	>0.433	>0.433	>0.433	0.335	0.333	0.337	0.359	>0.433	>0.433	>0.433	>0.433	>0.433	>0.433	>0.433	>0.433	>0.433
	3.5	>0.433	0.346	0.330	0.322	0.321	0.324	0.332	0.342	0.376	>0.433	>0.433	>0.433	>0.433	>0.433	>0.433	>0.433
	4.5	>0.433	0.332	0.321	0.312	0.311	0.314	0.322	0.331	0.341	0.363	>0.433	>0.433	>0.433	>0.433	>0.433	>0.433
	5.5	0.340	0.324	0.312	0.304	0.302	0.306	0.313	0.323	0.332	0.342	0.362	0.411	>0.433	>0.433	>0.433	>0.433
	6.5	0.333	0.318	0.305	0.297	0.294	0.299	0.306	0.315	0.325	0.334	0.345	0.365	0.407	>0.433	>0.433	>0.433
	7.5	0.328	0.312	0.300	0.291	0.288	0.292	0.300	0.310	0.320	0.328	0.337	0.349	0.370	0.410	>0.433	>0.433
Hs	8.5	0.323	0.306	0.293	0.285	0.283	0.286	0.293	0.303	0.313	0.323	0.332	0.341	0.354	0.376	0.416	>0.433
	9.5	0.318	0.302	0.289	0.282	0.280	0.282	0.289	0.298	0.308	0.318	0.327	0.335	0.345	0.360	0.384	0.425
	10.5	0.314	0.297	0.285	0.280	0.277	0.280	0.284	0.293	0.303	0.313	0.323	0.331	0.340	0.351	0.367	0.393
	11.5	0.310	0.293	0.282	0.277	0.275	0.277	0.282	0.289	0.299	0.309	0.319	0.327	0.335	0.345	0.357	0.375
	12.5	0.306	0.290	0.281	0.276	0.274	0.275	0.280	0.285	0.294	0.304	0.314	0.323	0.332	0.340	0.350	0.364
	13.5	0.302	0.287	0.280	0.275	0.274	0.274	0.278	0.283	0.291	0.301	0.311	0.320	0.328	0.336	0.345	0.357
	14.5	0.300	0.285	0.279	0.275	0.273	0.274	0.277	0.281	0.288	0.297	0.307	0.316	0.325	0.333	0.341	0.351
	15.5	0.297	0.284	0.278	0.274	0.273	0.274	0.276	0.281	0.285	0.294	0.303	0.313	0.322	0.330	0.338	0.347
	16.5	0.295	0.283	0.277	0.274	0.273	0.273	0.275	0.280	0.283	0.291	0.301	0.310	0.319	0.327	0.335	0.344

The critical Froude numbers, reported in Table 9.2, correspond to the critical nominal ship speed whose value or above it should be avoided in following to beam wave directions in each corresponding sea state. The table has been coloured to highlight the following:

- **green** if the sea states are not critical, when the critical Froude number is above the service speed.

- **from yellow to red**, corresponding to decreasing values, if the sea states are critical and the corresponding critical and higher Froude number must be avoided;

It can be observed that under wave heights $H_{S,UL}$=2 m there are no limitations for ship speed and the critical speed decreases together with wave heights for wave periods corresponding to wave lengths comparable to ship lengths.

It has to be underlined that Table 9.2 represents theoretical speed limit values regarding the surf-riding phenomenon only but in actual operations the ship could have speed reductions or heading changes to avoid violent slams or cargo lost or damage.

The provided Simplified Operational Guidance, corresponding to the considered loading condition, must be in compliance with the maximum value of 0.2 of the ratio of the total duration of all situations which should be avoided to the total operational time.

Therefore the probability of encountering each sea state defined by a zero crossing period and a significant wave height, $Pr(T_Z, H_S)$, has been multiplied by a coefficient that takes into account the considered heading range, $heading(range)$, and a coefficient which takes into account the deviation between the limit speed and the service speed, $\frac{Fn_{service} - Fn_{critical}}{Fn_{service}}$, as in the Equation (9.2):

$$Pr(T_Z, H_S) * heading(range) * \frac{Fn_{service} - Fn_{critical}}{Fn_{service}} \qquad (9.2)$$

The value obtained by Equation 9.2 defines the probability of unacceptable situations for the corresponding sea state, range of heading and speed. The sum of all the probabilities of the unacceptable cases gives the Total Probability of the cases to be avoided, whose value must be less than 0.2 in order to consider acceptable the loading condition for which the Operational Guidance has been provided.

The Total Probability of the cases to be avoided has been evaluated for the North Atlantic wave occurrence table and for the scatter diagram of AREA 26. The heading weight has been taken equal to 1/2, corresponding to uniformly distributed heading range from following to beam sea, therefore half of 360°. The speed range has been considered uniformly distributed from 0 to service speed (Fn=0.433) and the critical Fn taken from Table 9.2. The calculation of probability of each sea state weight on heading and speed and the Total Probability of situations to avoid are represented in Tables 9.3 and 9.4 for the North Atlantic and AREA 26 respectively.

It can be observed that for both wave scatter diagrams the Total Probability is less than 0.2, therefore the Operational Guidance defined in Table 9.2 are in compliance with the criterion and may be applied for hull D1 in the considered loading condition.

Table 9.3: Total Probability of the cases to be avoided for D1 hull evaluate for the North Atlantic wave scatter diagram

Probability of wave occurrences weighted with heading and critical speed for NORTH ATLANTIC																
Hs [m]	Tz [s]															
	3.5	4.5	5.5	6.5	7.5	8.5	9.5	10.5	11.5	12.5	13.5	14.5	15.5	16.5	17.5	18.5
0.5	0	0	0	0	0	0	0	0	0	0	0	0	0	0	0	0
1.5	0	0	0	0	0	0	0	0	0	0	0	0	0	0	0	0
2.5	0	0	0	0.0025	0.0072	0.0082	0.0042	0	0	0	0	0	0	0	0	0
3.5	0	2E-07	4E-05	0.0009	0.0042	0.0059	0.006	0.003	0.0007	0	0	0	0	0	0	0
4.5	0	0	8E-06	0.0003	0.0019	0.0045	0.0049	0.0032	0.0014	0.0004	0	0	0	0	0	0
5.5	0	0	1E-06	8E-05	0.0008	0.0024	0.0033	0.0026	0.0013	0.0005	0.0001	1E-05	0	0	0	0
6.5	0	0	3E-07	2E-05	0.0003	0.0011	0.0018	0.0017	0.001	0.0004	0.0001	3E-05	3E-06	0	0	0
7.5	0	0	0	5E-06	9E-05	0.0004	0.0009	0.001	0.0007	0.0003	0.0001	4E-05	7E-06	7E-07	0	0
8.5	0	0	0	1E-06	3E-05	0.0002	0.0004	0.0005	0.0004	0.0002	9E-05	3E-05	8E-06	1E-06	1E-07	0
9.5	0	0	0	3E-07	8E-06	6E-05	0.0002	0.0002	0.0002	0.0001	6E-05	2E-05	6E-06	1E-06	2E-07	9E-09
10.5	0	0	0	0	2E-06	2E-05	7E-05	0.0001	0.0001	7E-05	3E-05	1E-05	4E-06	1E-06	2E-07	0
11.5	0	0	0	0	5E-07	6E-06	2E-05	4E-05	5E-05	4E-05	2E-05	8E-06	3E-06	7E-07	2E-07	0
12.5	0	0	0	0	2E-07	2E-06	8E-06	2E-05	2E-05	2E-05	9E-06	4E-06	2E-06	4E-07	1E-07	0
13.5	0	0	0	0	0	5E-07	3E-06	6E-06	8E-06	7E-06	4E-06	2E-06	8E-07	2E-07	1E-07	0
14.5	0	0	0	0	0	2E-07	7E-07	2E-06	3E-06	3E-06	2E-06	9E-07	4E-07	1E-07	0	0
15.5	0	0	0	0	0	0	2E-07	7E-07	1E-06	1E-06	7E-07	4E-07	1E-07	1E-07	0	0
16.5	0	0	0	0	0	0	0	2E-07	3E-07	3E-07	3E-07	1E-07	1E-07	0	0	0

	PR TOT	0.084

Table 9.4: Total Probability of the cases to be avoided for D1 hull evaluate for the wave scatter diagram of AREA 26

Probability of wave occurrences weighted with heading and critical speed for AREA 26										
Hs [m]	Tz [s]									
	3.5	4.5	5.5	6.5	7.5	8.5	9.5	10.5	11.5	12.5	13.5
0.5	0	0	0	0	0	0	0	0	0	0	0
1.5	0	0	0	0	0	0	0	0	0	0	0
2.5	0	0	0	0.00569	0.00231	0.00066	8.6E-05	0	0	0	0
3.5	0	0.0009	0.00285	0.00294	0.00142	0.0005	0.00012	0	0	0	0
4.5	0	0.00035	0.00104	0.00125	0.0007	0.00028	0.00013	0	0	0	0
5.5	0	0.00013	0.00042	0.0006	0.0003	0.00015	0	0	0	0	0
6.5	0	0	0.00015	0.00032	0.00016	0.00015	0	0	0	0	0
7.5	0	0	0.00015	0.00016	0.00017	0	0	0	0	0	0
8.5	0	0	0	0	0	0	0	0	0	0	0
9.5	0	0	0	0	0	0	0	0	0	0	0
10.5	0	0	0	0	0	0	0	0	0	0	0
11.5	0	0	0	0	0	0	0	0	0	0	0
12.5	0	0	0	0	0	0	0	0	0	0	0
13.5	0	0	0	0	0	0	0	0	0	0	0
14.5	0	0	0	0	0	0	0	0	0	0	0

	PR TOT	0.024

Chapter 10

Conclusions and Future Works

In this thesis the surf-riding phenomenon is analysed both as a physical phenomenon and as a subject of the regulatory framework. Surf-riding/broaching phenomenon is one of the five failure modes defined by IMO working group within the Second Generation Intact Stability Criteria.

Surf-riding phenomenon occurs when a ship sailing in following or quartering waves, which have lengths and celerity comparable to ship length and speed, reaches and travels with wave celerity. Normally surf-riding precedes broaching, which has a more complex dynamics, therefore it is used as vulnerability assessment for the surf-riding/broaching criterion. The physics and dynamics of surf-riding phenomenon are described by the force's equilibrium in the forward speed direction: resistance, thrust and wave exciting force. The physically correct approach to develop a mathematical model, should consider all forces variations in wave condition: the wave exciting force should include Froude-Krylov and diffraction components calculated under actual wave profile, the resistance and thrust should incorporate actual wetted surface and estimation of wave systems for the test case.

The phenomenon has been studied by means of three different numerical approaches: 1-DOF bifurcation analysis, 3-DOF CFD simulations, 6-DOF potential theory simulations.

The Systematic Series D (Kracht and Jacobsen, 1992), a semi-displacement naval hull form representative of 90 m lengths European Corvettes, has been used as test case to study and analyse the surf-riding occurrence.

Following IMO procedures (SDC7/WP6, 2020), Level 1 and Level 2 vulnerability assessments have been performed on the 7 hulls of the Series D, that were all found vulnerable to surf-riding/broaching criterion at the service speed corresponding to Fn=0.433. Therefore, the maximum allowable ship speed that complies with Level 2 criterion has been searched and compared with the limit imposed by Level 1 assessment. Moreover, the effects of non linear wave celerity and diffraction component in the wave surging force, determined by a 3-D panel method, have been discussed. The limits found with these corrections provided less conservative results: including the non linear wave celerity, the speed limit, to comply with Level 2 criterion, increased in about half a knot according to Level 1, and including the diffraction effect in about 1 knot.

The 1-DOF surge mathematical model for regular following waves has been studied by a non linear dynamics procedure and bifurcation analysis. By a phase plane analysis surf-riding thresholds have been identified for the parent hull D1 of the Series D for different waves cases and ship speeds. The effect of diffraction has been analysed and

it has been found that it improves the 1-DOF approach with higher influence for higher wave heights.

The 1-DOF direct procedure has been compared with IMO criterion and proved to be less conservative than Melnikov's method used in Level 2 assessment.

The 6-DOF potential theory mathematical model (Acanfora and Matusiak, 2016) combines seakeeping and manoeuvring models. Resistance and thrust are approximated with calm water formulations, and added mass, damping and diffraction values are obtained by a 3-D panel method, Hydrostar ®, and the manoeuvring coefficients are evaluated by semi-empirical formulas in calm water conditions. The manoeuvring coefficients take into account an additional damping effect since damping coefficients tend to zero when encounter frequencies tend to zero in surf-riding conditions.

CFD simulations have been performed in 3-DOF for following regular waves with the Naval Hydro Pack of OpenFOAM software, that takes into account all the neglected non linearities and the approximations made in the 1-DOF simple approach.

To avoid time consuming calculations, PT and CFD simulation cases have been chosen starting from sailing conditions and wave cases for which the ship experienced surf-riding over the 2nd threshold by 1-DOF approach. The resulting motions of surge or surf-riding have been identified analysing the ship speeds and forces variations.

The differences between the wave heights at which surf-riding has been observed by CFD and 1-DOF approach, highlighted the great conservatism of the assumptions made in the 1-DOF approach. Taking into account the diffraction effect clearly decreased the differences. Throughout a comparison of 1-DOF and CFD forces, another improvement to include in the 1-DOF model has been identified in the wave velocity field influence. Wave particle velocity contributions included in resistance and thrust forces have highlighted small contributions that were more visible for longer waves according to the ship length.

The surf-riding limits found with the three approaches have been compared, knowing that 1-DOF approach defines clearly the first and second surf-riding thresholds, while CFD and potential theory simulations define surf-riding or surging conditions for specific environmental, operational and initial conditions. Therefore when performing various tests with CFD or 6-DOF no surf-riding limits can be defined and due to the uncertainties of the initial conditions the only certainties are:

- if surf-riding phenomenon is observed at least once, the considered sea state and sailing and loading condition falls above surf-riding first threshold;

- if surging phenomenon is observed at least once, the considered sea state and sailing and loading condition falls below surf-riding second threshold;

From the study of the surf-riding phenomenon by means of the different approaches, the Series D has been found vulnerable to this failure mode. Therefore, Operational Measures have been applied and discussed to reduce the stability failure when dangerous sea state conditions are encountered.

IMO working groups have long discussed on the procedure to adopt and the actual guidelines has brought to some uncertainties.

The Operational Guidance is based on three approaches: probabilistic, deterministic and simplified.

The simplified one is analysed in this thesis and the guidelines define a maximum ship speed in each sea state for which the short term exceeds the specified limit, but the text and the reference to the formula is misleading.

Another important aspect of the Operational Measures is the understanding of ships' safety when complying with the regulation. Since the Operational Limitations related to maximum wave heights are based on the long-term index, when the ship complies with the OL this does not mean that the ship may always operate in safe conditions when the wave height is lower than the selected one, but they state that the probability of failure in these sea states is sufficiently low. On the other hand, the Operational Guidance is based on the short-term and clearly indicate in which sea state the ship operates in safe conditions or and in which she does not.

A hypothetical route for the D1 ship has been chosen in the Mediterranean Sea corresponding to AREA 26 from the Global Wave Statistics (Hogben et al., 1986). The ship did not comply with the Operational Limitations related to this area for the defined service loading condition, and since no changes in ship design were considered feasible, Operational Limitation related to maximum wave height and Operation Guidance has been analysed.

The value of the maximum wave height has been checked if in accordance with the limitations of minimum allowable significant wave height in order to consider the loading condition acceptable, corresponding to 20% value of the ratio between the total duration of all situations which should be avoided and the total operational time.

The Operational Guidance has then been provided in coloured table form, reporting the limiting speeds achievable in each sea state condition. The considered loading condition for D1 has been tested acceptable for the North Atlantic and AREA 26 wave scatter diagram since the total probability of sea states to be avoided has been found less than 20% threshold.

The major difference between OL and OG is: the OL state that the considered sea state must be avoided independently from heading and speed, while the OG permit operations in the sea states but for limited headings and ship speed.

Overall results obtained by the application of the three numerical approaches highlight the following:

- The 1-DOF approach is limited to calm water approximations but including the diffraction component brought a significant improvement. The time duration to find surf-riding limits for each sea state condition was about few seconds.

- The 6-DOF approach has some limitations: the resistance and thrust are approximated for calm water conditions; the Froude-Krylov component is weakly nonlinear, because it is calculated under the linear wave profile; the diffraction component is obtained under calm water profile; and the maximum allowable wave height is limited to avoid green water effect. The time duration to find surf-riding limits for each sea state condition was about few minutes.

- The CFD simulations brought to the least conservatism since all non linearities due to force variation in waves are taken into account, but they were time consuming, reaching even one week for each case tested.

It is worth to underline that the diffraction force and the hydrodynamic coefficients could be evaluated under the actual wave profile, with Level 3 body non linear method, as described in Hirdaris et al. (2014), but authors state that no publications regarding the Level 3 methods appeared during the reporting period. Instead body exact methods (Level 4) and fully non-linear methods as CFD (Level 6) are used.

The 6-DOF potential theory methodology stands between the two approaches, the simple and fast 1-DOF and the direct but time consuming CFD, and turns out to be a good compromise in predicting surf-riding limits.

Following SDC7/WP6 (2020) for the Direct Stability Assessment, the motion of ships in waves can be predicted by means of numerical simulations or model tests that replicate ship motions in irregular waves. For the surf-riding/broaching failure mode ship motion simulations should include at least the following four degrees of freedom: surge, sway, roll and yaw, and an appropriate autopilot should be used.

Having underlined the limitations of the three approaches described in the thesis and knowing the time duration for each approach in regular following wave as well as the fact that the time would increase in case of irregular waves, here follows a discussion of applicability of each approach.

Although CFD simulations, extended to 4-DOF, would predict less conservative surf-riding limits since they embrace all the non linear effects due to waves, the performance of DSA would have impracticable time durations and costs;

Since the limits predicted with the 6-DOF potential theory approach are fairly comparable with limits obtained by the CFD method and the simulation time duration seems reasonable, this is considered the overall best approach for a Direct Stability Assessment.

The potential theory numerical code could be improved by including the randomization of irregular sea states and including manoeuvring coefficients evaluated for the specific hull. In this perspective the 1-DOF quickest approach would be a primary tool to define a first set of limits from which the other two approaches would start from to decrease time duration and costs.

Future improvements and studies may be carried out to extend CFD simulations in irregular wave conditions in 6-DOF to analyse the both surf-riding and broaching phenomena.

Moreover, simulations in wave results will need to be verified and the uncertainty of the results will need to be assessed following ITTC Uncertainty analysis in CFD Verification and Validation Methodology and Procedure. In this context, an experimental campaign of towing tank tests of self-propelled ship sailing in following regular and irregular sea, could be made to verify partial results of CFD simulations in wave.

It should be highlighted that the development of the surf-riding phenomenon, throughout the thesis, has been analysed considering the ship in open sea and the surf-riding limits have been related to maximum allowable speed and wave steepness underlining that the phenomenon could be avoided when ship speed decreases. Another important aspect of the occurrence of the phenomenon is in bar crossing conditions. In this situation of shallow water waves are steep and the ship could be more easily exposed to surf-riding. Some advices given to ships when crossing coastal sandbars and coming in from sea are: "Adjust the boats speed to match the speed of the waves but do not attempt to overtake the waves. Displacement boats may have to come in very slowly to avoid surfing and broaching-to (getting caught side-on to a wave). A future task could be the analysis and discussion on the bar crossing conditions.

Chapter 11

Appendix

Table 11.1: Total resistance for models of D-Systematic Series – scaled to ship of 90m length

F_n	v_S [m/s]	R_{TS} [N]						
		D1	D2	D3	D4	D5	D6	D7
0.15	4.46	35366.75	38128.07	35805.71	35286.63	38511.27	36515.11	35710.06
0.20	5.94	68260.71	78167.86	69976.26	69922.32	71521.82	71593.53	67525.90
0.25	7.43	124739.72	143382.49	128186.54	126546.44	129932.73	138793.71	126621.08
0.30	8.91	199939.25	231934.35	204570.25	203227.55	213005.99	242283.48	221001.01
0.35	10.40	283814.29	347967.80	288420.54	297885.67	310312.18	369313.51	333803.60
0.40	11.88	505457.66	581855.28	480200.48	512437.23	489906.81	619083.00	507392.46
0.45	13.37	809543.86	1039345.96	801151.67	833723.97	841181.35	1032966.81	814329.16
0.50	14.85	1055316.73	1391432.51	1069022.90	1112416.61	1089420.28	1375352.68	1067426.46
0.55	16.34	1263720.98	1661855.06	1287132.03	1336230.01	1288110.95	1648551.03	1277228.52
0.60	17.83	1446500.80	1872851.93	1463083.67	1505372.31	1470149.50	1860322.34	1453354.75
0.65	19.31	1598053.61	2034559.42	1605251.93	1633940.12	1629621.16	2019498.31	1599060.35
0.70	20.80	1701014.05	2143789.97	1718245.03	1742795.02	1731056.43	2131155.78	1710642.26
0.75	22.28	1760026.39	2204579.42	1799128.90	1836315.71	1777221.80	2192660.02	1787799.51

Table 11.2: Thrust for models of D-Systematic Series – scaled to ship of 90m length

F_n	v_S [m/s]	T_S [N]						
		D1	D2	D3	D4	D5	D6	D7
0.15	4.46	18107.89	19560.19	18315.63	18088.78	19735.17	18696.34	18281.00
0.20	5.94	35350.20	40475.70	36250.40	36257.67	37081.35	37060.93	34969.34
0.25	7.43	65264.57	75193.92	67064.97	66190.46	67999.79	72727.27	66268.64
0.30	8.91	105392.75	122530.33	107851.00	107245.16	112352.00	127880.54	116610.64
0.35	10.40	150368.18	184675.46	152826.42	157914.49	164563.65	196293.62	177097.22
0.40	11.88	269333.19	310582.37	255760.93	273228.81	260989.02	330554.99	270371.89
0.45	13.37	432788.91	556451.52	428253.28	446436.37	449788.85	552872.35	435351.02
0.50	14.85	564910.70	746039.23	572216.18	596298.15	583226.33	737545.97	571385.23
0.55	16.34	676535.62	890851.40	689069.18	716308.19	689657.78	883802.48	683806.47
0.60	17.83	773826.56	1003093.65	782690.08	805884.87	786567.87	996435.07	777531.24
0.65	19.31	853771.33	1088389.28	857545.25	873726.02	870702.03	1080460.93	854290.68
0.70	20.80	907021.68	1144840.71	916162.18	930355.79	923121.43	1138077.95	912145.90
0.75	22.28	936243.59	1174267.55	957017.45	977934.56	945453.33	1168001.98	951062.28

Table 11.3: Propeller's number of revolutions for models of D-Systematic Series – scaled to ship of 90m length

Fn	v_S [m/s]	N_S [rpm]						
		D1	D2	D3	D4	D5	D6	D7
0.15	4.46	72.5	72.5	72.5	72.5	72.8	72.3	72.5
0.20	5.94	97.3	97.4	97.3	97.4	97.4	97.1	97.3
0.25	7.43	123.5	123.8	123.5	123.5	123.6	123.6	123.5
0.30	8.91	152.0	152.4	152.0	152.1	152.4	152.6	152.4
0.35	10.40	184.4	185.1	184.4	184.7	185.0	185.6	185.3
0.40	11.88	222.5	222.9	222.0	222.6	222.3	223.4	222.5
0.45	13.37	262.0	263.1	261.8	262.3	262.3	263.1	262.0
0.50	14.85	298.5	300.1	298.5	299.1	298.8	300.1	298.7
0.55	16.34	330.6	332.1	330.8	331.2	330.9	332.1	330.8
0.60	17.83	357.4	358.8	357.4	357.7	357.6	358.8	357.4
0.65	19.31	379.1	380.5	379.1	379.4	379.4	380.5	379.1
0.70	20.80	397.2	398.5	397.2	397.5	397.4	398.5	397.2
0.75	22.28	413.0	414.3	413.2	413.5	413.2	414.3	413.2

Nomenclature And Acronyms

Nomenclature

List of symbols

Symbol	unit	definition
B	m	moulded breadth of the ship
β, μ	deg/rad	heading angle
C		long-term prediction index of Level 2
c, c_i	m/s	linear wave celerity
$C2\ (Hs, Tz)$		short-term index of Level 2
C_m		midship section coefficient of the ship in fully loaded condition in calm water
d	m	draft at considered loading condition
D	m	moulded depth
$d(x_m)$	m	draft at m-th station in calm water
D_P	m	propeller diameter
Δx_m	m	length of the ship strip associated with station m;
Fc_i, Fs_i		Froude-Krylov components
f_{ij}, f_X	N	amplitude of Wave Surging Force
Fn		Froude number
Fn_{cr}		critical Froude number corresponding to the critical number of revolutions
F_X	N	wave induced force
g	m/s^2	gravitational acceleration, 9.8065
G	m	ship centre of gravity
$G; x; y; z$		reference system fixed to the ship
GM	m	metacentric height
GZ	m	righting lever
H, H_{ij}	m	wave height
H_S	m	significant wave height
$H_{S,LIM}$	m	significant wave height limit to define limited wave scatter diagram
$H_{S,UL}$	m	upper limit of the significant wave heights, $H_{S,UL}$
$H_{S,UL\ (20\%)}$	m	upper limit of the H_S for which the ratio of the total duration of all situations which should be avoided to the total operational time is equal to 0.2

Symbol	unit	definition
J		advance ratio
k_0, k_1, k_2		approximation coefficients for propeller thrust
KB	m	height of the vertical centre of buoyancy corresponding to the loading condition under consideration
KG	m	height of the vertical centre of gravity
k_i / k	rad/m	wave number
K_T		propeller thrust coefficient
L	m	length of the ship
λ, λ_i	m	wave length
LCB	m	longitudinal position of centre of buoyancy
M	kg	mass of the ship
M_X	kg	added mass of the ship in surge approximated as 0.1*M
n	$1/s$	propeller's commanded number of revolutions
N		number of stations
n_{cr}	$1/s$	critical number of revolutions for surf-riding second threshold by Melnikov's analysis
N_P		number of propellers
$O;X,Y,Z$		fixed to Earth reference system
ρ	kg/m^3	sea density equal to 1025.87
R	N	calm water resistance
r_0, r_1, r_2, r_3, r_4, r_5		approximation coefficients for calm water resistance
R_C	N	calm water resistance at wave celerity
r_i		wavelength to ship length ratio, $r_i = (\lambda_i/L) = [1:0.025:3]$
R_{SR}		Level 2 threshold
$S(x_m)$	m^2	area of submerged portion of the ship at m-th station in calm water
s_j		wave steepness, $s_j = (H_{ij}/\lambda_i) = [0.03:0.0012:0.15]$
T	s	wave period
t	s	time
τ_0, τ_1, τ_2		thrust approximation coefficients
T_C	N	propeller's thrust at wave celerity
T_e	N	propeller's thrust
t_p		approximate thrust deduction
T_Z	s	zero crossing period

Symbol	unit	definition
u, v_S	m/s	ship speed in calm water
u_{cr}	m/s	critical ship speed of Level 2
$\dot{u}$	m/s^2	ship acceleration in calm water
ω	rad/s	wave frequency
$W2(H_S,T_Z)$		probability of wave occurrence in each sea state condition
ω_e	$1/s$	wave encounter frequency
W_{ij}		statistical weight of Level 2 representing the joint probability density function of local steepness and local wavelength under the stationary wave state with a Pierson-Moskwitz type wave spectrum
w_p		wake fraction
X	m	distance from the fixed to earth reference system and wave trough
x	m	surging displacement, distance between ship centre of gravity and the wave trough
$\dot{x}, x'$	m/s	surging velocity relative velocity between ship speed and wave celerity
$\ddot{x}$	m/s^2	surging acceleration
X_G	m	distance of the centre of gravity from the fixed to earth reference system
x_m	m	longitudinal distance from centre of ship mass to a m-th station, positive for a bow section
$\zeta(t)$	m	wave elevation

Acronyms

Acronyms

CFD	Computational Fluid Dynamics
CPL	Continuous Piecewise Linear
DOF	Degrees of Freedom
DSA	Direct Stability Assessment
EFD	Experimental Fluid Dynamics
FVM	Finite Volume Method
GFM	Ghost Fluid Method
IMO	International Maritime Organization
ITTC	International Towing Tank Conference
L1	Level 1
L2	Level 2
LS	Level Set
MSC	Maritime Safety Committee
ODE	Ordinary differential equations
OG	Operational Guidance
OL	Operational Limitations
OM	Operational Measures
ONRT	Office of Naval Research Thumblehome
PF	Phase Field
PT	Potential Theory
RANS	Reynolds-Averaged Navier Stokes
SDC	Sub-Committee on Ship Design and Construction
SGISC	Second Generation Intact Stability Criteria
SLF	Sub-Committee on Stability and Load Lines and on Fishing Vessels' Safety
SOLAS	International Convention for the Safety of Life at Sea
SWENSE	Spectral Wave Explicit Navier-Stokes Equations

Bibliography

Acanfora, M., Begovic, E., and Rinauro, B. (2019). Surf-riding failure mode: from IMO criterion to Direct Assessment procedure and application on Systematic Series D. Helsinki, Finland. 17th International Ship Stability Workshop.

Acanfora, M. and Matusiak, J. (2016). On the estimations of ship motions during maneuvering tasks in irregular seas. London, ISBN 978-1-138-03000-8. Maritime Technology and Engineering 3, Guedes Soares and Santos (Eds).

Backalov, I., Bulian, G., Rosen, A., Shigunov, V., and Themelis, N. (2015). Ship and safety in intact condition through operational measures. Glasgow, UK. In Proceedings of 12st International Conference on the Stability of Ships and Ocean Vehicles.

Bakica, A., Gatin, I., Vukcevic, V., Jasak, H., and Vladimir, N. (2019). Accurate assessment of ship-propulsion characteristics using CFD. *Ocean Engineering*, 175:149–162.

Begovic, E., Bertorello, C., Boccadamo, G., and Rinauro, B. (2018). Application of surf-riding and broaching criteria for the Systematic Series D models. *Ocean Engineering*, 170:246–265.

Begovic, E., Gatin, I., Jasak, H., and Rinauro, B. (2020). CFD simulations for Surf-riding Occurrence Assessment. *Ocean Engineering*, under 2nd revision.

Belenky, V. and Sevastianov, N. B. (2007). *STABILITY AND SAFETY OF SHIPS: Risk of Capsizing*. The Society of Naval Architects and Marine Engineers (SNAME), Pavonia Ave., Jersey City.

Belenky, V., Weems, K., and Spyrou, K. (2016). On probability of surf- riding in irregular seas with a split-time formulation. *Ocean Engineering*, 120:264–274.

Bo, W. and Grove, J. W. (2014). A volume of fluid method based Ghost Fluid Method for compressible multi-fluid flows. *Computers and Fluids*, 90:113–122.

Bonci, M., Renilson, M., Jong, P. D., Walree, F. V., and Veer, R. V. (2018). On the direct assessment of broaching-to vulnerability of a high speed craft. Kobe, Japan. 13th International Conference on the Stability of Ships and Ocean Vehicles.

Brix, J. (1993). *Manoeuvring Technical Manual*. Seehafen Verlag GmbH, Hamburg.

Carrica, P. M., Paik, K. J., Hosseini, H. S., and Stern, F. (2008). URANS analysis of a broaching event in irregular quartering seas. *J Mar Sci Technol*, 13:395–407.

Conolly, J. E. (1972). Stability and Control in Waves-A survey of the Problem. *J. Mechanical Engineering Science, I Mech E,*, 14(7):186–194.

Dean, R. G. and Dalrymple, R. A. (2002). *Water Wave Mechanics for Engineers and Scientists, Vol. 2: Advanced Series on Ocean Engineering.* World Scientific.

Du-Cane, P. and Goodrich, G. J. (1962). The following sea broaching and surging. *Royal Institution of Naval Architects, Quarterly Transaction*, 104(2):109–140.

Ducrozet, G., Engsig-Karup, A. P., Bingham, H. B., and Ferrant, P. (2014). A non-linear wave decomposition model for effcient wave-structure interaction; part a: formulation, validations and analysis. *Journal of Computational Physics*, 257:863–883.

Feng, P., Fan, S., and Liu, X. (2015). Study on the second generation intact stability criteria of broaching failure mode. Glasgow, UK. Proceedings of the 12th International Conference on the Stability of Ships and Ocean Vehicles.

Feng, P., Fan, S., Nie, J., and Liu, X. (2017). The influence of wave surge force on surf-riding broaching vulnerability criteria check. *Journal of Hydrodynamics*, 29:596–602.

Ferrant, P., Gentaz, L., and Touze, D. L. (2002). A new RANSE/potential approach for water wave diffraction. Pornichet, France,. Numerical Towing Tank Symposium.

Gatin, I., Vladimir, N., Malenica, S., and Jasak, H. (2019). Green sea loads in irregular waves with Finite Volume method. *Ocean Engineering*, 171:554–564.

Gatin, I., Vukčević, V., and Jasak, H. (2015a). CFD Validation of a Container Ship in Calm Water and Head Seas. In *18th Numerical Towing Tank Symposium, NUTTS*.

Gatin, I., Vukčević, V., and Jasak, H. (2015b). Validation and Verification of steady resistance KCS simulations with dynamic sinkage and trim of KCS using Embedded Free Surface Method. In *Tokyo 2015: A workshop on CFD in Ship Hydrodynamics*.

Gatin, I., Vukčević, V., Jasak, H., and Ruscheb, H. (2017). Enhanced coupling of solid body motion and fluid flow in finite volume framework. *Ocean Engineering*, 143:295–304.

Goldstein, S. (1929). On the vortex theory of screw propellers. *Proceedings of the Royal Society of London*, 123:440–465.

Grim, O. (1963). Surging motion and broaching tendencies in a severe irregular sea. *Ocean Dynamics*, 16:201–231.

Hashimoto, H., Umeda, N., and Matsuda, A. (2004). Importance of several nonlinear factors on broaching prediction. *J Mar Sci Technol*, 9:80–93.

Hashimoto, H., Yoneda, S., Tahara, Y., and Kobayashi, E. (2016). CFD-based study on the prediction of wave-induced surge force. *Ocean Engineering*, 120:389–397.

Hirdaris, S., W.Bai, D.Dessi, A.Ergin, X.Gu, O.A.Hermundstad, R.Huijsmans, Iijima, K., U.D.Nielsen, J.Parunov, N.Fonseca, A.Papanikolaou, K.Argyriadis, and A.Incecik (2014). Loads for use in the design of ships and off shore structures. *Ocean Engineering*, 78:131—-174.

Hogben, N., Dacunha, N. C., and Olliver, G. F. (1986). *Global Wave Statistics.* British Maritime Technology Limited, Feltham Middlesex TW14 0LQ.

Huang, J., Carrica, P. M., and Stern, F. (2007). Coupled ghost fluid two-phase level set method for curvilinear body fitted grids. *Int. J. Numer. Meth. Fluids*, 44:867–897.

Issa, R. I. (1986). Solution of the implicitly discretised fluid flow equations by operator-splitting. *J. Comput. Phys.*, 62:40–65.

J. O. De Kat and W. L. Thomas III (1998). Broaching and capsize model tests for validation of numerical ship motion predictions. St. John's, Newfoundland. 4th International Ship Stability Workshop.

Jasak, H. (1996). *Error analysis and estimation for the finite volume method with applications to fluid flows*. PhD thesis, Imperial College of Science, Technology and Medicine, London.

Jasak, H., Jemcov, A., and Tuković, Z. (2007). *OpenFOAM: A C++ library for complex physics simulations*. International Workshop on Coupled Methods in Numerical Dynamics, IUC, Dubrovnik, Croatia.

Jasak, H., Vukcevic, V., and Gatin, I. (2015). Numerical simulation of wave loads on static offshore structures. *CFD for Wind and Tidal Offshore Turbines, Springer Tracts in Mechanical Engineering*, 100:95–105.

Jasak, H., Vukcevic, V., Gatin, I., and Lalovic, I. (2018). CFD Validation and Grid Sensitivity Studies of Full Scale Ship Self Propulsion. *International Journal of Naval Architecture and Ocean Engineering*, pages 1–11.

Kan, M., Saruta, T., and Taguchi, H. (1994). Comparative Model Tests on Capsizing of Ships in Quartering Seas. volume 3, pages 1–20, Melbourne, Florida. 5th Int. Conference STAB.

Kracht, A. M. and Jacobsen, A. (1992). D-Series systematic experiments with models of fast twin-screw displacement ship. *SNAME Transactions*, 100:199–222.

Krasilnikov, V. I. (2013). Self-Propulsion RANS Computations with a Single-Screw Container Ship. Launceston, Australia. Third International Symposium on Marine Propulsors SMP 13.

Longuet-Higgins, M. S. (1983). On the joint distribution of wave periods and amplitudes in a random wave field. volume A, pages 241–258. Proceedings of the Royal Society of London.

Maki, A., Umeda, N., and Renilson, M. (2010). Analytical formulae for predicting the surf-riding threshold for a ship in following seas. *J Mar Sci Technol*, 15:218–229.

Maki, A., Umeda, N., Renilson, M., and Ueta, T. (2014). Analytical methods to predict the surf-riding threshold and the waveblocking threshold in astern seas. *J Mar Sci Technol*, 19(4):415–424.

Matusiak, J. (2013). *Dynamics of Rigid Ship*. SCIENCE + TECHNOLOGY, Aalto University, School of Engineering, Department of Applied Mechanics, Marine Technology.

Menter, F. R., Kuntz, M., and Langtry, R. (2003). Ten years of industrial experience with the sst turbulence model. *Turbulence, Heat and Mass Transfer*, 4:625–632.

MSC.1/Circ.1228 (2007). Revised guidance to the master for avoiding dangerous situations in adverse weather and sea conditions.

MSC.1/Circ.707 (1995). Guidance to the master for avoiding dangerous situations in following and quartering seas.

Muller, A. and Terze, Z. (2016). Geometric methods and formulations in computational multibody system dynamics. *Acta Mech.*, 227(12):3327—-3350.

Patankar, S. V. and Spalding, D. B. (1972). A calculation procedure for heat, mass and momentum transfer in three-dimensional parabolic flows. *Int. J. Heat Mass Transf.*, 15:1787–1806.

Pereira, F. S., Vaz, G., and Eca, L. (2015). On the Numerical Requirements of RANS and Hybrid Turbulence Models. *Proceedings of the MARINE 2015 Conference*, pages 886–902.

Perić, R., Vukčević, V., Abdel-Maksoud, M., and Jasak, H. (2018). Tuning the Case-Dependent Parameters of Relaxation Zones for Flow Simulations With Strongly Reflecting Bodies in Free-Surface Waves.

Petacco, N. and Gualeni, P. (2020). Imo second generation intact stability criteria: general overview and focus on operational measures. *J. Mar. Sci. Eng.*

Rahola, J. (1939). The Judging of the Stability of Ships and the Determination of the Minimum Amount of Stability – Especially Considering the Vessels Navigating Finnish Waters.

Saad, Y. (2003). *Iterative Methods for Sparse Linear Systems*. Society for Industrial and Applied Mathematics (SIAM), Philadelphia.

Sadat-Hosseini, H., Carrica, P., Stern, F., Umeda, N., Hashimoto, H., Yamamura, S., and Mastuda, A. (2011). CFD, system-based and EFD study of ship dynamic instability events: Surf-riding, periodic motion, and broaching. *Ocean Engineering*, 38(1):88–110.

Salmaso, M. (2018). *ANALISI DELLA DINAMICA DI SURF-RIDING E WAVE-BLOCKING*. PhD thesis, UNIVERSITÀ DEGLI STUDI DI TRIESTE.

SDC2/INF10 (2014). Second-generation intact stability criteria.

SDC2/WP4 (2015). Development of second generation intact stability criteria.

SDC3/INF10 (2015). Finalization of second generation intact stability criteria.

SDC3/WP5 (2016). Finalization of second generation intact stability criteria.

SDC4/5/4 (2016). Finalization of second generation intact stability criteria.

SDC4/5/6 (2016). Finalization of second generation intact stability criteria.

SDC6/WP6 (2019). Finalization of second generation intact stability criteria.

SDC7/5 (2019). Finalization of second generation intact stability criteria.

SDC7/WP6 (2020). Finalization of second generation intact stability criteria.

Seb, B. (2017). Numerical characterisation of a ship propeller. Master's thesis, Faculty of Mechanical Engineering and Naval Architecture, University of Zagreb.

Shigunov, V., el Moctar, O., Papanikolaou, A., Potthoff, R., and Liu, S. (2018). International benchmark study on numerical simulation methods for prediction of manoeuvrability of ships in waves. *Ocean Engineering*, 165:365–385.

Spyrou, K. J. (1996a). Dynamic instability in quartering seas-Part II: Analysis of ship roll and capsize for broaching. *Journal of Ship Research*, 40(4):326–336.

Spyrou, K. J. (1996b). Dynamic instability in quartering seas: The behavior of a ship during broaching. *Journal of Ship Research*, 40(1):46–59.

Spyrou, K. J. (2006). Asymmetric surging of ships in following seas and its repercussions for safety. *Nonlinear Dynamics*, 43:149–172.

Spyrou, K. J., Belenky, V., Themelis, N., and Weems, K. (2014). Detection of surf-riding behavior of ships in irregular seas. *Nonlinear Dynamics*, 78:649–667.

Sun, Y. and Beckermann, C. (2007). Sharp interface tracking using the phase field equation. *Comput. Phys*, 220:626–653.

Themelis, N., Spyrou, K. J., and Belenky, V. (2016). High runs of a ship in multichromatic seas. *Ocean Engineering*, 120:230–237.

Umeda, N. (1984). Resistance variation and surf-riding of a fishing boat in a following sea. *Bull Natl Res Inst Fish Eng*, 5:185–205.

Umeda, N. (1999). Nonlinear dynamics of ship capsizing due to broaching in following and quartering seas. *J Mar Sci Technol*, 4:16–26.

van der Vorst, H. A. (2003). *Iterative Krylov Methods for Large Linear Systems*. Cambridge University Press.

Versteeg, H. K. and Malalasekera, W. (2007). *An Introduction to Computational Fluid*. Pearson Education Limited, Edinburgh Gate, 2 edition.

Vukčević, V. (2016). *Numerical modelling of coupled potential and viscous ow for marine applications*. PhD thesis, Faculty of Mechanical Engineering and Naval Architecture, University of Zagreb.

Vukčević, V. and Jasak, H. (2015). Seakeeping Validation and Verification Using Decomposition Model Based on Embedded Free Surface Method. volume 3, pages 437–442. In Proceedings of the Tokyo 2015: A Workshop on CFD in Ship Hydrodynamics.

Vukčević, V., Jasak, H., and Gatin, I. (2017). Implementation of the Ghost Fluid Method for free surface flows in polyhedral Finite Volume framework. *Comput. Fluids*, 153:1–19.

Vukčević, V., Jasak, H., and Malenica, S. (2016a). Decomposition Model for Naval Hydrodynamic Applications, Part I: Computational Method. *Ocean Engineering*, 121:37–46.

Vukčević, V., Jasak, H., and Malenica, S. (2016b). Decomposition Model for Naval Hydrodynamic Applications, Part II: Verification and validation. *Ocean Engineering*, 121:76–88.

Weller, H. G., Tabor, G., Jasak, H., and Fureby, C. (1998). A tensorial approach to computational continuum mechanics using object oriented techniques. *Comput. Phys*, 12:620–631.

Wu, W., Spyrou, K. J., and McCue, L. S. (2010). Improved prediction of the threshold of surf-riding of a ship in steep following seas. *Ocean Engineering*, 37:1103–1110.

Yang, B. and Wang, X. (2017). Study on Ship's Stability Loss in Surf-riding Based on CFD. *4th International Conference on Information, Cybernetics and Computational Social Systems.*

Yu, L., Ma, N., and Gu, X. (2014). Numerical investigation into ship stability failure events in quartering seas based on time domain weakly nonlinear unified model. pages 229–235, Kuala Lumpur, Malaysia. Proceedings of the 14th International Ship Stability Workshop.

Yu, L., Ma, N., and Gu, X. (2017). On the mitigation of surf-riding by adjusting center of buoyancy in design stage. *ScienceDirect, International Journal of naval architecture and ocean engineering.*

List of Figures

List of Tables